Modeling of the fundamental mechanical interactions of unit load components during warehouse racking storage

Eduardo Molina Montoya

Dissertation submitted to the faculty of the Virginia Polytechnic Institute and State University in partial fulfillment of the requirements for the degree of

Doctor of Philosophy
In
Forestry and Forest Products

Laszlo Horvath, Chair
Joseph R. Loferski
Robert L. West
Marshall S. White

December 10, 2020
Blacksburg, VA

Keywords: pallets, packaging, unit load, unit load interactions, finite element analysis, gaussian process model, load bridging

Modeling of the fundamental mechanical interactions of unit load components during warehouse racking storage

Eduardo Molina Montoya

ABSTRACT (Academic)

The global supply chain has been built on the material handling capabilities provided by the use of pallets and corrugated boxes. Current pallet design methodologies frequently underestimate the load carrying capacity of pallets by assuming they will only carry uniformly distributed, flexible payloads. But, by considering the effect of various payload characteristics and their interactions during the pallet design process, the structure of pallets can be optimized. This, in turn, will reduce the material consumption required to support the pallet industry.

In order to understand the mechanical interactions between stacked boxes and pallet decks, and how these interactions affect the bending moment of pallets, a finite element model was developed and validated. The model developed was two-dimensional, nonlinear and implicitly dynamic. It allowed for evaluations of the effects of different payload configurations on the pallet bending response. The model accurately predicted the deflection of the pallet segment and the movement of the packages for each scenario simulated.

The second phase of the study characterized the effects, significant factors, and interactions influencing load bridging on unit loads. It provided a clear understanding of the load bridging effect and how it can be successfully included during the unit load design process. It was concluded that pallet yield strength could be increased by over 60% when accounting for the load bridging effect. To provide a more efficient and cost-effective solution, a surrogate model was developed using a Gaussian Process regression. A detailed analysis of the payloads' effects on pallet deflection was conducted. Four factors were identified as generating significant influence: the number of columns in the unit load, the height of the payload, the friction coefficient of the payload's contact with the pallet deck, and the contact friction between the packages. Additionally, it was identified that complex interactions exist between these significant factors, so they must always be considered.

Modeling of the fundamental mechanical interactions of unit load components during warehouse racking storage

Eduardo Molina Montoya

ABSTRACT (Public)

Pallets are a key element of an efficient global supply chain. Most products that are transported are commonly packaged in corrugated boxes and handled by stacking these boxes on pallets. Currently, pallet design methods do not take into consideration the product that is being carried, instead using generic flexible loads for the determination of the pallet's load carrying capacity. In practice, most pallets carry discrete loads, such as corrugated boxes. It has been proven that a pallet, when carrying certain types of packages, can have increased performance compared to the design's estimated load carrying capacity. This is caused by the load redistribution across the pallet deck through an effect known as load bridging.

Being able to incorporate the load bridging effect on pallet performance during the design process can allow for the optimization of pallets for specific uses and the reduction in costs and in material consumption. Historically, this effect has been evaluated through physical testing, but that is a slow and cumbersome process that does not allow control of all of the variables for the development of a general model. This research study developed a computer simulation model of a simplified unit load to demonstrate and replicate the load bridging effect.

Additionally, a surrogate model was developed in order to conduct a detailed analysis of the main factors and their interactions. These models provide pallet designers an efficient method to use to identify opportunities to modify the unit load's characteristics and improve pallet performance for specific conditions of use.

TABLE OF CONTENTS

List of Figures

List of Tables

Introduction

In a highly globalized world with intertwined supply chains, packages often move long distances across the globe, allowing products to reach remote locations. Companies in this extremely competitive environment are continuously searching for efficiency improvement opportunities. A popular target area for continuous improvements is packaging redesign, conducted at all levels, from primary packaging enhancements to secondary and tertiary packaging redevelopments.

The global supply chain has been built on the material handling capabilities provided by pallets, which allow for far more efficient mechanical handling of products (Gurvich & Thompson, 2004; LeBlanc & Richardson, 2003). The significance of pallets is backed up by the numbers. In the United States alone, there are over 2 billion pallets in circulation (McGinley, 2016). Pallets are traditionally built out of wood, but alternative materials, mainly plastics, are becoming increasingly common (McCrea, 2016).

One of the reasons that wooden pallets are so common is due to the simplicity of prototyping, the availability of tools to use in the development of new or improved designs and their low costs. Commercial software, such as *Best Pallet* ® and *The Pallet Design System* ®, are the most commonly used tools. These software solutions allow their users to predict pallet performance at multiple stages in the supply chain, such as in racking storage, floor stacking, and during dynamic handling on forklifts (National Wooden Pallet and Container Association, 2019; White and Company, 2019). Plastic pallets require a steeper initial investment during development, which entails creating complex mechanical analysis models (such as finite element analysis) to predict their performance. Prototyping and manufacturing involve large monetary investments due to the specialized equipment required.

Given the relevance of pallets in global logistics, and the importance of determining the limitations of each design due to safety considerations, pallet performance evaluation has been standardized. Pallet testing standards include ASTM D1185 - *Standard Test Methods for Pallets and Related Structures Employed in Materials Handling and Shipping* (2016) and *ISO 8611 – Pallets for material handling* (2011a). Most of the standard test methods assume a uniformly distributed load, or a close alternative, to replicate a generic payload.

Research behind improvements to package and pallet designs have been conducted independently of each other. A company may focus on redesigning a secondary package in order to increase its performance in the field, while ignoring pallet design. On the other hand, it is not uncommon for companies to optimize their pallet costs by reducing their quality, not considering the possible effects this may have on the packages and products that the pallet will carry. With this dissonance in mind, research efforts have been conducted to bridge this knowledge gap and explore how pallet design can affect package performance, or how a payloads' characteristics may impact pallet performance. This is what has become known as a systems-based design methodology, instead of the traditional component-based design method (White & Hamner, 2005).

Regarding the effect of payload characteristics and assuming a uniformly distributed load, such as an airbag, ASTM D1185 provides a reliable performance estimation for pallets, regardless of the product being transported. Naturally, pallets do not always transport uniformly distributed loads such as large bags of water. The most common type of unitized package is a stack of corrugated boxes (Twede, 2007). A significant number of pallets are specifically designed to transport one, or only a few, different payload configurations.

Pallets carrying a non-uniformly distributed load, such as in a stack of corrugated boxes, perform differently than when measured using uniform load testing methods. The rigidity of the load on the pallet redistributes the stresses across it, generates different load distributions, and can affect reactions by reducing pallet bending and increasing overall performance in the field. This effect is known as load bridging in unit loads. To account for these changes in the performance of pallets when loaded with known payloads, ISO 8611 Part 3 (ISO, 2011b), includes the determination of a maximum working load for each known payload for each different pallet support condition.

Research has been conducted to explore why load bridging occurs and which factors influence it. The factors that have been identified that affect the stiffness of the load, and therefore, the level of load bridging experienced are as follows: package size, package and pallet stiffness, containment force, number of layers, unit load height, coefficient of friction between components, and package stacking pattern (Center for Unit-Load Design, 1997; Collie, 1984; Fagan, 1982; Park, 2015; Park et al., 2017; White, Dibling, Rupert, & Mcleod, 1999; Yoo, 2011).

Fagan (1982) began characterizing types of unit loads in order to gain an understanding about how the type of load affects the pallet performance. He concluded that load type and pallet

stiffness have a significant effect on the deflection of the pallet. Collie (1984) continued investigating the load bridging effect in unit loads for stacked and racked palletized loads. He identified that load bridging is greater in pallets stored in a configuration that spans the pallet width because pallets are less stiff in this mode of support. Regarding the differences in deflection due to the load type, only on the lower stiffness pallets was it possible to find any significant differences.

Other research studies looking at understanding how a load redistributes or how the pallet bends have been conducted by Yoo (2011), Park (2017), Molina (2018),Clayton (2019), and Morrissette (2020). These investigations all had a common approach, where experimental methods were developed to study how pallet bending reacts to different payload characteristics. Research projects that study different payload configurations experimentally require extensive time and money investments, and provide results limited to the specific factors measured.

In an effort to develop more efficient packaging design methods, finite element analysis (FEA) is commonly utilized. The finite element method allows for the simulation of different scenarios without the need to actually create and test multiple, costly, experimental replicates, and FEA allows scientists to analyze how the unit load reacts to multiple inputs.

Extensive research has included FEA modeling of different packaging materials, such as wood (Mackerle, 2005), corrugated board (Djilali Hammou, Minh Duong, Abbès, Makhlouf, & Guo, 2012; Fadiji, Coetzee, Berry, Ambaw, & Opara, 2018; Zhang, Qiu, Song, & Sun, 2014), paperboard (Nygårds, Sjökvist, Marin, & Sundström, 2019; Zaheer, Awais, Rautkari, & Sorvari, 2018), and multiple others (Wang, Zhao, & Li, 2012).

A key step in the development of a finite element model for a unit load will be the frictional contacts between multiple components, such as the contact of a box against another box or between the boxes and the pallet. Frictional contacts in FEA are commonly regarded as complex mathematical problems given the computational analysis required and the additional possible convergence issues generated (Gurvich & Thompson, 2004).

The use of FEA has become commonplace in the design process of pallets for material handling. Wooden pallets can be designed using various commercial software available, which are mostly based on finite element models (Modern Material Handling, 2012).

Multiple studies can be found in literature that evaluate new pallet designs often using innovative materials, where the application of finite element models allow for the preliminary

evaluation of pallet performance (Mohammed & Baig, 2018; Ratnam, Lim, & Khalil, 2005; Waseem, Nawaz, Munir, Islam, & Noor, 2013).

Han, White and Hamner (2007) applied the finite element method to better understand and explain the load bridging effect in unit loads that are stacked on the floor of a warehouse. A single board segment was simulated, and experimental verification was conducted by using pressure sensitive film to study pressure distribution and also by measuring board deflection. The overall finite element solution provided results in close agreement to the experimental measurements. FEA confirmed the non-uniform pressure distribution experienced when a deck board is under load from a discrete payload.

Besides the static interactions of loading on pallets, studies can also be found looking at the dynamic interactions of pallets, containers, and products during transportation. During handling, unit loads are subjected to vibration. Weigel (2001) studied the resonant response of unit loads to vibration frequencies. For this, a computer model was developed using finite element analysis in order to identify the resonant frequencies of the unit loads; those at which vibration will be most magnified. The model allowed designers to understand the effect of different unit load design decisions on the vibratory responses of the load. This is especially critical for products that are sensitive to damage from small, repetitive impacts such as fresh fruit or electronics.

It can be concluded that there is a need for better understanding about how the payload interacts with the pallet. This will allow unit load designers to more accurately predict the performance of any specific pallet design, based on the product being carried. Even though the existing knowledge provides hints about the trends and effects, more fundamental knowledge is needed about how different factors, such as box size, frictional interaction, unit load aspect ratios, as well as payload weight, and pallet stiffness interact with each other and ultimately affect the bending of pallets. This knowledge gap is even more evident for plastic pallets. Their performance is mostly driven by bending limits. Finite element analysis stands out as a powerful tool that could accomplish this goal.

1 Objectives

Historically, approaches to pallet testing have left out the complex interactions between payloads and pallets, focusing instead on uniform loading to obtain performance values regardless of the actual product being carried and ignoring the load bridging effect. This approach tends to penalize the performance of low-stiffness, plastic pallets intended for a few specific loads, such as carrying only stacked corrugated boxes. In an effort to bridge this gap, existing methods allow for the determination of maximum working loads through laboratory testing of each pallet design and each payload configuration. Being able to determine the carrying capacity of a single pallet when carrying different packages, implies testing each configuration in time-consuming and expensive laboratory setups. Tests are required for each type and arrangement of packages, even when carried on the same pallet.

It is not uncommon to find custom evaluation methods from plastic pallet suppliers that do not adhere to standards, risking severe accidents, or at least supporting uncompetitive business practices. Efforts have been conducted to understand and model the load bridging effect, but the high number of factors, all of the possible levels, and the interactions amongst all of the factors have made this endeavor difficult, especially when limited to physical testing methods. The availability of advanced computing power and software that can conduct complex finite element analysis, provide the opportunity to model the interactions between payloads and pallets and can help us understand how load bridging works.

The main objective of this project is to quantify and model how the mechanical interactions between stacked boxes and the pallet deck affect the bending movement and load carrying capacity of pallets in the warehouse racking support condition.

To be able to attain the main objective of the project, specific objectives are defined.

1) To develop and validate a two-dimensional finite element model that can accurately simulate the deflection of a pallet carrying stacked boxes in a simulated storage rack.
2) To develop a simplified, general, load bridging model for use in the design and validation of unit loads, that will allow for the selection of the payload configurations which cause higher pallet deflection.
3) To quantify the effect of each of the factors that influence load bridging on unit loads on the resulting deflection and strength of the pallet simulator.

Literature Review

1 Pallets

1.1 Pallets in the global supply chain

A pallet is defined by the ANSI MH1 standard (2016) as a "*portable, horizontal, rigid, composite platform used as base for assembling, storing, stacking, handling, and transporting goods as unit load; […] described by providing the following information in the sequence listed: class, use, type, style, bottom deck size, and design.*" Even though pallets were initially developed in the 1920s, their utilization did not become widespread until World War II (1939-1945). During that time, there was a new urgency to be able to efficiently transport large amounts of goods in order to support the war effort. Along with the development of material handling equipment, pallets became commonplace due to the benefits of mechanized and unitized handling of products (LeBlanc & Richardson, 2003).

In 2018, an estimated 6.8 billion pallets were in circulation in the world, supporting the movement of goods in the global economy (Research and Markets, 2019). In the United States specifically, more than 500 million new, wooden pallets were manufactured in 2016. This represented an increase of 22% since 2011. These were in addition to the 341 million pallets that were repaired for continued use (Gerber, Horvath, Araman, & Gething, 2020). In 2018, the wooden pallet manufacturing industry in the U.S. generated an annual estimated revenue of $10.4 billion (McGinley, 2019), and the pallet rental business generated $3 billion (Masters, 2018). Given the size of the industry and the highly decentralized market, the competitive environment has driven companies to innovate, differentiate, offer additional services, and increase the automation of their operations (McGinley, 2019).

Pallets can be manufactured from different raw materials. The most common material, by a wide margin, is wood, which represents approximately 80% of the material demand, followed by plastic pallets (11%), and multiple other alternatives available in the market, such as composite wood, paper based pallets, and metal ones (McCrea, 2016; The Freedonia Group, 2008).

1.2 Pallet classifications, sizes and materials

To classify pallets, the ANSI MH1 standard (2016) proposes describing them in a sequential manner mentioning class, use, type, style, bottom deck size and design.

1.2.1 Pallet classes

The two main pallet classes are stringer and block pallets, whose schematics are shown in Figure 1 and Figure 2, respectively. According to Gerber et al. (2020), in the United States, by the year 2016, 76% of the wooden pallets manufactured were stringer class, while 21% were block class pallets. The remaining 3% corresponded to skids (pallets with no bottom deck) with custom designs. The popularity of stringer pallets is associated with lower costs, mainly due to ease of manufacturing (Clarke, 2004). Popularity of block class pallets has increased over the years. In 2011, only 6% of new wooden pallets were block class compared to the 21% in 2016 (Bush & Araman, 2014; Gerber et al., 2020).

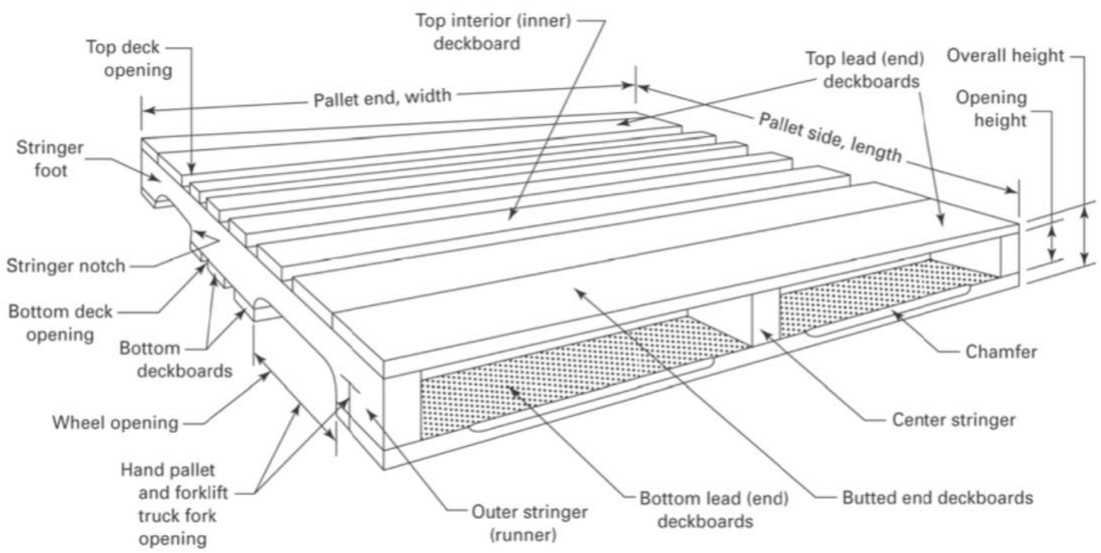

Figure 1. Diagram of Typical Stringer Class Pallet (MH1 Committee, 2016)

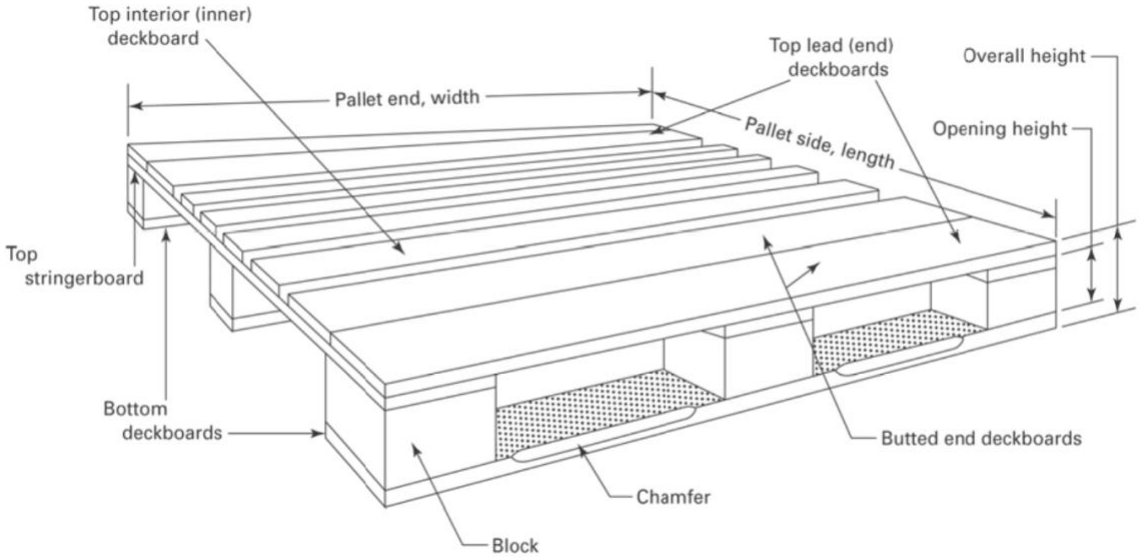

Figure 2. Diagram of Typical Block Class Pallet (MH1 Committee, 2016)

1.2.2 Use categories

Pallets can also be classified according to the number of trips for which they are intended to be used. Reusable pallets are those used multiple times to carry different unit loads. Single-use pallets are intended to be loaded once for one single trip (National Wooden Pallet and Container Association, 2014).

1.2.3 Entry type

One of the reasons for the increased popularity in block pallets is the ease of handling. Block pallets can be accessed from all four of their sides by the different handling equipment (4-way pallets). Stringer class pallets with no notches on their stringer boards can be accessed only from two ends (two-way pallets). When notches are used, the stringer pallet can be accessed from all four sides but only with limited equipment due to reduced clearance (partial 4-way pallets) (LeBlanc & Richardson, 2003; National Wooden Pallet and Container Association, 2014).

1.2.4 Pallet sizes

Probably the most important characteristic of pallets are their dimensions. Size will impact the efficiency of space and volume utilization throughout the supply chain. The fit of the pallet in different equipment and storage options can affect the smooth distribution of goods. Given that

companies continuously look for optimization opportunities, developing pallets with different dimensions has been common practice. This caused a sprawl in the number of available pallet sizes in the market, each optimized for specific operations, but ignored the cost that this lack of standardization caused in the large, global, interconnected markets (Raballand & Aldaz-Carroll, 2007).

With the goal of providing guidance towards standard pallet sizes, the International Standard Organization developed the standard ISO 6780 - Flat pallets for intercontinental materials handling - Principal dimensions and tolerances (ISO, 2003). Table 1 shows the standard pallet sizes as proposed by the organization. Even though there has been historically low standardization, recent studies have found a decrease in the production of pallets with custom dimensions. In 2018 only around 39% of the new pallets were custom sizes, compared to 60% ten years earlier. Of all of the new wooden pallets manufactured in the United States, 35% are now of the size 48 in. x 40 in. (Gerber et al., 2020).

Table 1. ISO Standard Pallet Dimensions (Adapted from ISO 6780: 2003)

Size, mm(in)	**Region**
1200 x 800 (47.2 x 31.5)	Europe
1200 x 1000 (47.2 x 39.4)	Europe, China
1219 x 1016 (48 x 40)	North America
1067 x 1067 (42 x 42)	North America
1100 x 1100 (43.3 x 43.3)	Japan, Korea
1140 x 1140 (44.9 x 44.9)	Australia

1.2.5 Pallet support conditions

The most common pallet support conditions for storage include the use of warehouse racks. Warehouse racks commonly support pallets along two beams, with an open, unsupported span in the middle. Depending on the rack design, this span can be parallel to the stringers of the pallet or perpendicular to them (for stringer pallets). A pallet that is being supported along the outside stringers is said to be supported in a “warehouse racking across the width condition,” shown in Figure 3(A). This is the common setup for drive-in and drive-through pallet racks. In these

conditions, the pallet components that are supporting most of the load are the deck boards, which are typically the weakest components. Pallets that are supported along the deck boards are said to be supported in a "warehouse racking across the length condition," and this is commonly seen in selective racks, shown in Figure 3 (B). In these scenarios, the weight of the load is supported by the stringers, which are typically stronger than the deckboards; hence, provide better performance. When designing pallets and unit loads, short but dynamic trips on forklifts must also be considered, as shown in Figure 3 (C). Pallets can also be stacked on the floor (Figure 3 (D)). In this floor stack condition, most of the load will be supported by the deck boards on the bottom of the pallet (Howie, 2008).

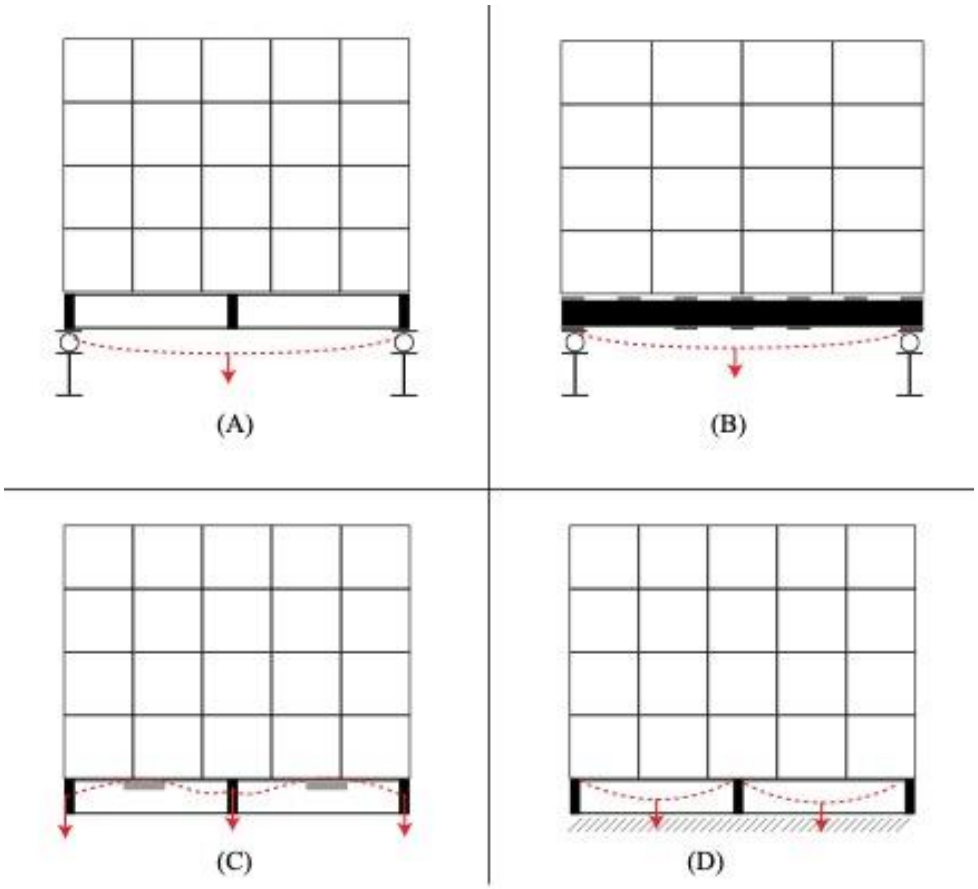

Figure 3. Common pallet support conditions and usual deflection pattern (dashed red line) for warehouse racking across the width (A), across the length (B), forklift support (C) and floor stacking (D).

1.3 Pallet design and performance testing

Historically, pallet design began as a combination of experience-based design and trial and error experimentation. But a clear need to engineer a reliable, better-performing structure became evident, and standardized pallet design methods began to be developed. Initial research to study the performance of pallet components can be traced back to Heebink (1959), who developed the mathematical basis used to study the load capacity of pallet deck boards. As part of his investigation, Heebink studied the different factors affecting the performance of wooden deckboards. Factors investigated were the quality and species of wood, moisture content of the wood, defects, load placement and duration of load.

Wallin (1979) developed the mathematical formulas for predicting the carrying capacity of combined pallets when racked across the width and across the length for both uniform and concentrated loads. He also came up with a basic procedure to determine expected deflection rates. Kyokong (1979) developed a pallet model using matrix structural analysis. Samarasinghe (1987) investigated the nail joint properties of wooden pallets and analyzed the rotational modulus of the joints. Based on these previous developments, Urbanik (1985) further refined and simplified the formulas for the pallet deflection of a pallet supported on a drive-in rack.

Fagan (1982) developed a method to evaluate the performance of pallets in a systematic manner, with consistent load application using airbags and simulated rack supports. His methods allowed for repeatability of the tests regardless of which laboratory conducted them. As a result, the load carrying capacity of the pallet could be determined independently of the payload it carried, since a uniformly distributed load was applied during testing.

Loferski, McLain and Collie (1985) developed a comprehensive procedure that could be used to analyze racked wooden stringer pallets, using a simplified pallet model to analyze using matrix structural analysis. The methodology allowed for the computation of stress and deflection levels for each pallet component. The advancement in theoretical methods to predict pallet performance, as well as better experimental evaluation techniques allowed for improved pallet design, increasing reliability, and improved safety of operations.

1.3.1 Standard test methods for pallets

To determine the performance of pallets, multiple standards have been published. These standards provide guidelines about how to conduct different tests to evaluate pallet strength and stiffness under different support conditions and for different payloads or load simulators. ISO 8611 - Pallets for material handling – Flat Pallets (2011a) provides methods to determine the nominal load for a pallet, which corresponds to "*the lowest safe load value for the specified support conditions, independent of the type of load*" (ISO, 2011a). Additionally, a maximum working load can be calculated for specific payloads. The maximum working load is the "*greatest payload that a pallet is permitted to carry in a specific loading and support condition*" (ISO, 2011a). Figure 4 shows the ISO 8611-1 (2011a) experimental test setup for the determination of the bending strength and stiffness of pallets in racking conditions. Load applicators consisting of 50 mm wide and 10 mm thick plates (key #4 in Figure 4) are used to apply a simulated line load across the pallet. ISO 8611 (2011a) also allows for the determination of the maximum working load using the actual payload that the pallet will carry, providing more targeted results for specific use pallets.

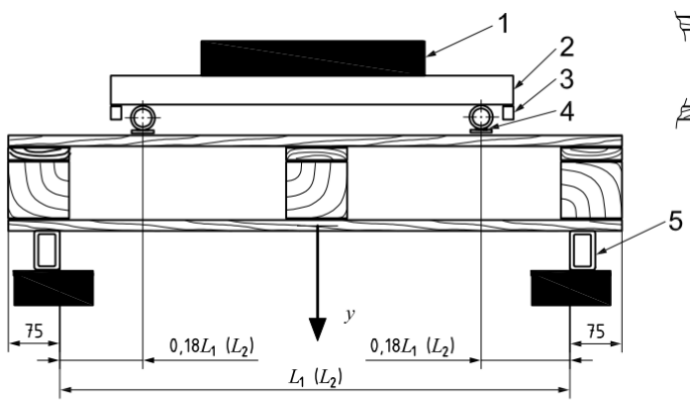

Key

1 test load
2 load board
3 safety stop
4 load applicator
5 support
6 wing
y deflection

Figure 4. Experimental test setup for the determination of bending strength and bending stiffness of pallets in racking, according to ISO 8611-1 (2011a).

ASTM D1185 Standard Test Methods for Pallets and Related Structures Employed in Materials Handling and Shipping (2009) also provides methods for the determination of the static and dynamic performance of a pallet. Focusing on static performance tests, this standard uses a uniform loading method to evaluate the bending of a pallet, commonly conducted with inflatable airbags restricted by a test rig. Figure 5 shows the ASTM D1185 experimental test setup for the determination of the bending strength and stiffness of pallets in racking conditions.

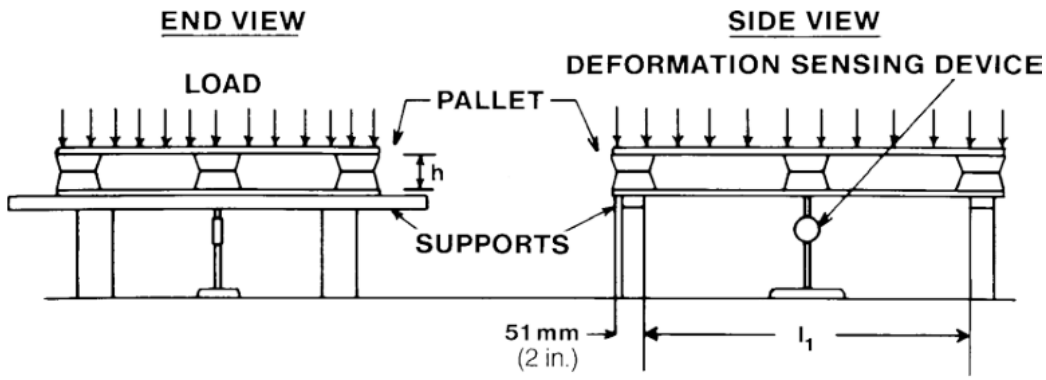

Figure 5. Experimental test setup for the determination of bending strength and bending stiffness of pallets in racking, according to ATSM D 1185.

2 Corrugated Boxes

Even though corrugated boxes have been around since the nineteenth century, they are still the most common shipping container used around the world. This widespread use is supported by their flexibility, excellent performance under different conditions, relatively low cost, as well as their high recyclability (Dekker, 2013).

2.1 Introduction and history of corrugated boxes

Corrugated fiberboard has been around since the late 1800s, and currently, it represents around 80% of the volume of shipping materials used in the United States. The corrugated fiberboard used in standard shipping boxes usually consists of two outside layers of paper, known as liners, with corrugated paper between them, known as the medium. Different arrangements can be made by changing the mediums' design (flutes) or adding additional liners and/or combinations

of fiberboard layers in order to adjust the container (box) for specific uses (Dekker, 2013; Twede, 2007).

Paper and paperboard packaging are currently the main materials used for packaging in the U.S., and they are tied with plastics in worldwide usage. Of the different package forms produced from paper and paperboard, the corrugated fiberboard package (common box) represented 64% of the total value of shipments in the year 2011, and $26.1 billion of the total production for the industry in the U.S. (Twede, Selke, Kamdem, & Shires, 2014).

2.2 Corrugated box classifications

2.2.1 Corrugated board

Corrugated fiberboard, from which corrugated boxes are made, is composed of two structural elements: linerboards and mediums. The facings of the corrugated board (the flat outside layers) are the linerboards, and mediums are the fluted structures adhered between the liners (Fibre Box Association, 2015). These two elements are glued together most commonly using a starch-based adhesive, which allows the layers to form a good bond at high manufacturing speeds (Twede et al., 2014).

Linerboards can be one of several types, but the most common is the Kraft liner. This type is made from virgin softwood fibers, but it can also be mixed with recycled fibers. In the United States, it is still considered “virgin” if at least 80% are new fibers (Maltenfort, 1988).

The mediums are made by a similar process as the linerboards but from a different type of wood pulp. It is normally made from either recycled corrugated board or from virgin hardwood fibers. This type of medium is known as semi-chemical, due to the recycling process of defibering by both mechanical and chemical processes. Although most packaging applications wouldn’t consider this type of fiber acceptable, in the production of fluting mediums, it is beneficial to facilitate the corrugating process without damaging the paper (Maltenfort, 1988; Twede et al., 2014).

These two different types of components are used together in different configurations. When only one layer of linerboard is attached to the medium, it is known as single-face corrugated board which is mostly used as wrapping material and is shipped and sold in rolls. When two liners are attached, one on either side of the medium, it is called a double-face or single wall corrugated

board. Double or triple wall corrugated boards are extensions of the arrangements possible between liners and mediums (Twede et al., 2014). Figure 6 shows drawings for these configurations.

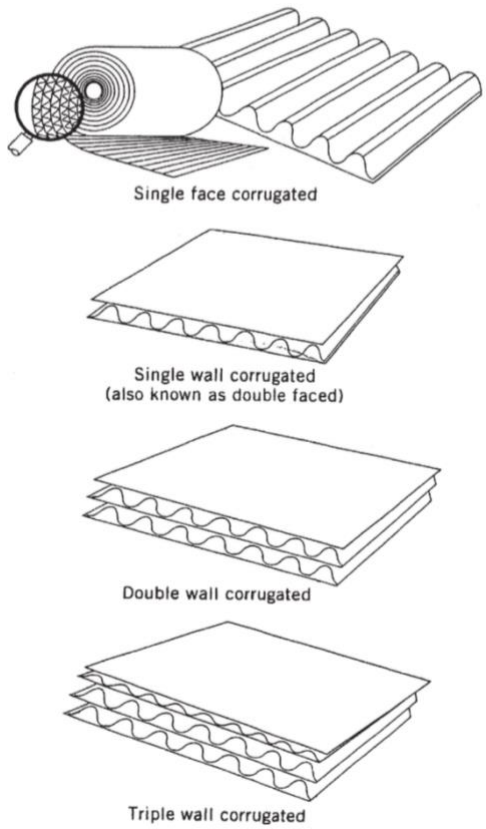

Figure 6. Possible corrugated configurations (from Foster 2010).

2.2.2 Flute types

The flutes or mediums can be made in several different common standard sizes. These sizes are characterized by the flute height and the number of flutes per linear distance (feet or meters) and identified with letters. The thickest flute type is A, and the most popular type is C-flute. The sizes are not ordered correspondingly to the alphabet order but as they appeared historically; A-flute was the first to be produced, followed by B-flute (Twede et al., 2014). Table 2 presents the four most common flute styles in the market, the number of flutes per meter or inch and the usual height range of the flute. It must be noted that it is common to have variations in factors such as

the flutes per meter, since these values are not completely standardized and depend on the manufacturing characteristics (Twede et al., 2014). It also includes a take-up factor, which is the ratio of the length of the medium divided by the length of the linerboard (Koning, 1983).

Table 2. Most common flute styles and characteristics (adapted from Dekker, n.d.; Foster 2010).

Flute Type	**Flutes per meter**	**Flutes per foot**	**Flute Thickness, mm (in.)**	**Take-up factor**
A	108 ± 10	33 ± 3	4.8 (3/16)	1.5
C	128 ± 10	39 ± 3	4.0 (5/32)	1.45
B	154 ± 10	47 ± 3	3.2 (1/8)	1.35
E	295 ± 13	90 ± 4	1.6 (1/16)	1.25

2.2.3 Board grades

Corrugated board grades are usually specified by flute type and by the basis weight (BW), which is the weight per unit of area and is also known as *grammage*. In the S.I. metric system, the BW is defined as the weight in grams of a square meter of the component (linerboard or medium), and in the U.S. customary system, it is the weight in pounds of 1000 ft^2 (Steadman, 2002).

A sample of the most common *grammages* is shown on Table 3, including the U.S. basis weight, the exact equivalent in metric units, and the corresponding similar metric grade. Additional values can be found on the market. It is a common practice to match low *grammage* mediums with low *grammage* linerboards so a balanced structure can be obtained (Steadman, 2002). Due to the modifications of the materials used for the manufacturing of corrugated board, such as the increased use of recycled fibers that reduce the strength, the basis weight is no longer enough to predict the physical capabilities of the board. Additional information is required, such as the results from an edge crush test or a Mullen burst test (see Section 2.3 Corrugated box performance and testing).

Table 3. Common nominal basis weights for linerboard and medium in the U.S. and similar international grades (adapted from Steadman 2002) .

Common Basis Weight or *Grammage*			
Linerboard		**Medium**	
U.S. customary (lb./1000ft^2)	Metric System (g/m^2)	U.S. customary (lb./1000ft^2)	Metric System (g/m^2)
26	125	26	125
33	150	28	140
38	175	30	150
42	200	36	175
47	225	40	200
69	339	42	200

Note: Relation between the common basis weights is not equivalent to the mathematical conversion of the units.

2.2.4 Corrugated box styles

In order to be able to identify the different box styles, a collaboration between the European Federation of Corrugated Board Manufacturers (FEFCO) and the European Solid Board Association (ESBO), developed a classification method, assigning numerical codes to the different styles of boxes according to their designs (Fibre Box Association, 2015).

The FEFCO classification groups all box styles in nine basic categories. The first two digits of the four digit FEFCO code represent the different categories while the last two digits identify the specific design with the category (FEFCO-ESBO, 2007). The different categories are 01 - Commercial rolls and sheets; 02 - Slotted-type boxes; 03 - Telescope-type boxes; 04 - Folder-type boxes and trays; 05 - Slide-type boxes, 06 - Rigid-type boxes; 07 - Ready-glued cases, 09 - Interior fitments.

The most common type of box is the Regular Slotted Container (RSC), code 0201. It is made from a single blank of corrugated, and normally, the lengthwise flaps meet at the center when

folded. It is a very efficient design with little material waste when manufacturing (Fibre Box Association, 2015).

Regarding the sizes of the boxes, although any design can be sized as needed to better fit a product, the standard ISO 3394 Packaging - Complete, filled transport packages and unit loads - Dimensions of rigid rectangular packages has been published to facilitate material handling operations by limiting the dimensions of packages to modular sizes, based on the proposed dimensions for pallets, and therefore having better utilization of the available space (ISO, 2012). Three different modules are proposed, 600 mm. x 400 mm., 600 mm. x 500 mm., and 550 mm. x 366 mm., and for each of them, the corresponding pallet sizes. Submultiples of the modules are given for users to make decisions according to their needs.

2.3 Corrugated box performance and testing

The Edge Crush Test (ECT) (TAPPI T 811:2002 Edgewise compressive strength of corrugated fiberboard (short column test), TAPPI T 839:1995 Edgewise compressive strength of corrugated fiberboard using the clamp method (short column test) and ISO 13821:2002 Corrugated fibreboard -- Determination of edgewise crush resistance -- Waxed edge method) is probably the most common and important test performed on corrugated boards. Since the ECT results are used to predict the compression strength of a box (in other words, its performance), these results are commonly used as the main value when specifying corrugated board, instead of grammage or thickness (Twede et al., 2014). The test consists of applying a constant force to a sample of corrugated board that is standing on its edge with its flutes parallel to the force until the board is crushed. The amount of force recorded when the failure occurs, divided by the length of the sample, gives the ECT value (lb.-force/in or kilonewtons/meter).

Using the simplified McKee Formula (1), the ECT value can be used to predict the compression strength of the box (BCT). This formula uses the perimeter of the box and the caliper of the board to estimate the box compression strength (McKee, Ganer, & Wachuta, 1963).

$$BCT = 5.87 * ECT * \sqrt{P * Z} \quad (1)$$

with,

ECT: Edge Compression test (lbf/in.)

P: Perimeter of the box (in).

Z: Caliper of combined corrugated board (in.)

Besides estimating the BCT from the ECT value, testing can also be performed to determine the box compression strength. TAPPI T804:2002 Compression test of fiberboard shipping containers, ISO12048:1994 Complete, filled transport packages – Compression and stacking tests using a compression tester, and ASTM D642:2000 Determining Compressive Resistance of Shipping Containers, Components, and Unit Loads are three testing standards that can be followed. ISO and TAPPI methods follow similar procedures of conditioning and testing. However, the ISO standard is limited to filled packages, while TAPPI T 804:2002 recommends testing empty containers. The ASTM test provides the option of testing containers with floating platens, and in general, tests a wider scope of possibilities for the same types of containers.

Another important performance characteristic of corrugated board is the bursting strength. The testing method for performing this test is the TAPPI T 810:1998 Bursting strength of corrugated and solid fiberboard, which is specifically for single and double wall corrugated fiberboard. After conditioning circular, corrugated test specimens, they are clamped on the edges in the bursting tester and pressure is applied by a piston inflating a diaphragm underneath the sample until it bursts. The pressure level at the moment of bursting is an important measure of board performance.

Flat crush testing (FCT) is a measure of the compression strength of the flutes of a corrugated sample when a force is applied perpendicular to the board surface. TAPPI T808:2001 Flat crush test of corrugated board (flexible beam method) gives a description of this test.

3 Containment Methods

In order to unitize loads and hold them together throughout the distribution process, the transportation industry utilizes many different containment methods. Common load stabilizers are stretch wrapping, stretch hooding, strapping, or the use of tie-sheets, among other alternatives. The quantity used and the force applied depend on the geometry and stability of the unit load itself, but excessive containment force can generate package and product damage.

Current design methodologies for the use of stretch films to build stable unit loads are based on the measurement of the resulting containment force after the application of the film. To generate this force measurement, various methods can be applied, some of which might provide results that are non-comparable with the others (American Society of Testing and Materials (ASTM), 2009). The results of these measurements, although accurate for auditing and quality control purposes, do not directly predict the performance of the unit load in the field. Using an instrumented test pallet from Highlight Industries to measure containment force, Dunno (2017) showed that many of the stretch wrapping configuration values could be changed and still obtain the same containment force. A designer can experiment with different values of film pre-stretch percentages, film stretch percentages on the pallet, number of top wraps, weight of the film, and number of revolutions, and still be able to obtain the same resulting containment force. In the field though, these unit loads will most certainly not perform the same.

Singh, et. al. (2017) approached the evaluation of stability by simulating the transportation hazards through tilt and incline impact tests. Even though valuable data was obtained by correlating these tests to load shift during distribution, no guidance was provided regarding how to improve unit load stability. All Singh's evaluations told us was whether the unit load with that particular containment force survived the simulated tests or not. It is relevant to note that the stability of the unit loads was affected by factors like the stacking pattern of the packages.

Bisha (2008) compared the effect of four load stabilizing methods: stretch hooding, two film gauges of stretch wrap, and strapping. The unit loads were subjected to vibration and inclined impacts. For the vibration tests, the natural frequency and transmissibility were identified. No significant differences were observed between the containment methods used. It is worth noting that the results of transmissibility and natural frequency were averaged for the random vibration tests that were conducted. As for the tests conducted to evaluate the unit load stability during side-impacts, clear differences were observed in the various containment methods' performances, as

measured by load shift. The correlation of the results to the containment force method applied were inconclusive; containment force alone is not a clear indicator of load stability.

Methods have been developed to measure the applied containment force, specifically for stretch wrapping. The standard ASTM D4649-03 Selection and Use of Stretch Wrap Films provides guidelines on measuring and comparing the wrap performance of films, but it measures the containment force only on the faces of a unit load and not at the corners, where higher pressure might exist; therefore, this generates a possible bias. This method performs measurements after applying the film to the unit load, so a trial-and-error process must be followed to reach specific containment forces. Efforts have been conducted in order to develop methods capable of predicting containment forces by following standardized calculations such as using film thickness and pre-stretch levels as inputs, but additional research is required in order to obtain more consistent results (Bisha, 2012).

4 Unit Loads and Components Interactions

Carrying products as unit loads is the most common distribution method, representing over 80% of the loads transported in the United States (Raballand & Aldaz-Carroll, 2007). Benefits from shipping in unit load form include reduction in product damages of up to 80%, when compared to non-palletized loads, and increased handling efficiency; although, space utilization is decreased significantly. Products stacked on standard ISO pallets can see a reduction of the available volume by as much as 30% (Goertz, 1976).

4.1 Unit Load Interactions

When all of the components of the unit loads are placed together, it has been shown that their performance is affected by their interactions with other unit load components. A small change in the stiffness of a pallet can affect the performance of corrugated boxes, or a change in the size of the boxes can affect the bending stiffness of the pallets. These interactions are important to consider when evaluating the performance of unit loads.

4.1.1 Effect of pallets in package performance

Extensive research has been conducted to understand the compression strength of boxes (Frank, Gilgenbach, & Maltenfort, 2010). Most of these studies are limited to specific box design characteristics, and their results are not always easily extrapolated to general use conditions. Popular box compression models such as the one developed by McKee et al.(1963) assumes boxes are mostly supported on flat surfaces. Corrugated boxes, when used in unit loads, are carried by pallets. As a whole unit, the pallets and the corrugated boxes will interact with each other. Each affects the performance of the other when any aspect changes.

To study the interactions between the pallets and the boxes, research has been conducted from different perspectives. Kellicut (1963) studied the effect of gaps between pallet top deck boards and how larger gaps reduce the compression strength of boxes. He concluded that boxes would see a 12-13% reduction in compression strength when stacked on pallets. In addition to these gap effects, boxes can also be stacked so that they overhang the pallet edges. This stacking condition also reduces the boxes' strength since the side panels and certain corners of the box might not be fully supported. Multiple studies can be found about pallet design characteristics and their impact on box compression strength (Baker, Horvath, & White, 2016b; DiSalvo, 1999; Ievans, 1975; Monaghan & Marcondes, 1992).

The stiffness of the pallet can also play a significant role in box performance. Studies have been conducted to determine how a less stiff pallet deck affects the performance of boxes and how to model it (Baker, Horvath, & White, 2016a; Baker, Horvath, White, & Scott, 2018; Quesenberry, Horvath, Bouldin, & White, 2020).

Packages stacked in a unit load are subjected to compression stresses of variable magnitudes. To create an effective package design, these forces must be known. Besides the common factors that determine compressive stresses, such as force applied or the effective bearing area, it has been discovered that in the case of unitized product, the stiffness of the pallet is a significant factor with a direct effect on the bearing area. If the stiffness of the pallets' deck is increased, the deflection of the deck boards is minimized, resulting in an increased effective bearing area, which reduces the compressive stresses on the packages (White, 2015).

4.1.2 Effect of packages on pallet performance (Load Bridging)

Current pallet design techniques assume a uniformly distributed load on the pallets. Laboratory testing based on ASTM D1185 (ASTM International, 2009) is conducted based on the same principle, commonly using airbags as uniform load applicators (Figure 7). But the actual loads being shipped on pallets differ from airbags and often don't distribute the load uniformly. The most common package type used is the corrugated fiberboard box. Based on previous investigations (McKee & Gander, 1957), it is known that when boxes are stacked in a column, most of the load distributes down along the perimeters of the boxes. McKee and Gander also showed that the load often concentrates at the corners of the boxes resulting in an uneven distribution of the load along the boxes' perimeters.

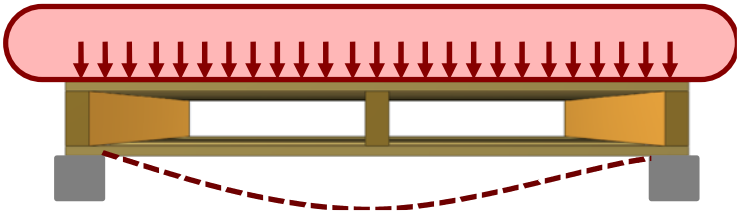

Figure 7. Pallet racked across the width under uniformly distributed loading with an airbag (From Molina, 2017).

In a unitized scenario, when pallet bending is present, the boxes also interact with each other, altering how the load is transferred from the stack of boxes to the pallet. As a result of this interaction, a certain percentage of the compression stresses are redistributed towards the supports, reducing the pallet deflection. This stress redistribution is called the load bridging effect on unit loads. Figure 8 shows a schematic of the experimentally observed unit load interactions and the stress redistribution that is present from the load bridging effect when the pallet is in a racking support condition. This specific behavior has not yet been mathematically characterized.

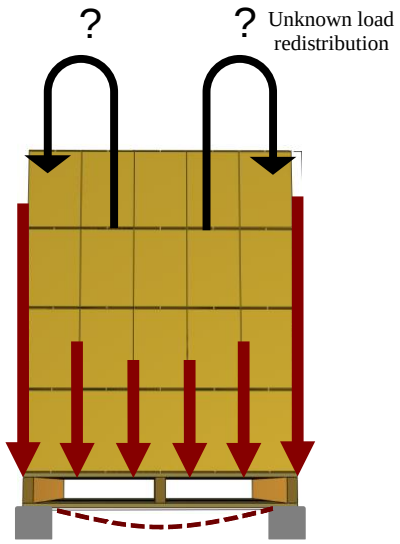

Figure 8. Experimentally observed load redistribution of a four-layer unit load on a racked across the width pallet (From Molina, 2017).

The factors that have been identified as possibly affecting the stiffness of the load, and therefore the load bridging effect, are as follows: package size, the stiffness of the package, the stiffness of the pallet, the containment method and the force applied, the number of layers, the height of the unit load, the friction of each of the contact interactions between the multiple components, and the stacking pattern of the packages (Center for Unit-Load Design, 1997; Collie, 1984; Fagan, 1982; Park, 2015; Park et al., 2017; White et al., 1999; Yoo, 2011).

Fagan (1982) began characterizing the loads, supports, and structural members of unit loads in order to be able to gain an understanding of how the type of load affects pallet performance. In his initial study, the author tested four different load types which were expected to have differing load bridging effects, and he then measured pallet deflection as the main response. The first load type was the uniform load with an airbag (no load-bridging), then a symmetrical box pattern (low load-bridging), next an asymmetrical box pattern (medium load-bridging), and finally the fourth a platen-type load (extreme load-bridging). Each load type was tested on four pallets with different stiffnesses (identified by the average MOE of the components of each pallet) and in two racking directions: racked across the length and racked across the width. Fagan concluded that the deflection of the pallet changes significantly depending on the load type and the stiffness of the pallet. It was hypothesized that the stiffness of the pallet is what drives the magnitude of the effect of the other factors.

Collie (1984) continued investigating the load bridging effect on unit loads. One of the studies that he performed evaluated the effect of stacking patterns and the number of unit loads stacked on top of one another. All of these tests were performed simulating floor stacking. No effect on deflection was identified for different stacking patterns. Adjustment factors were calculated for the effect due to the number of unit loads in the pile.

In additional studies, Collie (1984) worked toward identifying and characterizing the factors causing load-bridging when the unit load is in a racking support condition. For this experiment, five different types of loads were used, each with a different level of expected load bridging. For extreme load bridging, boxed goods that were the same size as half of the pallet were used. Two loads with the same boxes, but arranged in different stacking patterns, were used to estimate medium load bridging. A stiffer load with minimal load bridging was simulated with interlocked bagged goods. Finally, an airbag was used as the control with no load bridging at all. Each type of load was tested on three different types of pallets: low, medium and high stiffness. Each of these combinations was tested in both racking across the width and racking across the length. Pallet deflection was the main response measured during each of these tests. As with Fagan (1982), Collie concluded that load bridging decreases significantly when the stiffness of the pallet increases, making the load bridging effect almost negligible on very stiff pallets. Also, the racking direction was demonstrated to be a critical factor in the amount of load bridging experienced by unit loads. Load bridging is greater during racking spanning the pallets' width because pallets are less stiff in this direction of support. Regarding differences in deflection due to load type, only on the low stiffness pallets was it possible to find any significant variations.

When the size of the package is increased, the load is distributed along fewer points of the pallet, and a higher percentage of the load is directly supported by the supports of the pallet, mainly in a racking support (Collie, 1984). To better understand and model the distribution of stresses on pallet decks, Yoo (2011) developed research relating pallet stress distribution with the theory of a beam on an elastic foundation. It was identified that the compression stresses are higher near the supports and diminish towards the middle of the free span. The magnitude of the stress redistribution depends on the pallet stiffness and the stiffness of the load itself.

In order to quantify the effect of the size of a corrugated box on the performance of a unit load, Park (2017) measured pallet deformation while varying box sizes and flute types. He found that up to a 76% reduction in unit load deflection can be achieved by increasing package

dimensions. Park (2015) conducted an experiment to identify the effect of the containment force of stretch wrap on the load bridging of unit loads. Tests were conducted using two plywood boards as simulated pallets with low and high stiffness, three different package sizes, and three levels of containment force (0 lbs., 30 lbs., and 60 lbs.). The deformation of the simulated pallet was measured, and its deflection was compared to that of the same simulated pallet under a load applied using an airbag. It was concluded that pallet deformation decreases significantly with changes in the size of the box. This shows that an interaction happens when varying box size and containment force. Using a pressure mat it was also identified that the stress distribution on the simulated pallet changes with an increase in containment force. With little-to-no containment force, stresses are more evenly distributed across the pallet, but as the applied containment force increases, the stresses move towards the edges, applying more pressure to the packages and increasing the load bridging effect.

Following a similar methodology to Park, Phanthanousy (2017) studied the effect of the box contents on pallet deflection. It was concluded that for the different contents studied no clear effect in pallet bending was observed. The contents evaluated on these unit loads were boxes filled with free-flowing wooden pellets, boxes containing a chamfered board supporting a metal load that did not contact the box panels, and boxes containing a tightly fit rigid oriented strand board box filled with sand. These findings allowed for the decoupling of the box contents and the study of the load bridging effect, significantly reducing the complexity of factor interactions.

Further research of the load bridging effect on unit loads was conducted by Clayton (2019). In his research, the effect of the box size, as well as the effect of the available headspace inside the corrugated box was studied. Headspace was not previously studied as a factor in the load bridging effect. Six support conditions were studied to evaluate the deflection of stringer pallets. It was concluded that box size has a significant effect on pallet deflection, as it has been confirmed in previous studies. Additionally, a clear redistribution of the stresses on the pallet deck was observed when increasing the dimensions of the packages. These effects were evident for pallets racked across the width but not for the other supports. A similar research project was conducted using block style pallets (Morrissette et al., 2020). This study further confirmed the effect of box size on pallet deflection. Additional testing was conducted to evaluate the effect of package headspace and the effect of differently designed bottom bases of the pallets. Both of these factors did not significantly affect the pallet bending response.

Limited research has been conducted with the objective of determining the effect of stacking patterns on pallet deflection and ultimate load-carrying capacity. The load configuration, which is affected by the specifications of the stacking patterns, leads to significant changes in the bending behavior of the pallet.

Fagan (1982) and Collie (1984) conducted investigations where different load configurations were evaluated. A clear relationship trend between load characteristics and pallet bending was found, but no specific evaluations were conducted to measure the effect of the stacking patterns by themselves. White *et al.* (1999) also evaluated the effect of the application of different load stabilizers on pallet deflection. They looked at this effect on different stacking patterns including a comparison of column versus interlock stacking. Their results identified that load stabilizers had a significant effect on pallet deflection, but no conclusive results were obtained.

In general, it can be said that different stacking patterns modify the pressure distribution of the load on the pallet, and therefore they change the performance of the pallet. However, no specific knowledge is available regarding the exact effect of stacking patterns. Identifying simple alternatives that improve the performance of a unit load can translate into cost and material reductions and a more efficient supply chain.

Molina (2018) investigated the effect of the stacking patterns of the packages on pallet deflection. Research was conducted to account for different support conditions and three stringer pallets of different stiffnesses. Overall, five different pallet stacking patterns were investigated, ranging from a column stacking pattern to a fully interlocked stacking pattern. It was concluded that the interlocking of the packages increases the stiffness of the payload and reduces significantly pallet deflection.

The studies by Molina et al., Clayton et al., and Morrissette et al. compared pallet performance for different support conditions, including different combinations of warehouse racking across the width, warehouse racking across the length, floor stacking with single and double stacks, and supporting the unit loads on forklift tines. For all studies, warehouse racking presented the highest pallet deflection, with racking across the width being the support condition that limited pallet performance the most.

Throughout the different research projects, there has been a commonly observed correlation where the load bridging effect is present in lower stiffness pallets but not so on more

rigid structures. Molina hypothesized about the possibility of a relationship between the load level being carried and the pallet carrying capacity. If the load carried is close or even higher than the safe carrying capacity, the pallet will present large bending and therefore load bridging will be observable. If a pallet carries a load that is much lower than its maximum carrying capacity, the pallet will present low or negligible bending. Given the low bending present, the load bridging effect will not be possible to measure with the current testing techniques. If the load level is increased, load bridging might become evident and a stiff pallet will still present load bridging. Accuracy of the measurements would play a key role in identifying the load bridging effect.

4.2 Unit Load Design and Modeling

The packaging supply chain is composed of three main components: packages, such as bags, boxes, pails, etc.; the pallet itself, which works as a platform to support the product and allow for efficient handling; and the handling equipment. Typically, these components have been designed as isolated units with the goal of reducing the cost of each individual component. This approach commonly ignores the fact that when any of the components change, the performance of the other components is influenced (White & Hamner, 2005). This component-based design methodology can generate an increase in the cost of the overall supply chain. For example, reducing pallet costs could result in lower pallet stiffness, but as a consequence, higher compression stresses are applied to the corrugated containers, possibly damaging them and, in the end, increasing overall costs. To eliminate the above mentioned issues in the supply chain, White and Hamner (2005) proposed using a “System-based Design Methodology”, where every component is designed taking into consideration the interaction between all of the different elements. The result of this system-based design methodology is reduced overall costs for final consumers, reduction in the environmental impact of logistics, and higher human health and safety levels due to better-performing unit loads.

5 The Finite Element Method

5.1 Introduction and history to the Finite Element Analysis

The finite element method (FEM), also known as finite element analysis (FEA) is a numerical method that can be used to solve boundary value problems (BVP). These are problems where the differential equation is limited by boundary conditions, represented as a set of additional constraints. FEA is a method commonly used to solve field problems, such as heat transfer, solid mechanics, acoustics, magnetic fields, and more (Cook, Malkus, Plesha, & Witt, 2001). The Finite Element Analysis deals with the approximation of the solutions to partial differential equations (PDE) boundary value problems, but instead of solving over continuous domains through the assembly of continuum elements, it solves boundary value problems of ordinary differential equations (ODE) over discrete structures, through the assembly of structural elements, in the form of matrix structural analysis. The discretization of the structures, called meshing, simplifies the mathematical complexity and allows for a numerical approximation solution to be obtained.

FEM's advantages over other numerical analysis methods include its wide range of applications and the few-to-no restrictions regarding possible geometries, materials, and boundary conditions that can be modeled.

The earliest developments of the FE method, as it's currently known, are traced back to a paper published in 1943, where the torsional rigidity of a hollow shaft was determined by dividing its cross section into triangles and then interpolating a stress function over each triangle from the values at the nodes (Cook et al., 2001). Apparently, without direct knowledge of the FE solution, aerospace engineers in the 1950s developed the Matrix Structural Analysis by also applying a discrete mesh over a continuous domain, for which each sub-domain was called an element.

The technique was rapidly developed in the 1950s through multiple, independent accomplishments, commonly by engineers helped out by intuition and physical arguments. The term "finite element" was first used in 1960 (Cook et al., 2001). FEA became a respectable method in academia when, in 1963, it was recognized as a form of the Raleigh-Ritz method, a classical approximation technique. With this proof of convergence, FEA went from a trick used for stress analysis to a widely valid method having a solid mathematical foundation. Given that FEA approaches solutions through discretization, computational requirements are extensive, and the use of computer power is therefore mandatory for finding the solutions in practical applications. The

popularity of FE increased exponentially along with the computing power available to solve structural analysis problems.

5.2 General steps of the Finite Element Method

On a conceptual basis, following the outline of a finite element analysis project as proposed by Cook et al. (2001), the first step when solving field problems through finite element analysis must always be to establish a clear definition and understanding of the physical problem that is to be solved. It is in this stage that a mathematical approximation can be obtained if possible. The success of finite element analysis is tied to it appropriately representing the physical domain. Once the structure is represented correctly, it can be divided into subdomains, or 'finite 'elements', through the use of discretization methods. For larger projects, the next phase will involve the use of computer software to generate and assemble the equations that explain the field variable displacements at each one of the nodes. Loading and boundary conditions in the model are represented through nodal forces and displacements. Once the model is properly represented and then solved, the next major step is postprocessing the results. This is where the analyst must determine the validity of the results obtained. The accuracy of the simulation will depend on multiple factors, such as how well the element types selected represent the displacement fields being simulated. Other factors include the mesh selected, that is, the number and distribution of the elements used, proper identification and representation of the materials behavior, the boundary conditions, and the applied loads. Figure 9 represents an outline of a common workflow for a finite element analysis project.

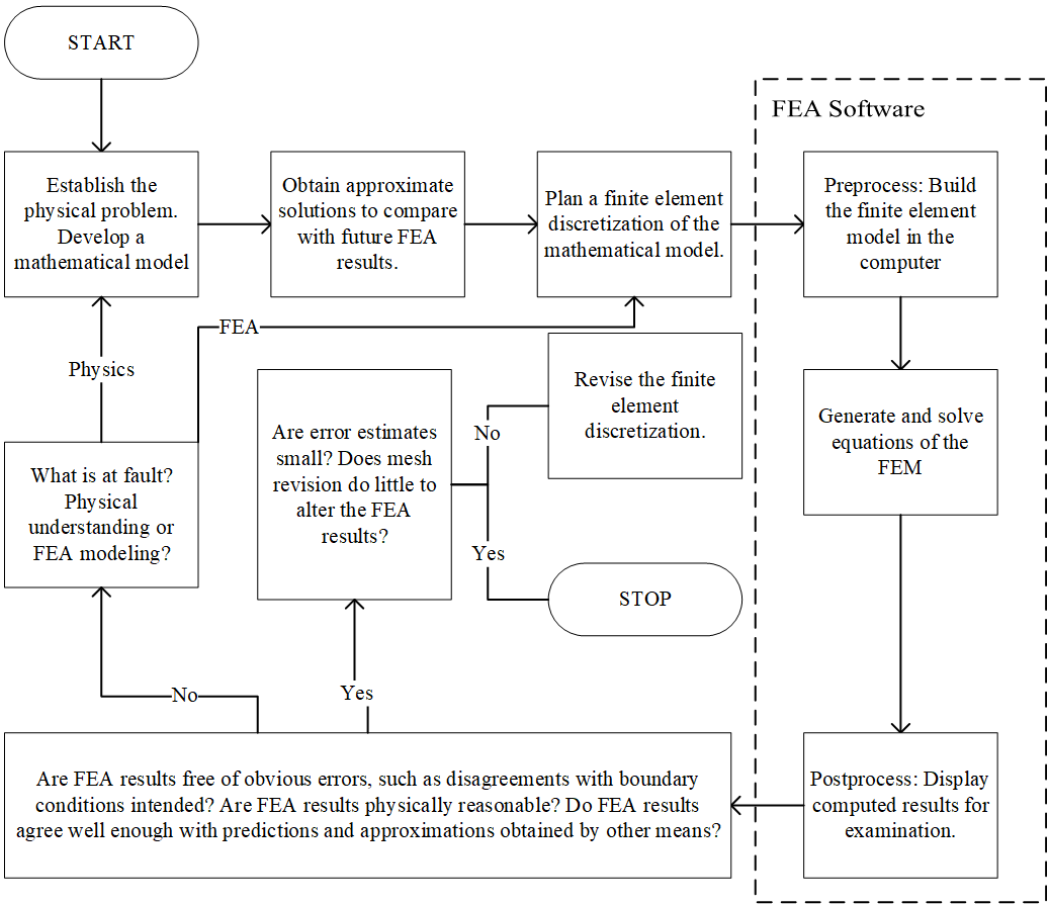

Figure 9. Outline of a finite element analysis project (Adapted from Cook et al., 2001).

5.2.1 Basics of Finite Element Simulations

Real-world problems usually contain enough significant complexity to be solved through analytical methods, especially when including nonlinearities and dynamic effects. The finite element method divides the bodies involved in the problem into small and geometrically simple bodies with specific shapes, called elements. These elements have finite sizes, hence the name "Finite Element Analysis". Instead of approaching a solution for the complete problem, equilibrium equations for each element are defined and then solved simultaneously.

At the vertices and edges of each element, there are nodes that connect the elements. In FEA, the method used to achieve results is to solve for the unknown displacements at each of the nodes, given that they are discrete values and not a field. The nodal displacement components fully define the response of a structure and as such, are known as the degrees of freedom (DOFs) and represented by a vector *{D}*.

To solve any FE problem, one must identify the nodal coordinates, the material properties, and the loading conditions. Then, one must assemble together all the individual equations in the system of equilibrium equations. In static analysis, (2) shows the system of equilibrium equations:

$$[K]\{D\} = \{F\} \tag{2}$$

where *{F}* is the vector of external forces acting upon the nodes as determined by the environmental conditions. The size of the system of equations is determined by the degrees of freedom. For a two-dimensional analysis, there are two degrees of freedom for every node. The stiffness matrix, $[K]$ can be explained using a common analogy with the one-dimensional spring analysis. Assuming that the stiffness matrix $[K]$ is the spring constant, k, the vector $\{F\}$ is the external force applied to the spring, then to solve the equilibrium $F = kx$, one must solve for x, or the displacement $\{D\}$ by inverting the equation. The same process must be conducted for finite element analyses. The stiffness matrix $[K]$ can also be understood as the values on its ith column are the forces required on all the of the DOFs to make the ith DOF move a unit displacement while preventing the other DOFs from any displacement.

While $[K]$ is a constant matrix for linear structures, it is a function of $\{D\}$ for nonlinear analyses. When dynamic cases need to be considered in the problems, those additional dynamic effects must be added into the equilibrium equations. A general model for dynamic, multi-degrees of freedom systems is generalized in (3) for a transient structural simulation.

$$[M]\{\ddot{D}\} + [C]\{\dot{D}\} + [K]\{D\} = \{F\} \tag{3}$$

Similar to the static linear analysis equation, the nodal displacement vector is represented by $\{D\}$., $\{F\}$ is the vector with the nodal external forces, and $[K]$ is the stiffness matrix. Additional components are added by the mass matrix $[M]$ and the damping matrix $[C]$. As previously done, this can be analyzed as a force equilibrium relation, with the external forces $\{F\}$ in the right-hand side and the left-hand side contains the *inertia forces* $[M]\{\ddot{D}\}$, *damping forces* $[C]\{\dot{D}\}$, and the *elastic force*s $[K]\{D\}$.

After obtaining the discrete nodal displacements $\{D\}$, the following step is to calculate the actual displacement fields $\{u\}$. For this, the nodal displacements must be interpolated, either using linear or quadratic functions. To obtain these displacement fields, (4) needs to be solved.

$$\{u\} = [N]\{d\} \tag{4}$$

Where $\{d\}$ are the individual components of the displacements at each node for each element. These interpolating functions establish a relationship between the displacement fields and the nodal displacements and are called shape functions. $[N]$ is the matrix of shape functions. Since the components of the nodal displacements, $\{d\}$, are discrete values and the components of displacements fields, $\{u\}$, are continuous functions of (X, Y, Z), the shape functions, $[N]$, work as a bridge between them and must contain functions of (X, Y, Z).

In a two-dimensional scenario, an element has a triangular or quadrilateral geometry and when it only has nodes at the vertices, the shape function must be linear. In this case, a linear function can accurately predict the linear displacement between the nodes. It is then capable of replicating the actual problem being solved. Such an element is called a linear element, first-order element, or lower-order element. If the characteristics of the problem so require, the element can be defined with a node in the middle of each of the edges, allowing for a quadratic polynomial to be the shape function. These elements are called quadratic elements, second-order elements, or higher-order elements (Cook et al., 2001; Lee, 2017).

5.2.2 Finite Element Discretization (Meshing)

After having established a physical model and calculated approximate solutions with the developed mathematical model when possible, one must plan the finite element discretization of the model. For this phase, the body to be analyzed is divided into a system of finite elements that is equivalent to the physical model to be studied. The analyst needs to decide what shape and size these subdomains will have. In general, the elements need to provide a balance between accurate results and computational complexity. Smaller and higher order elements might not provide any incremental benefits in the model results, but might increase exponentially the computing time (Logan, 2007).

A technique commonly utilized to determine if the mesh must be further refined is a convergency study. For this, the main result variable, such as principal stress or deformation is plotted against each iteration of a smaller mesh. When the variable does not change significantly anymore, it is considered to have converged. Any further refinements in the mesh will increase the computing requirements without increasing the accuracy of the results (Chang, 2006).

Aside from the element seed size, the analyst must select the right element type for a successful and accurate simulation of the problem at hand. The element will be defined by the shape and the order. Possible element shapes depend, first, on the dimension of the model. One-dimensional problems will use lines, and elements in two-dimensional simulations will be triangular or quadrilateral. Additional element shapes are shown in Figure 10.

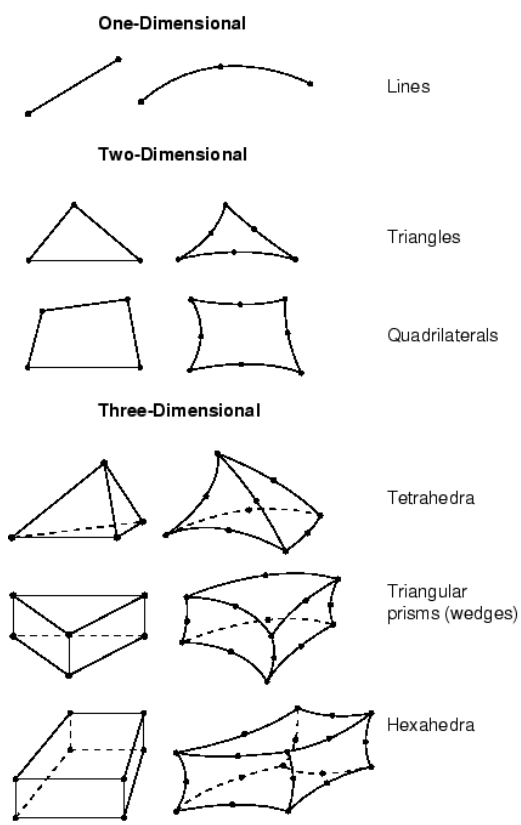

Figure 10. Element shapes for finite element models (From Dassault Systems, 2018).

5.2.3 Frictional Contacts in Finite Element Analysis

An important factor to study is how frictional contacts are defined and formulated when using the finite element method. The simple but powerful and empirically accurate Coulomb

Friction Model relates the maximum allowable frictional stress (shear stress) across an interface to the pressure of the contact between the bodies. In general, it establishes that two surfaces in contact are in the 'sticking' state when they can carry shear stresses up to a certain magnitude across their interface. After that point, they will start sliding relative to each other. The critical shear stress, τ_{crit}, is that at which the sliding of the surfaces begins as a fraction of the contact pressure, ρ, between the surfaces. Figure 11 shows graphically the critical shear stress as a function of contact pressure and equivalent shear stress. (5) defines the critical shear stress to pass the stick region to the sliding state (Dassault Systems, 2018). Given the characteristics of friction, it is modeled as a nonlinear effect in finite element modeling.

$$\tau_{crit} = \mu\rho \tag{5}$$

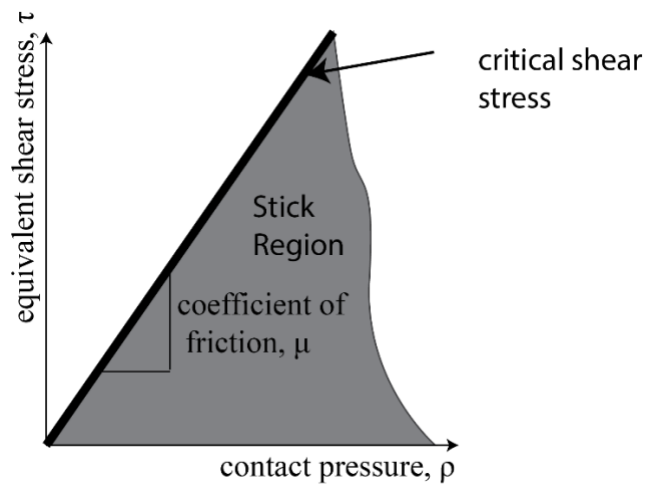

Figure 11. Coulomb model for friction and the identification of the critical shear stress (Adapted from Dassault Systems, 2018).

5.3 Finite element method applications in packaging science

Given the advantages obtained through the use of finite element modeling, multiple scientific areas have applied it extensively. The applications in packaging science, including structural analysis and material development, have increased significantly.

5.3.1 Study and FE modeling of packaging materials

5.3.1.1 Wood

Extensive research has been conducted in the application of finite element models for wood-based solutions in different areas. A review conducted by Mackerle (2005) covered over 300 different studies between 1995 and 2004. These studies and conference proceedings included a wide range of topics covering the use of wood as a construction material and FE models to simulate the performance of wood products and structures.

5.3.1.2 Corrugated Fiberboard

On the topic of generating models to study different performance factors affecting corrugated fiberboard, one can find research focused on the material performance in relation to structural support, heat dissipation, and the effects of environmental conditions, among others. Zhang et al. (2014) studied the effect of changing design elements, such as the number of flutes, height of flutes, and angle of the arcs of flutes on compression resistance, by applying static and dynamic pressure. This FE model utilized available literature for the material definitions of the board, and no experimental validations were conducted.

Dynamic models to study the design of corrugated boards and cushioning foams have also been developed. A finite element simulation was developed by Hammoum et al. (2012) to study the shock response from free fall drops, utilizing ABAQUS, and verifying the results with the measurement of accelerations on the simulated package. The model was considered accurate, and emphasis is made on the fact that the corrugated board has an effect on the cushioning properties of the protective packaging; therefore, it can’t be ignored in the simulation.

One field where the finite element analysis has already been applied extensively is in food packaging development utilizing corrugated board. The complexity of the material and its geometrical nonlinearities, as well as the effect of environmental conditions and additional factors, make it a difficult endeavor to simulate (Fadiji et al., 2018).

5.3.1.3 Paperboard

Nygårds et al. (2019) developed a general framework for the use of FEA to simulate paperboard packages, with the objective of improving the design process, without requiring expensive mill trials. Two simulations and validations were conducted. First, a simulated drop test was conducted. In order to reliably produce controllable shocks to the package, it was impacted by a hydraulic piston from the bottom instead of actually being dropped. The second test consisted of top-to-bottom compression of the gable top package being used. Continuum shell elements were used to define the material properties in the finite element simulation. Simulations were conducted for empty packages and ones filled with plastic granulates, simulated with discrete element sphere particles (DES). For the compression simulation, a pre-stress evaluation was conducted in the FE model in order to be able to simulate actual deformations; otherwise, the deformations wouldn't match experimental observations. As for the experimental validations conducted, the dynamic model is limited to a visual inspection and approximations of the tested samples versus the contour plots of the maximum principal stresses in the simulation. For the compression models, force-displacement was plotted for both the experiments and the simulations. There was no agreement in the initial deformation of the package, but the plots trended towards the same values of load-deflection after that initial deformation was experienced. In the simulations, significantly lower compression forces were required to achieve the same deformations as in the experimental tests. The loading history of folded edges was mentioned as a possible source of the discrepancies in the tests. Figure 12 shows the plotted results from this research.

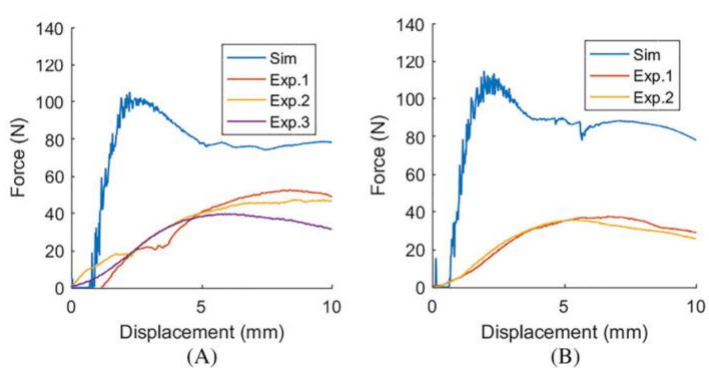

Figure 12. Comparison of compression force and deformation between experimental setups and Finite Element simulations for a paperboard gable top package. Source: (Nygårds et al., 2019).

Zaheer et al. (2018) developed a model to study the performance of paperboard boxes under compression. Paperboard was modeled as an orthotropic elastic material, and the effect of creases was also studied in the FEA model. No experimental validation of the simulation results was conducted.

5.3.1.4 Other containers

Multiple other research studies and applied projects have been conducted and published in order to improve on the design process of packaging containers made from different materials and for various uses. Finite element simulations can be used in conjunction with other design optimization techniques. Wang, et al. (2012) applied behavioral modeling techniques in order to optimize a bottle design of a specific required volume. Then, he studied the internal stresses of the container under compressing loads.

5.4 Finite element method research and applications in pallets and unit loads

The use of finite element analysis has become commonplace in the design process of many pallets for material handling. Wooden pallets can be designed using commercial software already available (see Section 1.3), which are mostly based on finite element models (Modern Material Handling, 2012). Multiple studies can be found in literature to evaluate new pallet designs or designs using innovative materials. The application of finite element models allows for the preliminary evaluation of these new pallets' performance. The technique has been applied to the development of pallets for many different uses.

Mohammed and Baig (2018) developed an optimized pallet model using finite element analysis with the software Solidworks and ANSYS. Waseem et al. (2013) conducted simulation of a pallet design built with five different materials and evaluated their resulting stiffness and strength. Other studies conducted using finite element analysis for pallet design include the development of a pallet made of recycled plastics. This pallet was modeled using the material as high density polyethylene (HDPE)(Kung, Chen, Liao, & Chou, 2012). Masood and Rizvi (2006) focused on the performance of current pallet designs in cold room applications. Five different pallet designs and materials were evaluated with the finite element models developed.

A significant factor in pallet design is how different payloads affect the distribution of compressive stresses across the pallet top deck boards, and ultimately, overall pallet performance. This is part of the load bridging effect previously discussed (See Section 4). Han, White and Hamner (2007) applied the finite element method to better understand and explain this effect on unit loads stacked on the floor of a warehouse. Using a simulated section of a pallet, composed of a single bottom deckboard, two equivalent stringer sections and a top deck board made out of acrylic, they studied non-uniform load applications from rigid packages. This was experimentally simulated by a rigid, metal load applicator and a corrugated board medium between the pallet and the load. Experimental verification was conducted using a pressure sensitive film to measure pallet deflection. The finite element model was developed for the different joint methods studied. The overall finite element solution provided results in close agreement with the experimental measurements. This confirmed that there is non-uniform pressure distribution when a deck board is under load from a discrete payload.

Additional studies were conducted to further characterize the load redistribution on pallet top decks and to understand the resulting pallet deformation (Yoo, 2008). Following a similar experimental setup as Han (2007), Yoo applied the load utilizing different foams and products like flour bags to simulate non-rigid payloads with different characteristics. The results of the racking simulations show a clear correlation between the rigidity of a load and pallet deflection. The results also showed that, when analyzing the rate of change in pallets' deflection while carrying different package stiffnesses, the pallets' stiffness does not seem to have any effect, even though the absolute deflection is evidently different.

Besides the static interactions of loaded pallets, studies can be found on the dynamic interactions of pallets, containers, and products during transportation. During handling, the unit loads are under different dynamic vibration events. Weigel (2001) studied the resonant response of the unit loads to vibration frequencies. For this, a computer model was developed using finite element analysis in order to predict the resonant frequencies at which those vibrations will be magnified in the unit loads. The model allowed designers to understand the effect of different unit load design decisions on the vibratory responses of the load. This is especially critical for products sensitive to damage from repetitive minor impacts, like fresh fruit.

6 References

American Society of Testing and Materials (ASTM). (2009). ASTM D4649-03 - Standard Guide For Selection and Use of Stretch Wrap Films (pp. 1–11). pp. 1–11. West Conshohocken, PA.

ASTM International. (2009). ASTM D1185-98a(2009) Standard test methods for pallets and related structures employed in materials handling and shipping. https://doi.org/10.1520/D1185-98AR09

Baker, M., Horvath, L., & White, M. (2016a). Effect of Pallet Deckboard Stiffness on Corrugated Box Compression Strength. Packaging Technology and Science, 29(4–5), 263–274. https://doi.org/10.1002/pts.2201

Baker, M., Horvath, L., & White, M. S. (2016b). Predicting the effect of gaps between pallet deckboards on the compression strength of corrugated boxes. Journal of Applied Packaging Research, 8(3), 30–42. https://doi.org/10.14448/japr.08.0017

Baker, M., Horvath, L., White, M. S., & Scott, M. (2018). Application of beam on elastic foundation to the interaction between a corrugated box and pallet deckboard. Packaging Technology and Science, 31(5), 377–385. https://doi.org/10.1002/pts.2338

Bisha, J. V. (2008). The effect of load stabilizer selection on load shift within unit loads (Master's Thesis). Virginia Polytechnic Institute and State University, Blacksburg, VA.

Bisha, J. V. (2012). Correlation of the elastic properties of stretch film on unit load containment. Virginia Polytechnic Institute and State University, Blacksburg, VA.

Bush, R. J., & Araman, P. A. (2014). Trends in the use of wood products for distribution packaging - Cooperative Agreement No. 11-CA11330142-137. Blacksburg, VA.

Center for Unit-Load Design. (1997). The effect of load bridging on unit-load deflection. In Research Update. Blacksburg, VA.

Chang, H. (2006). Seven techniques for finding FEA Errors. The Journal of Virtual Product Development, 1–5. Retrieved from https://www.mscsoftware.com/Submitted-Content/Resources/alpha-vol8-jun2006.pdf

Clarke, J. (2004). Pallets 101 : Industry overview and wood , plastic , paper & metal options. Retrieved from ISTA.org website: http://www.ista.org/forms/Pallets_101-Clarke_2004.pdf

Clayton, A. P., Horvath, L., Bouldin, J., & Gething, B. (2019). Investigation of the effect of column stacked corrugated boxes on load bridging using partial four-way stringer class wooden pallets. Packaging Technology and Science, 32(9), 423–439. https://doi.org/10.1002/pts.2438

Collie, S. T. (1984). Laboratory verification of pallet design procedures (Master's Thesis). Virginia Polytechnic Institute and State University, Blacksburg, VA.

Cook, R. D., Malkus, D. S., Plesha, M. E., & Witt, R. J. (2001). Concepts and applications of finite element analysis (4th ed.). Madison, WI: John Wiley & Sons, Ltd.

Dassault Systems. (2018). Dassault Systèmes 2018 SIMULIA User Assistance (Abaqus CAE). Retrieved March 2, 2019, from https://help.3ds.com

Dekker, A. (2013). Corrugated fibreboard packaging. In M. J. Kirwan (Ed.), Handbook of Paper and Paperboard Packaging Technology (2nd ed., pp. 313–339). https://doi.org/10.1002/9781118470930

DiSalvo, M. H. (1999). Interactive effects of palletizing factors on fiberboard packing strength (Master's Thesis). San Jose State University, San Jose, CA.

Djilali Hammou, A., Minh Duong, P. T., Abbès, B., Makhlouf, M., & Guo, Y.-Q. (2012). Finite-element simulation with a homogenization model and experimental study of free drop tests of corrugated cardboard packaging. Mechanics & Industry, 13(3), 175–184. https://doi.org/10.1051/meca/2012013

Dunno, K. D., Wyns, J., & Cook, J. (2017). Evaluation of Containment Force Variability between Different Grades of Stretch Film. International Journal of Advanced Packaging Technology, 5(1), 267–274. https://doi.org/10.23953/cloud.ijapt.318

Fadiji, T., Coetzee, C. J., Berry, T. M., Ambaw, A., & Opara, U. L. (2018). The efficacy of finite element analysis (FEA) as a design tool for food packaging: A review. Biosystems Engineering, 174, 20–40. https://doi.org/10.1016/j.biosystemseng.2018.06.015

Fagan, B. (1982). Load-support conditions and computerized test apparatus for wood pallets (Master's Thesis). Virginia Polytechnic Institute and State University, Blacksburg, VA.

FEFCO-ESBO. (2007). International fibreboard case code (Vol. 1, pp. 1–8). Vol. 1, pp. 1–8. https://doi.org/10.1017/CBO9781107415324.004

Fibre Box Association. (2015). Fibre Box Handbook (22nd ed.). Elk Grove Village, IL.

Foster, G. A. (2010). Boxes, Corrugated. In K. L. Yam (Ed.), The Wiley Encyclopedia of Packaging Technology (3rd., pp. 162–170). New York: John Wiley & Sons, Ltd.

Frank, B., Gilgenbach, M., & Maltenfort, M. (2010). Compression testing to simulate real-world stresses. Packaging Technology and Science, 23(5), 275–282. https://doi.org/10.1002/pts.898

Gerber, N., Horvath, L., Araman, P., & Gething, B. (2020). Investigation of New and Recovered Wood Shipping Platforms in the United States. BioResources, 15(2), 2818–2838. https://doi.org/10.15376/biores.15.2.2818-2838

Goertz, J. (1976). Unitization in Distribution. In P. M. Van Buytenen (Ed.), Business Logistics (pp. 200–217). Belgium: H.E. Stenfert Kroese B.V.

Han, J., White, M., & Hamner, P. (2007). Development of a Finite Element Model of Pallet Deformation and Compressive Stresses on Packaging within Pallet Loads. Journal of Applied Packaging Research, 1(3), 149–162.

Heebink, T. B. (1959). Load-carrying capacity of deckboards for general purpose pallets Report No. 2153. Madison, WI.

Howie, A. (2008). Fundamentals of Warehousing and Distribution (1st ed.). Charlotte, NC: Material Handling Institute of America.

Ievans, U. I. (1975). The effect of warehouse mishandling and stacking patterns on the compression strength of corrugated boxes. TAPPI Journal, 58(8), 108–111.

ISO. (2003). ISO 6780:2003(E) Flat pallets for intercontinental materials handling - Principal dimensions and tolerances (pp. 1–12). pp. 1–12. Geneva.

ISO. (2011). ISO 8611-1:2011(E) Pallets for materials handling — Flat pallets. Geneva, Switzerland.

ISO. (2012). ISO 3394:2012 Packaging - Complete, filled transport packages and unit loads - Dimensions of rigid rectangular packages. Geneva, Switzerland.

Kellicut, K. Q. (1963). Effect of contents and load bearing surface on compressive strength and stacking life of corrugated containers. Tappi, 46(1), 151A-154 A.

Koning, J. W. (1983). Corrugated Fiberboard. In R. E. Mark (Ed.), Handbook of Physical and Mechanical Testing of Paper and Paperboard (pp. 385–408). New York: Marcel Dekker, Inc.

Kung, C., Chen, S. Y., Liao, T. T., & Chou, T. M. (2012). Finite element modeling to a pallet with repeated lattice pattern. Applied Mechanics and Materials, 145, 88–92. https://doi.org/10.4028/www.scientific.net/AMM.145.88

Kyokong, B. (1979). The development of a model of the mechanical behavior of wooden pallets (PhD dissertation). Virginia Tech.

LeBlanc, R., & Richardson, S. (2003). Pallets: A North American perspective (1ed.). Ontario, Canada, Canada: PACTS Management Inc.

Lee, H.-H. (2017). Finite Element Simulations with ANSYS Workbench 17 (1st ed.). Mission, KS: SDC Publications.

Loferski, J. R. (1985). A Reliability Based Design Procedure for Wood Pallets (PhD Dissertation). Virginia Tech.

Logan, D. L. (2007). A first course in the finite element method. In Finite Elements in Analysis and Design (4th ed., Vol. 3). https://doi.org/10.1016/0168-874x(87)90008-4

Mackerle, J. (2005). Finite element analyses in wood research: a bibliography. Wood Science and Technology, 39(7), 579–600. https://doi.org/10.1007/s00226-005-0026-9

Maltenfort, G. G. (1988). Corrugated Shipping Containers. New York: Jelmar Publishing Co., Inc.

Masood, S. H., & Rizvi, S. H. (2006). An investigation of pallet design using alternative materials for cold room applications. Int J Adv Manuf Technol, 29, 1–8. https://doi.org/10.1007/s00170-004-2485-9

Masters, N. (2018). Pallet & Skid Rental in the US.

McCrea, B. (2016). Pallet usage report: Pallets remain critical in the modern-day warehouse. Retrieved March 6, 2017, from Modern Materials Handling website: http://www.mmh.com/article/pallets_remain_critical_in_the_modern_day_warehouse

McGinley, D. (2019). Wood Pallets & Skids Production in the US. Melbourne, Australia.

McKee, R. C., & Gander, J. W. (1957). Top-load compression. TAPPI, 40(1), 57–64.

McKee, R. C., Ganer, J. W., & Wachuta, J. R. (1963). Compression strenght formula for corrugated boxes. In G. G. Maltenfort (Ed.), Performance and Evaluation of Shipping Containers (1st ed., pp. 62–73). New York: Jelmar Publishing Co., Inc.

MH1 Committee. (2016). MH1-2016 Pallets, Slip Sheets, and Other Bases for Unit Loads. Charlotte, NC: MH1 Secretariat.

Modern Material Handling. (2012). Pallet design and analysis software tool released. Retrieved from Supply Chain Management Review website: https://www.scmr.com/article/pallet_design_and_analysis_software_tool_released

Mohammed, M., & Baig, A. (2018). Designing novel grooved pallets for industrial application (Master's Thesis). Cleveland State University.

Molina, E. (2017). Investigation of pallet stacking pattern on unit load bridging. Virginia Tech.

Molina, E., Horvath, L., & White, M. S. (2018). Investigation of pallet stacking pattern on unit load bridging. Packaging Technology and Science, 31(10), 653–663. https://doi.org/10.1002/pts.2406

Monaghan, J., & Marcondes, J. (1992). Technical notes: Overhang and pallet gap effects on the performance of corrugated fiberboard boxes. Transactions of the ASAE, 35(6), 1945–1947. https://doi.org/10.13031/2013.28820

Morrissette, S. M., Horvath, L., & DeLack, K. (2020). Investigation into the load bridging effect for block class pallets as a function of package size and pallet stiffness. Packaging Technology and Science, 1–19. https://doi.org/10.1002/pts.2539

National Wooden Pallet and Container Association. (2014). Uniform standard for wood pallets. Retrieved from www.palletcentral.com

Nygårds, M., Sjökvist, S., Marin, G., & Sundström, J. (2019). Simulation and experimental verification of a drop test and compression test of a gable top package. Packaging Technology and Science, (March), 1–9. https://doi.org/10.1002/pts.2441

Park, J. (2015). Investigation of fundamental relationships to improve the sustainability of unit loads (Ph.D. Dissertation). Virginia Polytechnic Institute and State University.

Park, J., Horvath, L., White, M. S., Phanthanousy, S., Araman, P., & Bush, R. J. (2017). The influence of package size and flute type of corrugated boxes on load bridging in unit loads. Packaging Technology and Science, 30(1–2), 33–43. https://doi.org/10.1002/pts.2279

Phanthanousy, S. (2017). The Effect of the Stiffness of Unit Load Components on Pallet Deflection and Box Compression Strength. Retrieved from https://vtechworks.lib.vt.edu/handle/10919/86203

Quesenberry, C., Horvath, L., Bouldin, J., & White, M. S. (2020). The effect of pallet top deck stiffness on the compression strength of asymmetrically supported corrugated boxes. Packaging Technology and Science, (July), 1–12. https://doi.org/10.1002/pts.2533

Raballand, G., & Aldaz-Carroll, E. (2007). How do differing standards increase trade costs? The case of pallets. The World Economy, 30(4), 685–702. https://doi.org/10.1111/j.1467-9701.2007.01009.x

Research and Markets. (2019, June). Pallet Market: Global Industry Trends, Share, Size, Growth, Opportunity and Forecast 2019-2024. Research and Markets.

Samarasinghe, S. (1987). Predicting rotation modulus for block pallet joints (Master's Thesis). Virginia Tech, Blacksburg, VA.

Singh, J., Sewell, T., Newton, L., & Saha, K. (2017). Evaluation of Stability of Unit Loads for Tilt and Shock Events During Distribution. Journal of Applied Packaging Research, 9(3). Retrieved from https://scholarworks.rit.edu/cgi/viewcontent.cgi?article=1102&context=japr

Steadman, R. (2002). Corrugated Board. In R. E. Mark, C. C. Habeger, J. Borch, & M. B. Lyne (Eds.), Handbook of Physical Testing of Paper (2nd ed., pp. 563–660). New York.

The Freedonia Group. (2008). Pallets - Industry Study 2359. Retrieved from http://www.freedoniagroup.com/brochure/33xx/3314smwe.pdf

Twede, D. (2007). The History of Corrugated Fiberboard Shipping Containers. CHARM, 241–246. Retrieved from http://learn.quinnipiac.edu/charm/CHARM proceedings/CHARM article archive pdf format/Volume 13 2007/249-254-twede.pdf

Twede, D., Selke, S. E. M., Kamdem, D.-P., & Shires, D. (2014). Cartons, crates and corrugated board: handbook of paper and wood packaging technology (2nd.). DEStech Publications, Inc.

Urbanik, T. J. (1985). Deckboard bending theory for 3-stringer wood pallets in drive-in racks. Journal of Testing and Evaluation, 13(1), 3–8. https://doi.org/10.1520/JTE10754J

Wallin, W. B. (1979). Analysis for Safe Load and Deflection for Wooden Pallets and Related Structures. Princeton, West Virginia.

Wang, M., Zhao, R. L., & Li, K. T. (2012). Application of the Behavioral Modeling Technique to Structure Optimization in Packaging Container Design. Applied Mechanics and Materials, 200, 592–596. https://doi.org/10.4028/www.scientific.net/AMM.200.592

Waseem, A., Nawaz, A., Munir, N., Islam, B., & Noor, S. (2013). Comparative analysis of different materials for pallet design using ANSYS. International Journal of Mechanical and Mechatronics Engineering, 13(2), 26–32.

Weigel, T. G. (2001). Modeling the Dynamic Interactions between Wood Pallets and Corrugated Containers during Resonance (Ph.D. Dissertation). Virginia Tech.

White, M. S. (2015). The Effect of Pallet Deck Design on Package Compression. ISTA TransPack Forum. Retrieved from http://www.whiteandcompany.net/news-events/PackageCompression.pdf

White, M. S., Dibling, W., Rupert, R., & Mcleod, J. (1999). Determining pallet maximum working loads from nominal load measurements. Blacksburg, VA.

White, M. S., & Hamner, P. (2005). Pallets move the world: the case for developing system-based designs for unit loads. Forest Products Journal, 55(3), 8–16.

Yoo, J. (2008). Quantitative Analysis of the Compressive Stress Distributions across Pallet Decks Supporting Packaging in Simulated Warehouse Storage (Master's Thesis). Virginia Tech.

Yoo, J. (2011). Modeling compressive stress distributions at the interface between a pallet deck and distribution packaging (Doctoral dissertation). Virginia Tech.

Zaheer, M., Awais, M., Rautkari, L., & Sorvari, J. (2018). Finite element analysis of paperboard package under compressional load. Procedia Manufacturing, 17, 1162–1170. https://doi.org/10.1016/j.promfg.2018.10.008

Zhang, Z., Qiu, T., Song, R., & Sun, Y. (2014). Nonlinear finite element analysis of the fluted corrugated sheet in the corrugated cardboard. Advances in Materials Science and Engineering, 2014, 1–8. https://doi.org/10.1155/2014/654012

Chapter 1: Development of a friction-driven finite element model to simulate deflection of a unit load segment

Abstract

Current pallet design methodology frequently underestimates the load capacity of the pallet by assuming the payload is uniformly distributed and flexible. By considering the effect of payload characteristics and their interactions during pallet design, the structure of pallets can be optimized, and raw material consumption reduced.

The objective of this study was to develop and validate a simplified finite element model to simulate the bending of a pallet supporting a payload made of corrugated boxes and stored on a warehouse load beam rack. Using a two-dimensional, nonlinear, implicit dynamic model, it allowed for the evaluation of the effect of different payload configurations on the pallet bending response. Factors considered included pallet stiffness, package dimensions, friction levels between packages, friction between packages and the pallet, payload weight, and height of the unit load. The model accurately predicted the deflection of the pallet segment and the movement of the packages for a simplified unit load segment with 3 or 4 columns of boxes supported in a warehouse rack support. Further refinement of the model would be required to predict the behavior of unit loads carrying larger boxes.

Accurately accounting for the reduction in pallet deflection for specific payloads can reduce the ecological impact of the supply chain. The model presented provides an efficient solution to the study of the affecting factors to ultimately optimize pallet design.

1 Introduction

Most consumer products are handled and transported predominantly in unit load form, commonly using wooden pallets and corrugated fiberboard boxes (Fibre Box Association, 2015; Twede et al., 2014). Pallets are key along the whole supply chain, such as in agricultural operations and retailers (McGinley, 2019). The design of pallets for material handling has evolved from a trial and error method to the development of advanced modeling systems (Fagan, 1982; LeBlanc & Richardson, 2003; J R Loferski, Mclain, & Collie, 1988; Joseph R Loferski, 1985;

Samarasinghe, 1987). The need for better models is supported by the material consumption present in pallet manufacturing and by the overall resources utilized in transportation operations. Estimates place the number of pallets in circulation at over 2 billion units in the United States and 6.8 billion units globally (McGinley, 2019; Research and Markets, 2019). In 2016 in the United States, more than 500 million new pallets were manufactured, and 341 million were repaired for continued use. The volume consumed for pallet manufacturing represented 21.8% of the total lumber production of the United States. Pallets for material handling represent one of the largest segments in consumption of sawn hardwoods in the United States, with 45% of the total production being dedicated to them (Gerber et al., 2020). The need for an efficient use of the natural resources consumed to support supply chains is critical and requires the proper design of each component in the system.

The load carrying capacity of most pallets is determined using a uniformly distributed load for each support condition of use, such as for warehouse racking or floor stacking (ASTM International, 2009; ISO, 2011a). Research conducted as early as 1982 shows that when pallets are loaded with specific payloads, instead of uniform loads, pallet bending is reduced due to the redistribution of the stresses on the pallet towards the supports (Collie, 1984; Fagan, 1982). Further exploration of this redistribution of stress across the pallet's top deck, known as the load bridging effect, has been conducted mostly through physical tests and by measuring the change in pallet deflection. The international standard, ISO 8611-Part 3 (ISO, 2011b), recognizes the effect of load bridging by allowing for the determination of a maximum working load of a pallet for a specific payload.

Research efforts have been made to further understand which aspect of the pallet, or its load, significantly influences load bridging for specific payload configurations. One of the first studies was conducted in 1997, by first determining five differing levels of rigidity for a payload and then measuring how much the deflection changed under each level (Center for Unit-Load Design, 1997). Although a clear effect in the results was observed (deflection decreased in direct relation to the payload rigidity), the results can only be considered preliminary since the effect of individual factors were not isolated from each other. The isolated effect of multiple palletizing characteristics such as containment force (Park, 2015), box size (Clayton et al., 2019; Morrissette et al., 2020; Park et al., 2017), flute size (Park et al., 2017), box contents (Phanthanousy, 2017), and interlock stacking (Molina et al., 2018) were investigated by many researchers. All of these

studies used physical testing which involved the construction of unit loads or segments of unit loads and subsequent laboratory measurements. Physical testing of unit loads can provide valuable information but has drawbacks. Physical testing is a time-intensive endeavor, interactions between variables is hard to investigate, and the control of experimental variables is not a simple task.

Simulations using the finite element method have been used extensively in the mechanical engineering field and recently have been widely adopted by packaging science. Research includes finite element analysis (FEA) of different packaging materials, such as wood (Mackerle, 2005), corrugated board (Djilali Hammou et al., 2012; Zhang et al., 2014), paperboard (Nygårds et al., 2019; Zaheer et al., 2018) and multiple others (Wang et al., 2012), including the extensive use of finite element models in the development of food packaging (Fadiji et al., 2018).

The use of finite element analysis has also become commonplace when designing pallets for material handling systems. Wooden pallets can be designed using commercial software that are already available; most of which are based on finite element models (Modern Material Handling, 2012). Multiple studies that evaluate new pallet designs with innovative materials can be found in the literature. These studies show that the application of finite element models allow for preliminary evaluations of pallet performance (Mohammed & Baig, 2018; Ratnam et al., 2005; Waseem et al., 2013). Han, White, and Hamner (2007) applied the finite element method to better understand and explain the distribution of stresses on a single board of the pallet's top deck. Weigel (2001) developed a finite element model to study the resonant frequencies of unit loads of palletized apples and peaches.

The application of the finite element method to study the load bridging effect can be a cost and time efficient alternative. FEA allows researchers to analyze the effect of multiple variables and their interactions with a scope not possible in physical testing. The finite element method has not been previously utilized for the modeling of unit loads and their effects on pallet deformation.

2 Objectives

The main objective of this investigation was to develop and validate a two-dimensional finite element model that can accurately predict the deflection of a pallet analog carrying stacked boxes in a simulated warehouse storage rack.

To be able to complete this main objective of the project, specific sub-objectives were defined.

1) To develop a finite element model to predict the behavior and deflection of a simulated unit load segment.
2) To validate the ability of the finite element model to accurately replicate the deflection of a unit load segment on a racking support for different payload configurations.

3 Unit Load Selection and Simplification

This research project limits the support conditions studied to warehouse racking across the pallet width. Previous research studies have identified this support condition as the one that most often limits the pallet load carrying capacity, given that it commonly presents the greatest pallet deformation (Clayton et al., 2019; Molina et al., 2018; Morrissette et al., 2020). The warehouse racking condition where the pallet is racked across its width will be referred to as simply "racking support." Additionally, it is assumed that under this condition, as shown in Figure 13, the displacement due to bending of the supporting pallet and box movement is primarily along the *xy*-plane, with negligible displacement along the *z*-axis. This assumption is supported by the results in the study by Molina et. al (2018). In this study, when varying different load bridging factors such as pallet design and package orientation, the rate of changes in pallet deflection generated were consistent for the center and the ends of the pallet, indicating that the effect of load bridging is not dependent on the location of the pallet deflection measurement. Based on the series of tests conducted by Molina et al., the bending phenomena can be accurately described by a two-dimensional model. Therefore, a single row of boxes, shown shaded in Figure 13, was modeled to represent the unit load and the payload's interactions. The pallet geometry was simplified to be just one board deep enough to support a single row of boxes. A similarly simplified unit load segment has been used for physical testing in previous studies (Park, 2015; Park et al., 2017; Phanthanousy, 2017). All measurements of pallet bending were considered initial, ignoring the effects of long-term creep on the bending response.

Corrugated boxes were modeled as nondeformable solid objects, subject to gravitational forces and frictional interactions. It is well-known that corrugated boxes are prone to buckling and other deformations while loading, especially the boxes located at the bottom of the stack in a unit load. While, undoubtedly, boxes with significant deformation would impact the results obtained in this study, it was assumed that most unit loads carry new, relatively undamaged packages, each

engineered to provide enough carrying capacity to support loading without significant deformation. Furthermore, the boxes used for the experimental validations contained rigid OSB containers closely fitted inside, preventing any buckling deformation from handling and loading during the tests.

Box contents were not considered in this model. This simplification is supported by research previously conducted that investigated the effects of box contents on pallet deflection (Phanthanousy, 2017). Even though the strength of a corrugated box can be influenced by its contents, the shape or form of the contents does not affect overall pallet deflection as long as the boxes are not deformed.

The pallet was represented in the model using a board as a pallet analog; thus, the effect of the pallet structure was not considered. Pallets can be designed in many different ways with many different materials, and some of these variations might have characteristics that affect the bending profiles. Other structural elements of pallets, such as the effect of stringers and deck boards, were also not considered. Only unit loads of boxes that provided full coverage of the pallet or pallet simulator deck were used. Under or overhanging packages on a pallet could possibly behave in a different manner. Pallet dimensions were based on the Grocery Manufacturers Association specification of 1,219 mm. x 1,016 mm.

This model did not include the effects of additional containment mechanisms such as stretch wrapping. Containment forces increase unit load rigidity and should decrease further the pallet deflection. This should be properly validated, but the conservative approach, which produces a higher deflection, provides a reliable starting point for modeling of unit loads through the application of finite element analysis.

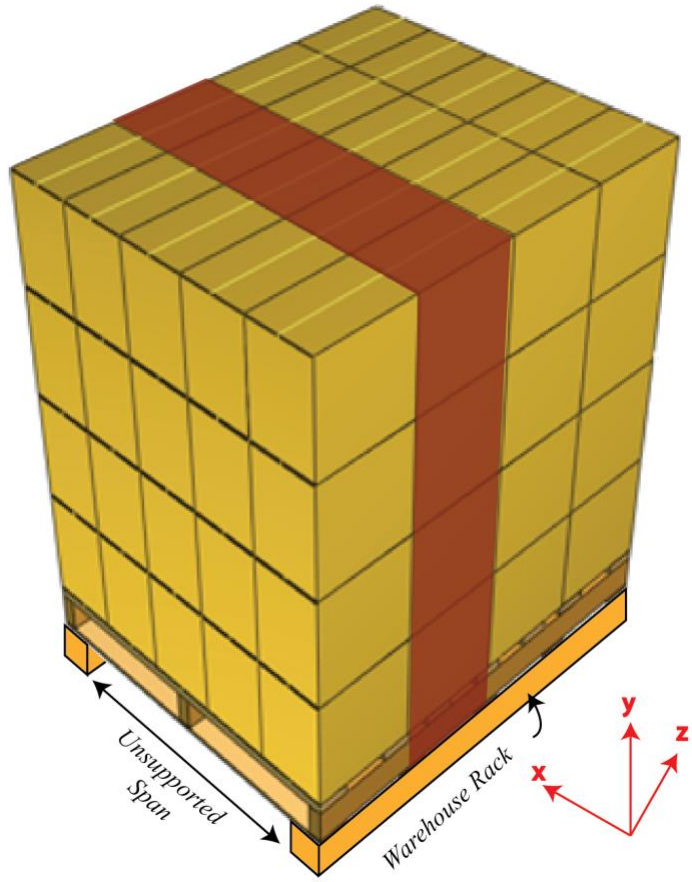

Figure 13. Unit load supported on a warehouse rack across the width. Shaded segment represents the section modeled.

4 Development of a Two-Dimensional Finite Element Model of a Unit Load Segment

A two-dimensional finite element model was developed using Abaqus CAE 16, to replicate the segment of a unit load of stacked corrugated boxes on a board, as shown in Figure 14. The initial model was developed for a unit load segment of 3 columns with 3 layers of boxes and then modified to present different combinations.

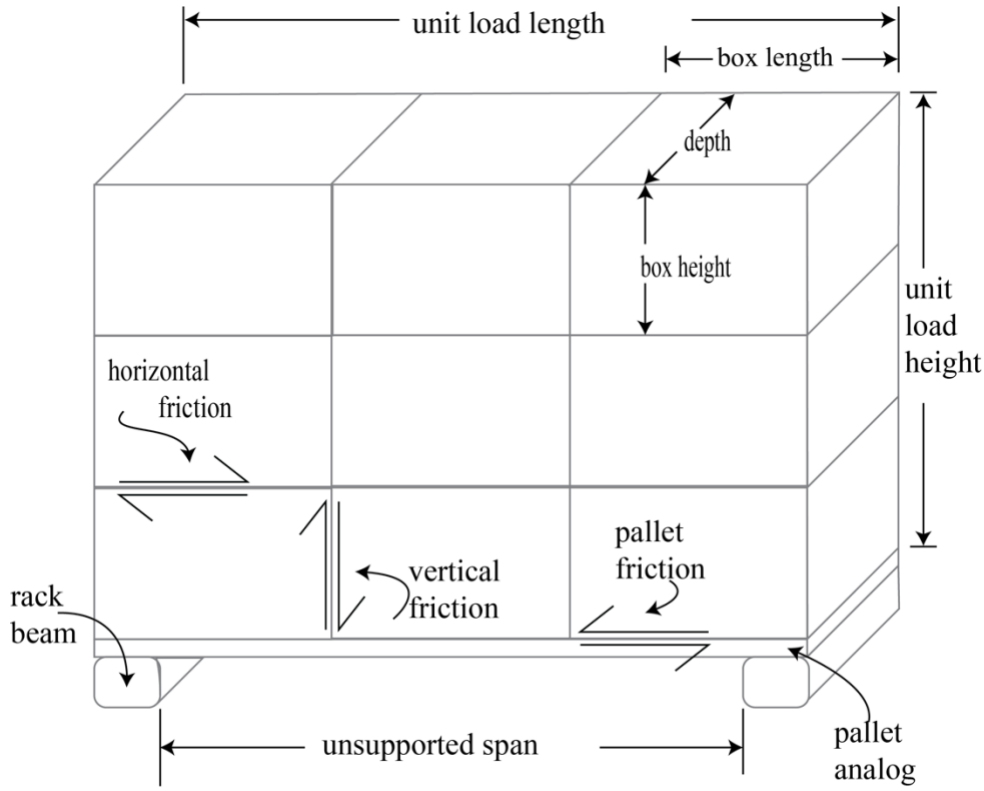

Figure 14. Diagram of the unit load segment modeled.

4.1 FEA Material and Section Assignments

The pallet analog, or board, was modeled as a two-dimensional object with dimensions of 1,016 mm along the length and a thickness of 19 mm, made out of Poly-methyl methacrylate (PMMA). Boxes were also 2D objects with dimensions 338 mm x 318 mm. A homogeneous solid section thickness of 254 mm was used for all instances as the material depth along the *z*-axis. The materials utilized for the pallet analog and boxes were defined as homogeneous, isotropic and linear elastic, specified by the Young's modulus and Poisson's ratio. A stiffness value of 600 GPa was used for the boxes or packages to simulate non-deformable objects under the loading events presented but maintaining the additional material properties of linear elastic objects. Additionally, the mass density of the board and boxes was required, since loading was applied through gravitational acceleration. A summary of the model's material properties is presented in Table 4. The aluminum rack beams of a warehouse rack were modeled as 2D discrete rigid objects measuring 50.8 mm x 50.8 mm with their corners rounded to a 5 mm radius in order to replicate

the same contact properties experienced by the board, representing the pallet analogue, and the beams in the racking condition simulated.

Table 4. Material properties for the unit load analogue components used for the model development.

Component	Property	Value	Source
PMMA board	Dimensions	1,016 x 254 x 19 mm	Experimental measurement
	Young's modulus	3.34 GPa	Experimental measurement using ASTM D198 (2015) (Altuglas International, 2006)
	Poisson's ratio	0.35	
	Mass density	1180 kg m^{-3}	Experimental measurement
Corrugated fiberboard boxes	Dimensions	338 x 254 x 318 mm	Experimental measurement
	Young's modulus	600 GPa	Model input for non-deformable object (Gilchrist, Suhling, & Urbanik, 1999)
	Poisson's ratio	0.44	
	Mass density	438 kg m^{-3}	Experimental measurement

4.2 Boundary Conditions and External Forces

Considering that the model being replicated was affected mostly by weight and not by the application of specific externally applied loads, the loading was simulated through the addition of gravitational forces along the negative *y*-axis, using the standard acceleration on the surface of the Earth of 9.81 m s^{-2}. The specification of mass density for each instance in the model was required. The finite element model was solved with a nonlinear incremental solver to account for the nonlinear mechanics associated with the frictional contact mechanics as well as the large deflections developed in the model. Racking supports, or in this case the aluminum rack beams,

were fixed in place using the Abaqus encastre condition, not allowing for displacement or rotation on any axis. A summary is shown in Table 5.

Table 5. Loading and boundary conditions used for the unit load segment model.

Property	**Location**	**Type/Value**
Loading	Entire model	Gravitational Acceleration -9.81 m s^{-2} along *y*-axis
Boundary conditions	Rack beams (2)	Fixed (encastre)
	Pallet analog	Frictional contacts
	Boxes (9)	Frictional contacts

4.3 Contact modeling

In order to model the contact properties of the unit load segment, the static friction coefficient between the different components were measured. The coefficient of friction was measured for the corrugated fiberboard before it was converted into boxes following the slide angle method from the industry standard TAPPI T-815 (2018). This test method was used to evaluate the specific material's property and ignores any additional variations that might be present when the boxes are fully converted. Figure 14 shows the location of the contacts for the horizontal, vertical and pallet frictions. Friction coefficients were measured for each of the identified contacts and the corresponding alignment of the fluting structures. Horizontal box to box contact was measured as the contact between both boards along the machine direction. Vertical contact was measured as cross direction for both specimens. The payload contact with the pallet was evaluated with the corrugated board aligned along the machine direction, given the direction of box movement along the *x*-axis. Table 6 shows the coefficients of friction for each contact interaction. Experimental measurements of the coefficients of friction were replicated 10 times for each contact, reducing the commonly occurring variability in frictional forces on natural materials. For simplicity, the friction corresponding to the horizontal contact between boxes will be referred to as horizontal friction, the vertical contact between boxes as vertical friction, and the contact

between the pallet and the payload simply as pallet friction. All measurements were conducted under standard laboratory conditions (50% Relative Humidity ± 2%; 23°C ± 1°C).

Table 6. Coefficients of friction for each contact condition in the unit load simulator, obtained according to TAPPI T-815 (2018), with an average of 10 replicates per contact interaction.

Contact interaction [a]			**COF**	
Contact	**Surface 1**	**Surface 2**	**Average**	**Std. Dev.**
Horizontal friction	MD	MD	0.55	0.05
Vertical friction	CD	CD	0.58	0.04
Pallet analog friction	Pallet analog top deck (PMMA)	MD	0.30	0.07
Rack beam- Pallet analog	Aluminum	Pallet analog bottom deck (PMMA)	0.15	0.03

[a] MD: machine direction of corrugated fiberboard; CD: cross direction of corrugated fiberboard; Std. Dev: Standard Deviation

All the components were assembled together to replicate the pallet analog supporting a unit load of stacked boxes and resting on aluminum rack beams. In order to establish boundary conditions for the model and assure proper loading of the parts, surfaces were generated so every contact region could be explicitly declared. Toward this goal, all the frictional contacts were created in the initial step and propagated to the subsequent loading steps. Every contact interaction was defined with friction properties, with tangential behavior using the penalty friction formulation. The specific coefficients of friction for each contact interaction are shown in Table 6. The normal behavior for the frictional contacts was determined using a penalty function as the constraint enforcement method. This was done to allow for separation of the components after the contact is established. Small sliding was permitted in the formulation of the model to represent the small relative motions expected between boxes and between the boxes and the pallet analog. Each contact interaction was defined as a surface-to surface contact with a node-to-surface discretization method. The unit load with 3 columns and 3 layers included 2 frictional contact interactions for the pallet analog with the rack beams, 3 contacts between the top deck of the pallet analog and the

bottom of the 3 boxes at the bottom layer, 6 contacts between the vertical edges of the boxes and 6 contacts for the horizontal edges of the boxes, for a total of 20 defined contact areas.

4.4 Model Discretization

Meshing was assigned individually to each object in the model. The pallet analog was discretized using the Abaqus CPE4I element type, which includes incompatible deformation modes, to include additional degrees of freedom in order to capture the bending kinematics more accurately. The quadrilateral elements for the pallet segment were sized at 2.54 mm, with a total of 3,200 elements.

In order to arrive at the optimal number of elements for the pallet analog, a mesh convergence study was conducted for a unit load consisting of 3 columns of 3 layers of boxes. The goal was to select the ideal seed size for each mesh element that would converge the results into a stable value without unnecessarily increasing the number of equations needing to be solved. An element size of 2.54 mm provided that ideal size. Coarser meshes associated with larger elements reduced calculation time but impacted the deflection results. Finer meshes defined by smaller element sizes provided solutions with almost the same values but increased exponentially the computing requirements. When decreasing the element size from 2.54 mm to 1.27 mm, the resulting change was less than 1% but it increased 2.5 times the computing requirements, generating 11,200 elements compared to 3,200. The percentual difference due to change in vertical displacement was calculated by dividing the difference in vertical displacement by the vertical displacement of the previous simulation. Table 7 and Figure 15 show the summary of the results obtained from the mesh refinement and convergence studies.

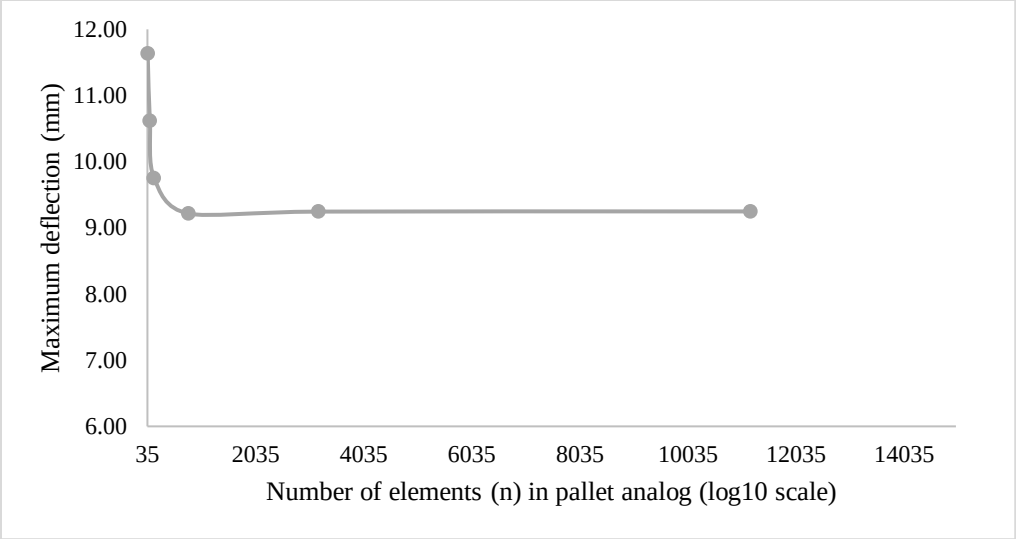

Figure 15. Pallet simulator mesh convergence results for 3 columns, 3 layer unit load. Maximum pallet deflection (U2, mm) at the board midspan versus total number of elements.

Table 7. Mesh convergence for pallet analog for maximum deflection.

Global Seed Size (mm)	**Pallet analog Elements (n)**	**Deformation, U2 (mm)**	**Difference on displacement**
50.8	40	11.63	-
25.4	80	10.61	9.60%
12.7	160	9.75	8.83%
5.08	800	9.22	5.82%
2.54[a]	3200	9.25	-0.33%
1.27	11200	9.25	-0.03%

[a] Optimal seed size selected for the current and further models

Boxes were generated as 2D solid elements, formulated as a plane/strain linear elastic material with reduced integration, specifically the Abaqus CPE4R element. The elements were globally sized at 12.7 mm for every box, regardless of its size. To select this element size, a mesh convergence study was conducted. Figure 16 and Table 8 show the results, conducted specifically for the scenario where 3 columns of boxes of 3 layers were loaded on the board. The midspan pallet analog deflection results were considered converged after the number of elements reached 6,075 for the 9 boxes, or when the seed size was 12.7 mm. Decreasing the box element size further,

to a 5.08 mm seed, changed the results by 1.09% but increased the number of elements 6.3 times, making it unnecessarily demanding.

The racking beam supports were discretized as 2-node, linear, discrete, rigid elements with a length of 2.54 mm and rigid link formulation, represented in Abaqus as rigid 2-noded 2D (R2D2) element. A summary of the mesh properties for each object is shown in Table 9.

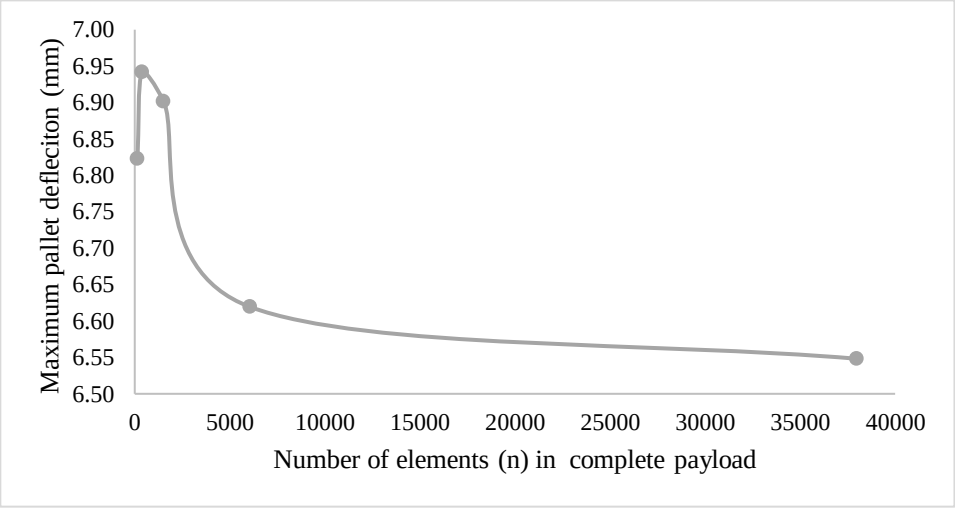

Figure 16. Payload mesh convergence results for 3 columns, 3 layers unit load. Maximum pallet deflection (U2, mm) at the board midspan versus total number of elements.

Table 8. Payload mesh convergence study results for 3 columns, 3 layers unit load.

Global Seed Size (mm)	Payload Elements (n)	Deformation, U2 (mm)	Change (%)
76.20	144	6.82	
50.80	378	6.94	1.72%
25.40	1521	6.90	-0.59%
12.70[a]	6075	6.62	-4.26%
5.08	37989	6.55	-1.09%

[a] Optimal seed size selected for the current and further models

Table 9. Mesh properties for each object in the model.

Part	Element Type	Seed Size	Number of elements
Board	CPE4I	2.54 mm	3,200
Box	CPE4R	12.7 mm	6,075 [a]
Rack Beam	R2D2	2.54 mm	80

[a] Correspond to the total elements in the 3 columns - 3 layers, 954 mm high unit load.

4.5 Model solver

The overall model was formulated as nonlinear, implicit dynamic. The dynamic formulation includes the representation of inertial forces into the system equations of dynamic equilibrium in order to account for the transient characteristics of the model, including the quick movements of all boxes, the large deflections experienced by the pallet segment, and all of the frictional contacts. An extended time step of 5 seconds was used to aid the convergence of the nonlinear contacts and deformations across the unit load segment and they were considered initial board deflections, not accounting for creep effects on the structure.

5 Model Validation

In order to validate the accuracy of the model, a series of experimental tests were conducted and then simulated with the same input values in the finite element model.

5.1 Materials

5.1.1 Pallet analog

Pallet analogs were simulated using a board of Poly-methyl methacrylate (PMMA), with dimensions of 1,016 mm length, 254 mm width and a thickness of 19 mm. PMMA is a commonly used material; its material properties are shown in Table 4. This type of board allowed for experiments to be conducted on an isotropic material with consistently repeatable properties in order to allow for more controllable experimentation and modeling than wooden pallet segments.

5.1.2 Corrugated Boxes

Regular-slotted container-style (RSC) corrugated boxes made of single-wall C-flute corrugated board with 7.2 kN m^{-1} Edge Crush Test (ECT) value were used. More information on this corrugated board can be found in Table 10. The box sizes and weights used for the study are shown in Table 11. Each corrugated box contained a box insert made of 12.7 mm thick oriented-strand-board (OSB) built to fit tightly the inside of the corrugated boxes and avoid any box deformation from repetitive loading. Weight was added using wooden pellets inside the OSB box in order to have boxes with a consistent density of 438 kg/m^3. Contact interaction properties for the boxes are shown in Table 6. The boxes were manufactured on a computerized cutting table (Esko Kongsberg XL44, Manufacturer: Esko, Miamisburg, Ohio, US). Top and bottom flaps of the boxes were sealed using a 50.8 mm packaging tape (3M, Saint Paul, MN, United States).

Table 10. Material properties of the corrugated board.

Property	**Standard**	**Mean**	**Std. Dev.**	**No. of Samples**
ECT (kN m^{-1})	ISO 3037:2013	7.20	0.21	10
FCT (kPa)	ISO 3035:2011	154.22	24.94	10
Thickness (mm)	ISO 3034:2011	4.17	0.03	10
Combined Board Weight (g m^{-2})	ISO 536:2019	654.7	5.4	5
Combined Board Dry Weight (g m^{-2})	ISO 536:2019	601.4	5.4	5
Grammage after separation (g m^{-2})	ISO 3039:2010	Inside liner: 203.18	2.81	5
		Medium: 182.55	3.71	5
		Outside liner: 207.14	7.01	5

Table 11. Weight and dimensions of boxes used for model validation.

Box	**Dimensions (mm)**	**Weight per box (kg)**
Small	254 x 254 x 318	9.07
Medium	338 x 254 x 318	12.11
Large	508 x 254 x 318	18.14

5.2 Methods

The model validation for this research was conducted in two sequential phases. First, the experimental analog of a pallet bending while in a warehouse rack support across its width was validated. This initial step allowed the researchers to confirm the accuracy of the model in replicating the pallet analog bending, before including additional complexities from the payload characteristics. Second, the complete unit load segment was tested, validating the model's ability to replicate the pallet analog's deflection response while under the different payloads being studied.

5.2.1 Validation of the FE simulation of a warehouse racking support analog

In order to measure pallet deflection while under each unit load configuration, a simulated pallet rack was built. The objective of this was to validate the support model without including boxes. Two square, 50.8 mm x 50.8 mm, hollow aluminum beams acted as direct supports and the pallet simulator rested on them. A free span of 914 mm between the inside ends of the aluminum beams simulated the common warehouse racking condition where the pallet is racked across its width. The aluminum beams were placed on top of two I-beams (101 mm wide flange, 101 mm high), which were secured to a rigid, flat platen on the floor.

To record board deflection, string potentiometers were attached to the center of each side of the pallet simulator (i.e., the PMMA board). Two additional string potentiometers were connected to the racking setup in order to measure and adjust the effects of the test setup when compressed downward from loading. This method assured measurement of only the board's deflection while eliminating any influence from external loading on the test setup.

While the pallet simulator was being loaded, it was supported from underneath using two car jacks. This was done to avoid any additional bending of the pallet during the loading of the payload. The removal of the car jack supports was done at a slow rate, manually lowering the supports until they had no further contact with the board. Maximum deflection at board midspan was recorded one minute after the supports were removed. All measurements were conducted under standard laboratory conditions (50% ± 2% Relative Humidity and 23°C ± 1°C) and every material that was used had been acclimated to those conditions for at least 72 hours. Figure 17 shows the experimental test setup for the warehouse racking support simulator.

To evaluate board bending under a specific loading condition and subsequently simulate it, the PMMA pallet analogue was loaded with a steel box, as shown in Figure 17, and the absolute deflection at the center of the board was measured and recorded. Weight box dimensions were 318 mm x 114 mm x 89 mm, with a weight of 22.7 kg. The experiment was conducted five times.

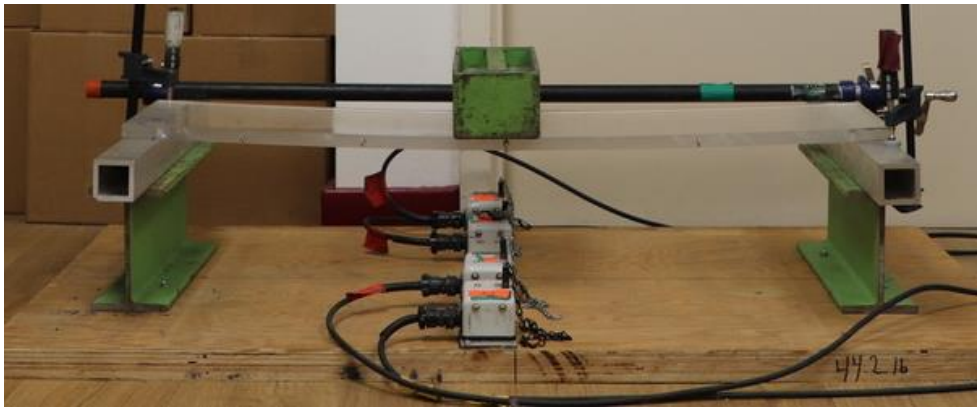

Figure 17. Experimental test setup for a center loading with a steel weight box on the pallet simulator.

5.2.2 Validation of the FE simulation of a unit load segment

Unit loads with different configurations were developed to measure the bending moment response of the pallet. Different configurations were achieved by changing the unit load's main variables such as the number of columns, number of layers, and the total weight supported by the pallet. It is known from previous experimental research that these factors are the ones generating the main effects on load bridging (Clayton et al., 2019; Collie, 1984; Fagan, 1982; Molina et al., 2018; Park et al., 2017). Representing a wider range of unit loads during the experimental studies allows for more robust model validation afterwards. The number of layers and total weight of each unit load evaluated are shown in Table 12. Each test was replicated five times. Figure 18 shows an example of a loaded unit load segment of two columns and two layers, supported to prevent bending while under deflection. To simplify the identification of the unit loads, a notation of "columns X layers" will be used; a unit load composed of four columns and three layers will be referred as a 4x3 unit load.

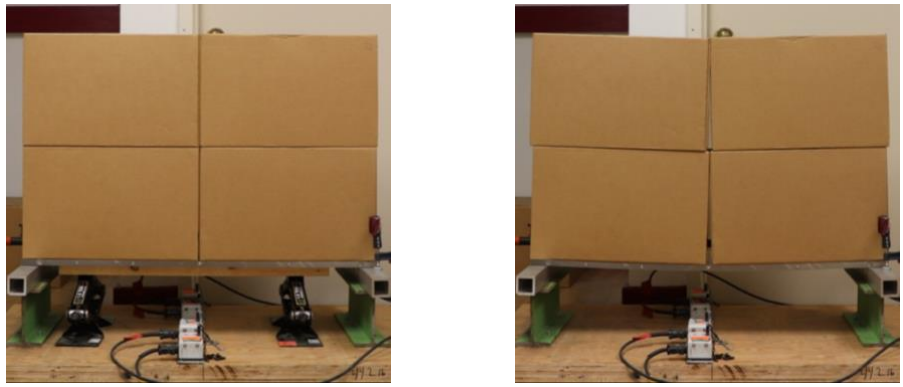

(a) Supported Unit Load (b) Unit load under load

Figure 18. Picture of unit load segment with 2 layers of large boxes, fully supported (a) and showing deflection under load (b).

5.3 Experimental Design

To conduct the validation of the finite element model of the unit load segment, each of the seven analogues studied was simulated and compared directly to the results of the experimental tests.

In order to calculate the accuracy of the model, the Mean Absolute Percent Error (MAPE) was calculated, using (6), comparing the experimental results, A_t (mm) against the finite element model results, F_t (mm), for the seven different models (n). MAPE was considered to provide an accurate description of the model, given that it weighs individually each model, accounting for the differences in the absolute deflection values.

$$MAPE = \frac{1}{n}\sum_{t=1}^{n}\left|\frac{A_t - F_t}{A_t}\right| \tag{6}$$

6 Results and Discussion

6.1 Warehouse racking simulation results

To validate the model without the addition of any payload complexities, the pallet segment was loaded with a steel weight box, as shown in Figure 17. The average initial deflection recorded

for the plate under load was 9.40 mm with a standard deviation of 0.56 mm. To replicate this, the finite element model was modified to have only a single box matching the size of the weight box centered along the board.

For this initial validation, the main response of interest after running the simulation was the deformation of the pallet segment along the *y*-axis. The largest deflection was identified at the midspan of the pallet analogue board. The predicted deflection was 9.25 mm (0.364 in). Figure 19 shows the Abaqus model results of the deformed structure. The color scheme corresponds to the deformation along the negative region of the *y*-axis, with sections shaded blue as the ones with larger displacements. When compared with the experimental test measurement, the result had a deviation of -1.62%, which was deemed acceptable for the validation of the test setup and confirmed the model's ability to accurately replicate the racking across the width pallet support test analogue.

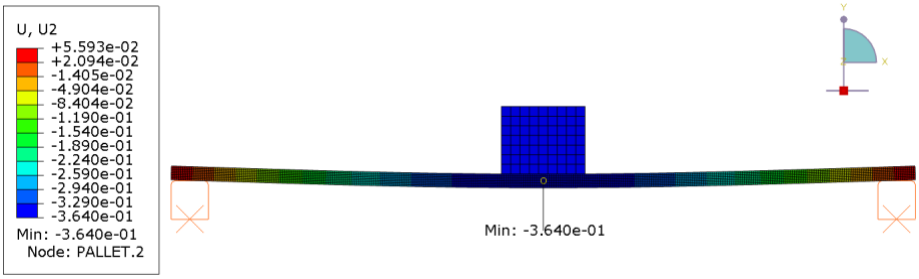

Figure 19. Two-dimensional FE model result for the simulated pallet segment and weight box, deformed. Figure values shown in inches.

6.2 Unit load segment simulation results

Using the support test setup that has already been validated and the methods previously described, experimental trials were conducted by loading the board with different box sizes. Small (254 x 254 x 318mm), medium (338 x 254 x 318mm), and large (508 x 254 x 318mm) boxes were tested. The initial deflections recorded at the end of the simulation at the board midspan are shown in Table 12 for the seven different unit load combinations of columns and layers of boxes.

Parallel to this, the finite element model was adjusted to the same box sizes and number of layers combinations. Table 12 shows the results for each of the analyses. The mean absolute percent error (MAPE) of the model is 22%. The greatest error with 59% MAPE was observed for the unit loads with the largest boxes (two columns). By limiting the prediction scope of the model

to those unit loads with three or four columns, model accuracy improves to a MAPE of 7.8%, which is considered an acceptable accuracy for such a general unit load bending model. Unit loads with three columns presented a MAPE of 12% and those with four columns a MAPE of 1.3%, suggesting an increased accuracy with smaller boxes.

The scenario of unit loads of two columns present a special case that needs to be formulated as a different model in order to accurately predict pallet deflection. The assumptions and simplifications in this project do not properly represent the actual unit load behavior. The boxes in the designed experiment present a large 'rotation' movement when they are under load. This movement is accurately predicted by the model, as seen in Figure 20 (a). The absolute value predicted, on the other hand, diverges by 29% from the measured experimental value for the 2x2 unit. A similar case occurs for the unit load of 2x3. For this scenario, the model underpredicted the overall pallet deflection, with an error of 88%. This specific two-column scenario presented significant differences from the rest of the unit loads studied. When using the friction values obtained by evaluating the linerboard contact properties, as conducted for this study, the actual properties of the contact might not have been properly represented. Corrugated boxes have imperfections. One example could be that there was compression of the flutes or of the linerboard between the fluting structure, albeit small, but that can affect the characteristics of the horizontal or pallet frictions. Additional variations could come from the use of packaging tape for the closures and any other environmental impurities when testing, such as dust, that could affect more directly the horizontal surfaces. When measuring the friction with the slide angle method, only the actual contact properties between the linerboards are evaluated, with low weight and perfect samples.

Another reason for the deviation of the model with the two-column unit load can be attributed to the use of non-deformable boxes in the simulations. Unit loads with smaller boxes, such as three and four-column units, presented no deformation and therefore, they are more accurate in their prediction. The larger boxes could have slight deformations in the experimental tests, changing the contact interactions; therefore, changing how the load is transferred to the pallet and ultimately affecting the pallet's deflection. Additionally, the use of no containment force in these experiments allowed the boxes to be freely displaced during the rotation generated through bending. This movement will be much more constrained in an actual unit load, given the use of containment mechanisms. By constraining larger displacements, the behavior of the boxes will be closer to the other scenarios, and hence could be better simulated.

For all the five scenarios where the unit loads had three or four columns, the model was capable of accurately predicting the deflection and the movement of the boxes. This movement is closely linked to their load bridging behavior. Figure 20(b) and 20(c) show the behavior of the boxes in the experimental tests and in the FE simulation for the 3x3 and 4x3 units. Visually, this model reasonably replicates the box movement. The 3x3 unit load shows a slight box rotation at the outer columns while the center column is displaced straight downwards. Although the boxes rotate, the model is capable of accurately predicting the pallet segment's deflection. The smaller rotation does not significantly affect the contact properties or cause any box deformation, as discussed for the two-column unit loads. The four-column unit load is also represented correctly in the model and shows high accuracy in the deflection results and in the visual inspection of box behavior. Small boxes kept their form, and the movements of these boxes were mostly along the *y*-axis, confirming the model's ability to represent the load bridging accurately. The model was able to simulate a unit load's bending accurately for three and four-column scenarios without requiring the further complexity that would be added by having to simulate corrugated panels and their potential buckling.

Overall, the model can simulate, with acceptable margins of error, the deflection of unit load segments and the box movements for unit loads with three and four columns of boxes. This can translate into better understanding of the load bridging effect by conducting further simulations with a wider range of variables, such as different numbers of columns, layers of boxes, payload heights, pallet stiffnesses, and all of the friction characteristics of each contact.

Table 12. Physical properties of each experimental unit with its corresponding deflection (mm) result for the experimental measurement and the finite element model simulation deflection result (mm) for each source of friction and its corresponding error.

Box Size	**Unit Load (Columns x Layers)**	**Payload Weight (kg)**	**Height (mm)**	**Experimental Test Results**			**FEA Simulation Results**	
				Average Deflection (mm)	**Std. Dev. (mm)**	**COV (%)**	**Deflection (mm)**	**Percent Error**
Large	2x2	72.6	636	4.38	0.48	11.11	3.12	29%
	2x3	108.9	954	2.65	0.41	5.45	0.31	88%
Medium	3x2	72.6	636	7.43	0.41	5.45	5.65	24%
	3x3	108.9	954	6.85	0.30	4.56	6.18	10%
	3x4	145.1	1272	8.38	0.41	4.93	8.09	3.4%
Small	4x2	72.6	636	6.89	0.2	3.11	6.93	-0.6%
	4x3	108.9	954	9.92	0.43	4.35	9.79	1.3%

(a) 2 Columns – 2 Layers Unit Load

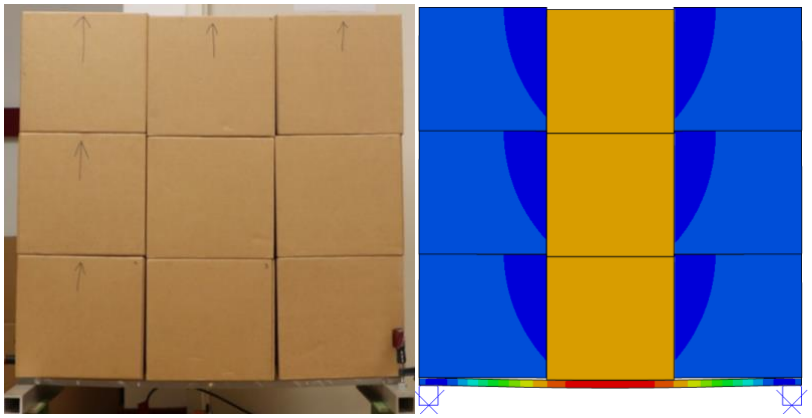

(b) 3 Columns – 3 Layers Unit Load

(c) 4 Columns – 3 Layers Unit Load

Images shown for the model (left) are colored based on deflection. Red equals large displacements, blue represents no movement.

Figure 20. Comparison of movement of unit load components under deflection for experimental (left) and finite element analysis (right) for two layers and (a) two columns, (b) three columns, and (c) four columns of packages.

7 Conclusions

In this paper, a finite element model to simulate unit load bending under warehouse load beam racking support was developed and validated. The following can be concluded:

- The two-dimensional model presented can accurately replicate the load bridging effect that has been observed in physical experimentation for unit load segments of three and four columns with an average error of 8%.
- Unit loads with very large boxes, such as a two-column unit load, present a different box movement behavior when deflecting. Refinement to the model must be developed in order to study these unit loads, considering the different contact interactions, possible box deformations, and the use of additional containment methods.
- This model is capable of replicating the behavior of the multiple unit load segments when modifying payload configurations, such as changing height, weight and number of columns.

Further exploration is required to determine how each of the many variables affects pallet bending. Load bridging in unit loads has been extensively studied in physical environments. The model developed allows for the exploration of the effects and interactions which is not feasible to conduct in controlled experiments.

8 Acknowledgements

This work was financially supported by the Industrial Affiliate Membership of the Center for Packaging and Unit Load Design at Virginia Tech. The corrugated boxes were donated by the Roanoke, VA facility of Packaging Corporations of America.

9 References

Altuglas International. (2006). Plexiglass General Information and Physical Properties. Retrieved May 28, 2019, from http://www.plexiglas.com/export/sites/plexiglas/.content/medias/downloads/sheet-docs/plexiglas-general-information-and-physical-properties.pdf

ASTM. (2015). D198-15 Standard Test Methods of Static Tests of Lumber in Structural Sizes. https://doi.org/10.1520/D0198-15

ASTM International. (2009). ASTM D1185-98a(2009) Standard test methods for pallets and related structures employed in materials handling and shipping. https://doi.org/10.1520/D1185-98AR09

Center for Unit-Load Design. (1997). The effect of load bridging on unit-load deflection. In Research Update. Blacksburg, VA.

Clayton, A. P., Horvath, L., Bouldin, J., & Gething, B. (2019). Investigation of the effect of column stacked corrugated boxes on load bridging using partial four-way stringer class wooden pallets. Packaging Technology and Science, 32(9), 423–439. https://doi.org/10.1002/pts.2438

Collie, S. T. (1984). Laboratory verification of pallet design procedures (Master's Thesis). Virginia Polytechnic Institute and State University, Blacksburg, VA.

Djilali Hammou, A., Minh Duong, P. T., Abbès, B., Makhlouf, M., & Guo, Y.-Q. (2012). Finite-element simulation with a homogenization model and experimental study of free drop tests of corrugated cardboard packaging. Mechanics & Industry, 13(3), 175–184. https://doi.org/10.1051/meca/2012013

Fadiji, T., Coetzee, C. J., Berry, T. M., Ambaw, A., & Opara, U. L. (2018). The efficacy of finite element analysis (FEA) as a design tool for food packaging: A review. Biosystems Engineering, 174, 20–40. https://doi.org/10.1016/j.biosystemseng.2018.06.015

Fagan, B. (1982). Load-support conditions and computerized test apparatus for wood pallets (Master's Thesis). Virginia Polytechnic Institute and State University, Blacksburg, VA.

Fibre Box Association. (2015). Fibre Box Handbook (22nd ed.). Elk Grove Village, IL.

Gerber, N., Horvath, L., Araman, P., & Gething, B. (2020). Investigation of New and Recovered Wood Shipping Platforms in the United States. BioResources, 15(2), 2818–2838. https://doi.org/10.15376/biores.15.2.2818-2838

Gilchrist, A. C., Suhling, J. C., & Urbanik, T. J. (1999). Nonlinear finite element modeling of corrugated board. American Society of Mechanical Engineers, Applied Mechanics Division, AMD, 231, 101–106.

Han, J., White, M., & Hamner, P. (2007). Development of a Finite Element Model of Pallet Deformation and Compressive Stresses on Packaging within Pallet Loads. Journal of Applied Packaging Research, 1(3), 149–162.

ISO. (2011a). ISO 8611-1:2011(E) Pallets for materials handling — Flat pallets. Geneva, Switzerland.

ISO. (2011b). ISO 8611-3:2011(E) Pallets for materials handling - Maximum Working Loads. ISO. Geneva, Switzerland.

LeBlanc, R., & Richardson, S. (2003). Pallets: A North American perspective (1ed.). Ontario, Canada, Canada: PACTS Management Inc.

Loferski, J R, Mclain, T. E., & Collie, S. T. (1988). Analysis of racked wood pallets. Wood and Fiber Science, 20(3), 304–319.

Loferski, Joseph R. (1985). A Reliability Based Design Procedure for Wood Pallets (PhD Dissertation). Virginia Tech.

Mackerle, J. (2005). Finite element analyses in wood research: a bibliography. Wood Science and Technology, 39(7), 579–600. https://doi.org/10.1007/s00226-005-0026-9

McGinley, D. (2019). Wood Pallets & Skids Production in the US. Melbourne, Australia.

Modern Material Handling. (2012). Pallet design and analysis software tool released. Retrieved from Supply Chain Management Review website: https://www.scmr.com/article/pallet_design_and_analysis_software_tool_released

Mohammed, M., & Baig, A. (2018). Designing novel grooved pallets for industrial application (Master's Thesis). Cleveland State University.

Molina, E., Horvath, L., & White, M. S. (2018). Investigation of pallet stacking pattern on unit load bridging. Packaging Technology and Science, 31(10), 653–663. https://doi.org/10.1002/pts.2406

Morrissette, S. M., Horvath, L., & DeLack, K. (2020). Investigation into the load bridging effect for block class pallets as a function of package size and pallet stiffness. Packaging Technology and Science, 1–19. https://doi.org/10.1002/pts.2539

Nygårds, M., Sjökvist, S., Marin, G., & Sundström, J. (2019). Simulation and experimental verification of a drop test and compression test of a gable top package. Packaging Technology and Science, (March), 1–9. https://doi.org/10.1002/pts.2441

Park, J. (2015). Investigation of fundamental relationships to improve the sustainability of unit loads (Ph.D. Dissertation). Virginia Polytechnic Institute and State University.

Park, J., Horvath, L., White, M. S., Phanthanousy, S., Araman, P., & Bush, R. J. (2017). The influence of package size and flute type of corrugated boxes on load bridging in unit loads. Packaging Technology and Science, 30(1–2), 33–43. https://doi.org/10.1002/pts.2279

Phanthanousy, S. (2017). The Effect of the Stiffness of Unit Load Components on Pallet Deflection and Box Compression Strength. Retrieved from https://vtechworks.lib.vt.edu/handle/10919/86203

Ratnam, M. M., Lim, J. H., & Khalil, H. P. S. A. (2005). Study of three-dimensional deformation of a pallet using phase-shiff shadow moiré and finite-element analysis. Experimental Mechanics, 45(1), 9–17. https://doi.org/10.1007/BF02428985

Research and Markets. (2019, June). Pallet Market: Global Industry Trends, Share, Size, Growth, Opportunity and Forecast 2019-2024. Research and Markets.

Samarasinghe, S. (1987). Predicting rotation modulus for block pallet joints (Master's Thesis). Virginia Tech, Blacksburg, VA.

TAPPI. (2018). T 815 om-18 - Coefficient of static friction (slide angle) of packaging and packaging materials (including shipping sack papers, corrugated and solid fiberboard) (inclined plane method) (pp. 1–6). pp. 1–6. TAPPI/ANSI.

Twede, D., Selke, S. E. M., Kamdem, D.-P., & Shires, D. (2014). Cartons, crates and corrugated board: handbook of paper and wood packaging technology (2nd.). DEStech Publications, Inc.

Wang, M., Zhao, R. L., & Li, K. T. (2012). Application of the Behavioral Modeling Technique to Structure Optimization in Packaging Container Design. Applied Mechanics and Materials, 200, 592–596. https://doi.org/10.4028/www.scientific.net/AMM.200.592

Waseem, A., Nawaz, A., Munir, N., Islam, B., & Noor, S. (2013). Comparative analysis of different materials for pallet design using ANSYS. International Journal of Mechanical and Mechatronics Engineering, 13(2), 26–32.

Weigel, T. G. (2001). Modeling the Dynamic Interactions between Wood Pallets and Corrugated Containers during Resonance (Ph.D. Dissertation). Virginia Tech.

Zaheer, M., Awais, M., Rautkari, L., & Sorvari, J. (2018). Finite element analysis of paperboard package under compressional load. Procedia Manufacturing, 17, 1162–1170. https://doi.org/10.1016/j.promfg.2018.10.008

Zhang, Z., Qiu, T., Song, R., & Sun, Y. (2014). Nonlinear finite element analysis of the fluted corrugated sheet in the corrugated cardboard. Advances in Materials Science and Engineering, 2014, 1–8. https://doi.org/10.1155/2014/654012

Chapter 2: Development of a simplified unit load model to study the factors influencing load bridging in racked pallets

Abstract

Currently, general purpose pallets are designed assuming a uniformly distributed payload will be carried. This assumption provides a safe estimate for general use pallets but limits the optimization potential of pallets designed for specific uses, such as carrying corrugated fiberboard boxes. Knowing the effect of the payload characteristics on the pallet performance can help unit load designers develop better and more sustainable pallets.

The objective of this study was to characterize the effects, significant factors and interactions influencing load bridging in unit loads. This will provide a clear understanding of the load bridging effect and how it can be successfully applied during the unit load design process. Using a previously developed finite element model, the unit load factors that significantly influence load bridging were identified. To provide a more efficient and cost-effective solution, a surrogate model was developed using the Gaussian Process method. A full analysis of payload effects on pallet deflection was conducted. Four factors were identified as generating significant influence: the number of columns in the unit load, the height of the payload, the friction coefficients of the payload's contact with the pallet deck, and the contact friction between packages. Additionally, it was identified that complex interactions exist between the significant factors and must always be considered.

1 Introduction

More than 6.8 billion pallets are in circulation around the world (Research and Markets, 2019). Over 80% of shipping volume utilizes some form of corrugated fiberboard packages (Twede et al., 2014). Previous research has shown that the performance of corrugated boxes is affected by the characteristics of the pallet that supports them, including factors such as deck board stiffness and gaps between the boards causing unsupported box corners (Baker, 2016; Kellicut, 1963; Monaghan & Marcondes, 1992; Quesenberry et al., 2020). Pallet performance is affected by the condition of use, such as being stored on a warehouse rack or on the floor. An extensive body

of knowledge has been developed to understand pallet performance for the most common supply chain environments, for different pallet materials and other design characteristics (Fagan, 1982; Hamner & White, 2005; Joseph R Loferski, 1985; Wallin, 1979). Studies have been conducted to evaluate the pallet performance when unit loads are supported on conditions such as warehouse racking across the length and across the width, supported on forklift tines, or stacked on the floor (Clayton et al., 2019; Molina et al., 2018; Morrissette et al., 2020).

Research has also been conducted to understand how the characteristics of the payload affects the performance of pallets, commonly showing that when a pallet carries a more rigid payload, pallet deformation decreases. This behavior is known as the load bridging effect and entails the redistribution of the compressive forces towards the rigid supports and away from the critical pallet components that might be more susceptive to failure (Collie, 1984; Park, 2015). To characterize this effect, studies were conducted evaluating specific factors that can potentially influence the load bridging effect level. Factors such as the dimensions of the packages, their contents, package stacking patterns, number of layers of packages, total height of the unit load and load containment methods have been evaluated (Clayton et al., 2019; Collie, 1984; Molina et al., 2018; Morrissette, 2020; Park et al., 2017; Phanthanousy, 2017). This research has historically been conducted through physical experimentation with a limited evaluation of the potential interactions between these factors. The load bridging effect has been measured through the change in overall deformation of the pallet structure and by evaluating the changes in the pressure distribution across the pallet top decks (Clayton et al., 2019; Han et al., 2007; Morrissette et al., 2020; Park et al., 2017; Yoo, 2011).

Physical experimentation for large systems, such as pallets carrying multiple packages, presents low repeatability due to the potential variation in uncontrollable factors. To account for this, simplified general models have been developed. Han et al. (2007) developed a finite element (FE) model to predict the deformation of pallet top deck boards under non-uniform load applications, but limited to rigid loads. Chapter 1 presented a model simulating the bending behavior of a simplified unit load segment using an implicit dynamic, two-dimensional finite element analysis approach. Unlike previous models, it provides a method to generically analyze a unit load when stored on a warehouse rack beam support to determine the predicted level of load bridging for the specific load characteristics.

Although the developed finite element model represents a robust baseline to use in studying which characteristics of a unit load influence the pallet performance, a full analysis of the trends and interactions of all of the identified factors increases the computing requirements exponentially. A surrogate model is commonly utilized in such scenarios, providing not only a more efficient analysis tool but also an accessible method for industry practitioners to design unit loads using acceptable approximations (Jones & Johnson, 2009; Keprate, Ratnayake, & Sankararaman, 2019; Maatouk & Bay, 2017; Vasudevan, Ramos, Nettleton, & Durrant-Whyte, 2009).

Being able to better understand the effect of the payload characteristics that influence the load bridging effect can allow for an improved design methodology for unit loads. Designers would be enabled to identify critical factors on unit loads that might be negatively impacting the pallet performance. Such a comprehensive knowledge on the load bridging effect factors is not currently available.

1.1 Objectives

The main objective of this investigation was to characterize the effects, significant factors, and interactions influencing load bridging on unit loads. This will provide a clear understanding of the load bridging effect and how it can be successfully applied during the unit load design process.

To attain the main objective of this project, specific objectives are defined as follows.

1) To evaluate the significance of the seven identified factors and their interactions that characterize load bridging for unit loads of stacked corrugated boxes on warehouse racking support.
2) To develop and validate a Gaussian process regression model that can efficiently and accurately replicate the finite element simulations.
3) To quantify and describe the effect of all identified significant load bridging factors influencing pallet bending, as well as the interactions between them.

1.2 Methodology

This research was structured to be presented in three main sections. First, a fractional factorial screening design was conducted to identify the significance of multiple factors that could have an influence on the load bridging effect on racked unit loads. Then, second, a Gaussian Process model was developed as a surrogate model to increase the efficiency of the analysis and the potential of its application. In the third and final section, the developed Gaussian Process model was used to conduct a detailed analysis on each of the significant factors. Special attention was paid to the interactions and trends observed. Figure 21 shows these steps in a summary flowchart of the research project.

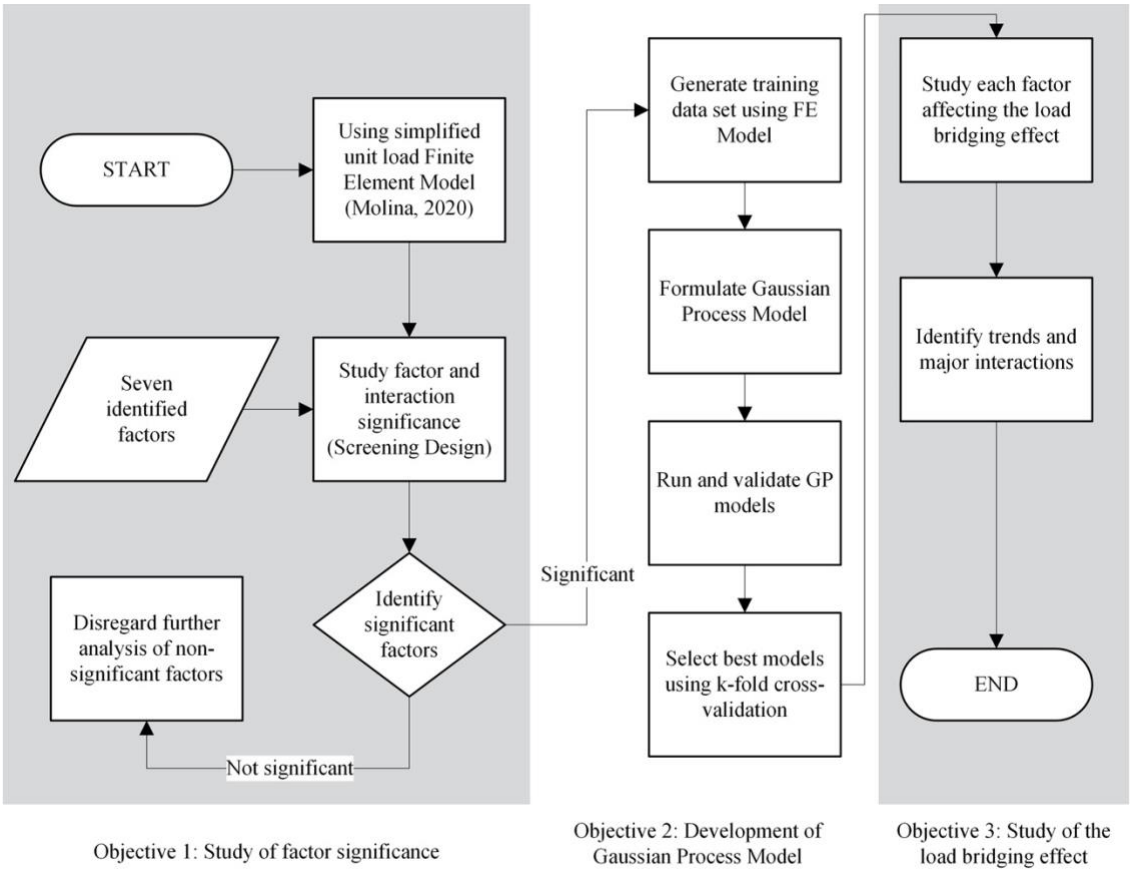

Figure 21. Steps followed to study the effect of load bridging on racked unit loads.

2 Study of the significance of the factors in the load bridging model

2.1 Materials and Methods

The finite element model of a unit load segment used in this paper was a two-dimensional implicit dynamic model. The full model description is provided in Chapter 1. In it, a segment of a unit load, supported on a warehouse storage racking condition across its width, was simulated. This model simplified the packages to non-deformable boxes with frictional contacts. Boxes were defined by density, and loading was conducted through gravitational acceleration. This model provided an average prediction accuracy of 8% for unit load segments with three or more columns of packages.

After the development of the finite element analysis for the unit load segment, multiple factors were identified as necessary inputs for an accurate simulation. The goal of this research endeavor was to understand and characterize the load bridging effect in unit loads. It was hypothesized that not all input variables would have the same degree of influence on load bridging. Screening for the significant factors and interactions, and then simplifying the load bridging model was a key first step towards comprehending the complex interactions occurring among payloads of stacked corrugated boxes.

Seven variables were identified as necessary to fully describe the unit load segments being replicated in the finite element model; therefore, these variables were selected as the initial factors for the screening design. The variables were as follows: the number of columns, which corresponds to the unit load length divided by the box length; the number of layers, which corresponds to the height of the payload divided by the box height; the payload height (m); the coefficient of friction between the pallet and the payload (pallet friction); the coefficient of friction between the boxes (box friction); the Young's Modulus of the pallet segment simulator (pallet stiffness, GPa); and the total payload weight (kg). All other model inputs were either constants or were derived from the main input variables, such as the material density of the boxes or the specific box dimensions, which depends on the combination of the number of columns, layers, and payload height. Figure 22 shows the unit load segment replicated and graphically depicting each factor.

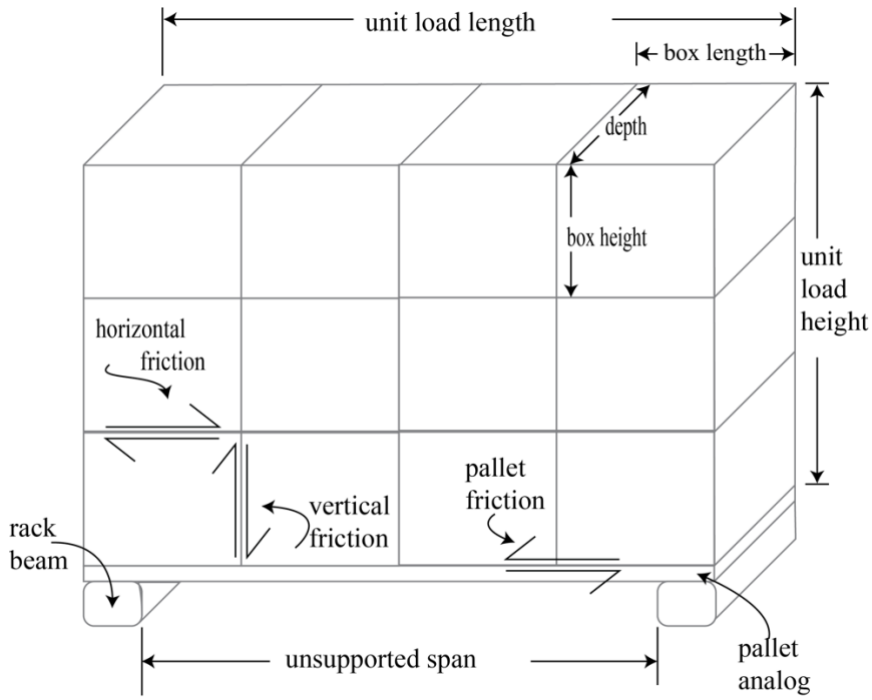

Figure 22. Diagram of the unit load segment and the variables studied (From Chapter 1).

To capture the effects of these variables, values for the study were determined from the trends observed in the model development process in Chapter 1. For the screening design, the unit load segments created consisted of three and five columns, and three and five layers. The coefficient of frictions of the different interactions were selected from a low friction of 0.20 to a higher value of 0.60. This covered the ranges of coefficients of friction (CoFs) observed in material handling operations for different common materials (O'Dell, Clarke, & White, 1998). The Modulus of Elasticity of the pallet was selected for an analog of a flexible plastic pallet of 2.76 GPa and a more rigid wooden pallet of 8.27 GPa. Pallet stiffness values were estimated based on the expected adjusted bending stiffness rates as developed by Park et. al (2017), with a deflection value of 5 kg/mm for the low stiffness board and 14 kg/mm for the high stiffness board. The payload weight was evaluated for both 109 kg and 218 kg, which generated an equivalent loading of 538 kg and 1,045 kg, respectively, on a standard pallet size of 1,219 mm x 1,016 mm. As for the unit load's height, the lowest value selected was 0.762 m and the highest value was 1.778 m.

Parallel to the study of the factors describing the payload, the finite element model was also modified to calculate the deflection under the same payload weight but as a uniformly distributed load across the pallet deck. These values allowed for the comparison of the relative

effects of different factors, controlling for changes on pallet stiffness and payload weight. Deflection ratios have been previously used as a measure of the load bridging levels and can provide a simpler measurement of the rate of change when altering the factors studied. Uniformly distributed loading represents the worse-case scenario for pallet bending and can be experimentally replicated using air or water bags (Fagan, 1982). The ratio is calculated by dividing the absolute deflection by the deflection of the pallet analog under uniform loading with the equivalent weight.

2.2 Design of Experiments

To identify the relevant factors in unit load bridging, a screening design was formulated. The design utilized was a fractional factorial orthogonal 2_{IV}^{7-1} design which allowed for the study of all of the seven main effects and the 2-factor interactions between the independent factors included in the model. This generated 64 representations of unit load configurations for the finite element model, with just one partition of the full factorial, thus reducing by half the required experiments from the full factorial design. The resolution *IV* of the statistical model avoided the main effects being confounded with any of the two-factor interactions. Possible confounding was at worst with the three-factor interactions. This model simplification is based on the sparsity-of-effects principle. This states that a system, such as the unit load representation at hand, will be dominated by the main effects and low-order interactions and only rarely by higher order interactions. No replication was possible, given that the finite element model as formulated provided a deterministic solution. The selection of this statistical model provided enough confidence in a screening design that there was no need for the development of a full factorial, considering the number of runs required. The values for the low and high levels of the seven variables are presented in Table 13. The main response variable of the model was the absolute pallet segment deflection measured at the center along the *y-axis*. Additionally, the same statistical analysis was conducted for the ratio of the deflection of each experimental test to the deflection of the uniform loading for the pallet segment when loaded with the same load level. The screening model formulation is presented in (7) , where y is the deflection or deflection ratio response, β's are the effect coefficients, x represents the coded factors considered in the model and n equals seven variables.

$$y = \beta_0 + \sum_{i=1}^{n} \beta_i x_i + \sum_{\substack{i,j=1 \\ j \neq i}}^{n} \beta_{ij} x_i x_j + \sum_{i=1}^{n} \beta_{ii} {x_i}^2 + \epsilon \tag{7}$$

Based on the results of the screening design, the significant main effects were subsequently analyzed as a 2^k-full factorial. Removing the factors classified as non-significant after the screening analysis provided enough degrees of freedom from the same data set to conduct a test with a full resolution, given a $k < 7$. This is based on the projection properties of the fractional factorials.

Table 13. Factor level combinations for the fractional factorial 2_{IV}^{7-1} design.

Variable	**Name**	**Levels**	
		Low (-)	**High (+)**
x_1	Payload Weight	109 kg	218 kg
x_2	Unit Load Columns	3	5
x_3	Unit Load Layers	3	5
x_4	Pallet Friction	0.20	0.60
x_5	Box Friction	0.20	0.60
x_6	Pallet Stiffness	2.76 GPa	8.27 GPa
x_7	Payload Height	0.762 m	1.778 m

2.3 Results and Discussion

2.3.1 Screening design

The finite element simulation for uniform loading was conducted for both low and high stiffness pallet segments. Table 14 shows the deflection results for the simulations of low and high stiffness boards when loaded with uniformly distributed forces of 109 kg and 218 kg, respectively, equivalent to 4.14 kPa and 8.27 kPa across the pallet segment's top deck.

Table 14. Simulation results for low and high stiffness pallet segments deflection (mm) under uniformly distributed loading.

Pallet Segment	**Stiffness (GPa)**	**Deflection (mm)**	
		108 kg	**218 kg**
Low stiffness	2.76	22.7	44.9
High stiffness	8.27	7.51	14.7

The complete unit load finite element (FE) model was solved for the 64 factor level combinations. Results for each simulation are presented in Appendix B and show the absolute pallet deflection results for each of the simulations, as well as the deflection ratios. Table 15 shows the individual p-values for each of the main factors and all of the second order interactions when using absolute pallet deflection as the main response. Effects and interactions were considered significant when they had a p-value lower than the selected p-value of 0.10 or when a higher order interaction included such effects. The p-value limit of 0.10 was selected to decrease the probability of rejecting variables with lower levels of influence. These are considered to be the factors influencing the load bridging effect which require further exploration.

As expected, the stiffness of the board and the load applied are very significant factors influencing the resulting bending moment. Alternatively, when looking at the effect from the perspective of change in deflection, that is the deflection ratio, weight and stiffness are non-significant factors. From a fundamental perspective, this is understandable since the ratio of deflection accounts for changes in stiffness and weight. It is important to note that these variables are not influencing the effect of other variables. No significant interaction for the deflection ratio analysis includes either payload weight or board stiffness. With this, it can be assumed that the rate of effect for the other factors, such as number of columns or payload height, are independent of the overall payload weight and pallet stiffness. Previous experimental studies have observed that, while maintaining the payload weight as a constant, load bridging is not relevant for high stiffness pallets. This suggests an interaction between pallet stiffness and load bridging (Clayton et al., 2019; Collie, 1984; Fagan, 1982; Molina et al., 2018; Park et al., 2017). Very high stiffness pallets present very low deflection results. Therefore, in order to be able to identify minute changes, extremely high consistency between experimental units and precise measurements are

required. Such precision levels cannot always be achieved for current unit load testing methods. Molina et al. (2018) briefly explored the load bridging effects of modifying pallet stiffnesses but not the weight of the payload. It was noted that higher stiffness pallets carrying a lighter load do not experience significant load bridging. There is a complete absence of a measurable bending response of the pallet.

Besides pallet stiffness and payload weight, it is worth noting that the number of layers in the unit load does not seem to influence the pallet segment's bending results, neither as a main effect nor as part of an interaction of higher order for either of the two analyses. The other four effects that were analyzed were considered significant regardless of the response variable studied. Multiple interactions were also identified as significant, supporting this study's hypothesis that interactions between multiple factors are significant and have not been properly studied before.

Table 15. Fractional factorial *p-values* for the factors and 2nd-interactions of the initial screening design by board deflection (mm) and deflection ratio as main response. Factors below divider were considered non-significant (p-value > 0.10).

Response: Deflection (mm)			**Response: Deflection ratio**		
Term	**P-value**		**Term**	**P-value**	
Pallet Stiffness	< 0.0001		Pallet Friction	< 0.0001	
Pallet Friction	< 0.0001		Columns	< 0.0001	
Weight	0.0001		Height*Pallet Friction	< 0.0001	
Pallet Stiffness*Weight	0.0001		Height	< 0.0001	^
Box Friction	0.0002		Columns*Height	0.0001	
Height	0.0002		Box Friction	0.0001	
Box Friction*Pallet Stiffness	0.0009		Height*Box Friction	0.0006	
Columns	0.0010		Columns*Pallet Friction	0.0309	
Pallet Friction*Pallet Stiffness	0.0015		Pallet Friction*Box Friction	0.0693	
Columns*Height	0.0017		Box Friction*Pallet Stiffness	0.1511	
Height*Pallet Friction	0.0023		Layers*Box Friction	0.2088	
Columns*Pallet Stiffness	0.0104		Columns*Box Friction	0.2088	
Height*Box Friction	0.0134		Weight	0.2789	
Pallet Friction*Weight	0.0328		Columns*Layers	0.3396	
Pallet Friction*Box Friction	0.0397		Layers	0.3489	^
Height*Pallet Stiffness	0.0432		Height*Weight	0.4402	
Columns*Weight	0.0695		Layers*Pallet Friction	0.4586	
Box Friction*Weight	0.1127		Height*Pallet Stiffness	0.4966	
Layers*Pallet Friction	0.1460		Pallet Stiffness*Weight	0.6204	
Columns*Box Friction	0.2057		Layers*Pallet Stiffness	0.6424	
Columns*Pallet Friction	0.2075		Layers*Height	0.7101	
Height*Weight	0.5336		Pallet Friction*Weight	0.8768	
Layers*Pallet Stiffness	0.6632		Layers*Weight	0.9013	
Layers*Height	0.7221		Box Friction*Weight	0.9013	
Layers*Weight	0.8300		Pallet Stiffness	0.9714	^
Layers*Box Friction	0.8668		Columns*Pallet Stiffness	0.9753	
Columns*Layers	0.9477		Columns*Weight	1.0000	
Layers	0.9577	^	Pallet Friction*Pallet Stiffness	1.0000	

2.3.2 2^4 full factorial design projection

A 2^4 full factorial design analysis was conducted using the model results from the screening design. This took advantage of the projection properties of the fractional designs. Deflection ratios were considered the main model response. The main factors were number of columns, payload height, pallet friction, and box friction. According to the screening design results, pallet stiffness, payload weight, and number of layers do not significantly affect the pallet bending ratio and therefore were excluded. Table 16 shows the effect summary p-values of the analysis. It was confirmed that there are four main effects significant in load bridging. Certain second order interactions were also found to be of significance in the load bridging effect, as well as multiple third-order interactions. This preliminary exploration shows the complexity of the load bridging effect, where every factor must be studied in coordination with the changes to other factors. It is not feasible to conduct such experimentation with traditional physical experimental methods.

Table 16. Results of the 2^4-full factorial design ANOVA (p-values) for the significant effects of on the board deflection ratio.

Source	***p-value***	
Pallet Friction	<0.0001	
Columns	<0.0001	
Height	<0.0001	
Box Friction	<0.0001	
Height*Pallet Friction	<0.0001	
Columns*Height	<0.0001	
Height*Box Friction	<0.0001	
Columns*Height*Pallet Friction	0.0002	
Columns*Height*Box Friction	0.0013	
Columns*Pallet Friction	0.0025	^
Height*Pallet Friction*Box Friction	0.0032	
Columns*Box Friction	0.0749	^
Columns*Pallet Friction*Box Friction	0.2725	
Pallet Friction*Box Friction	0.2773	^
Columns*Height*Pallet Friction*Box Friction	0.5086	

3 Development of a simplified model to predict unit load segment bending

3.1 Development and cross-validation of a Gaussian Process model

From the results of the screening analysis of the unit load bending model, four main factors were identified as significant. In order to develop a model that could accurately predict the bending behavior of the boards supporting the payload and the influence of different payload characteristics, each variable was limited to specific ranges, as follows. The number of columns, which relate to the box sizes, was limited to 3, 4, 5 and 6 columns of stacked boxes along the length of the board. Larger boxes were not part of the validated scope of the model, and smaller boxes, having seven or more columns, were considered too small to be commonly handled on unit loads without any additional shippers. The height of the boxes, in the model referenced as the overall height of the payload, was limited from relatively short unit loads of 508 mm to tall unit loads of 2.03 m. Very short unit loads, or abnormally tall ones, were not included in the model scope.It is important to reinforce that the number of layers, or the number of divisions that the unit load has along its height, was not considered a significant factor within these ranges. Even though pallet stiffness was not considered a significant factor, this was validated only within the ranges studied, from 2.76 GPa to 8.27 GPa. These values are equivalent to a multiple use plastic pallet and a wooden pallet with characteristics similar to a standard pool pallet (Park, 2015). Stiffer pallets using different materials, such as metal, might present different behavior, as well as very lightweight plastic pallets; therefore, these are not included in the model. The payload weight range for the unit load segment modeled was the same as for the screening design study, from 109 kg to 218 kg. When comparing the payload weight for a full unit load on a standard GMA pallet (1,219 mm x 1,016 mm), this range correlates to 523 kg to 1045 kg, using the same pressure level. Although this model's accuracy is expected to be acceptable, even around the limits, moving further away from this range could drastically reduce the prediction's accuracy.

The coefficient of friction (CoF) ranges for the different contact interactions were limited based on the commonly identified ranges for each material. The CoFs of the pallet's top deck's contact with corrugated fiberboard were based on the findings by O'Dell et al. (1998), where multiple pallet decks were evaluated for friction characteristics. Plastic pallets with little-to-no surface treatment presented coefficients around 0.30, while wooden pallets had values under 0.60. To account for variability, the model input was limited to between 0.20 and 0.70. Higher frictions

or the use of lips at the edges of the pallets might affect the movement of the components and therefore were not considered. Contacts between corrugated boxes were shown to be between 0.50 and 0.60 (See Chapter 1). To account for the possibilities of different packaging materials, the model range for the coefficient of friction between the box contacts was between 0.20 and 0.70. Using material treatments that significantly increase friction, such as tie sheets, could generate different interactions between the components.

In the more traditional approach developing response surfaces, the experimenter uses the sequential experimentation philosophy, working towards the identification of a small region of interest in order to determine an optimum solution, typically approximated as a low-order polynomial. This study sought to replicate the actual response throughout the whole response region, not only the lowest or highest pallet deflection, since optimization was not the only objective. In order to satisfy this, a space filling design was used in a manner that could cover the complete response region. Additionally, no replication was possible since the finite element model developed was a deterministic model. A space filling design that satisfied the requirements by spreading the design points evenly throughout the region of experimentation was the Latin Hypercube Design (LHD). A Latin Hypercube, with 40 runs and 4 dimensions (*40x4* matrix), was generated using the computer software JMP Pro 15 which conducts a random permutation to determine the values of each variable for each run. Table 17 presents the factor level combinations for each model run. The same design was used independently for the model of each quantity of columns (3, 4, 5, or 6 columns). A total of 160 finite element model simulation responses were required.

To fit the deterministic responses from the finite element simulations, a Gaussian process model was used. The Gaussian Process model is $y = \mu + z(\mathbf{X})$, where $z(\mathbf{X})$ is Gaussian stochastic process with covariance matrix $\sigma^2\mathbf{R}(\boldsymbol{\theta})$. $\mathbf{R}(\boldsymbol{\theta})$ is a correlation matrix with the elements shown in (8). Values for r_{ij} are the correlations between responses at two design points. The parameters μ and θ_s, s = 1, 2,…,k were estimated using the method of maximum likelihood.

$$r_{ij} = e^{-\sum_{s=1}^{k} \theta_s (x_{is} - x_{js})^2} \qquad (8)$$

Predicted values for the responses of the Gaussian Process Model are generated from (9). $\hat{\mu}$ and $\hat{\theta}$ are the maximum likelihood estimates of the model parameters μ and θ, and $r'(x) = [r(x_1, x), r(x_2, x), \ldots, r(x_n, x)]$. This prediction equation contains one term for each of the design points in the original experiment.

$$\hat{y}(x) = \hat{\mu} + r'(x)R(\hat{\theta})^{-1}(y - j\hat{\mu}) \tag{9}$$

In order to generate the most accurate model and to validate the prediction results from the Gaussian Process model, a *k*-fold cross validation was conducted. The response data set for each per column model was divided into five equal parts. The GP model was run five separate times with only four-fifths of the data. The remaining data points were used to conduct the cross validations. The model with the data set that provided the highest accuracy was selected as the resulting statistical model. Goodness of fit and predictive performance was evaluated by comparing the Root Mean Square Error (RMSE, **Error! Reference source not found.**) of the predictions against the finite element model simulation results, as well as the Mean Absolute Percent Error (MAPE, **Error! Reference source not found.**). Both error measurements together provided enough confidence to determine model accuracy.

$$RMSE = \sqrt{\sum_{i=1}^{n} \frac{(\hat{y}_i - y_i)^2}{n}} \tag{10}$$

$$\text{MAPE} = \frac{1}{n} \sum_{i=1}^{n} \left| \frac{y_i - \hat{y}_i}{y_i} \right| \tag{11}$$

Were $\hat{y}_i$ is the deflection ratio value predicted by the Gaussian Process Model and y_i is the resulting value from the simulation using the finite element model. n corresponds to the number of data points for each individual analysis. For the specific 5-fold cross-validations conducted for each number of columns, $n = 32$.

Table 17. Latin Hypercube Design factor levels for Gaussian Process model training data and corresponding finite element model simulation results as a ratio of deflection per unit load model.

ID	Height (mm)	Pallet Friction	Box Vertical Friction	Box Horizontal Friction	Deflection Ratio by Model			
					3 columns	4 columns	5 columns	6 columns
Run 001	508.00	0.66	0.48	0.41	0.38	0.36	0.33	0.39
Run 002	547.08	0.47	0.26	0.64	0.35	0.42	0.56	0.64
Run 003	586.15	0.61	0.24	0.34	0.35	0.37	0.53	0.64
Run 004	625.23	0.43	0.39	0.43	0.37	0.42	0.61	0.64
Run 005	664.31	0.33	0.67	0.61	0.20	0.44	0.48	0.65
Run 006	703.38	0.46	0.52	0.23	0.48	0.41	0.46	0.65
Run 007	742.46	0.28	0.30	0.30	0.65	0.43	0.58	0.62
Run 008	781.54	0.48	0.61	0.44	0.15	0.33	0.44	0.49
Run 009	820.62	0.25	0.34	0.55	0.36	0.42	0.56	0.65
Run 010	859.69	0.70	0.29	0.53	0.26	0.47	0.55	0.64
Run 011	898.77	0.24	0.57	0.25	0.60	0.38	0.55	0.65
Run 012	937.85	0.65	0.64	0.29	0.10	0.20	0.30	0.34
Run 013	976.92	0.56	0.44	0.60	0.22	0.43	0.55	0.62
Run 014	1016.00	0.69	0.62	0.52	0.14	0.24	0.30	0.34
Run 015	1055.08	0.35	0.49	0.69	0.29	0.43	0.62	0.63
Run 016	1094.15	0.60	0.41	0.33	0.20	0.45	0.55	0.66
Run 017	1133.23	0.52	0.66	0.67	0.17	0.31	0.41	0.57
Run 018	1172.31	0.29	0.65	0.46	0.27	0.44	0.57	0.66
Run 019	1211.38	0.42	0.25	0.56	0.32	0.43	0.58	0.64
Run 020	1250.46	0.20	0.43	0.39	0.34	0.46	0.59	0.64
Run 021	1289.54	0.38	0.42	0.24	0.29	0.42	0.63	0.63
Run 022	1328.62	0.41	0.47	0.48	0.28	0.43	0.57	0.64
Run 023	1367.69	0.30	0.23	0.37	0.32	0.45	0.59	0.64
Run 024	1406.77	0.53	0.20	0.32	0.34	0.45	0.60	0.64
Run 025	1445.85	0.49	0.70	0.38	0.14	0.32	0.42	0.66
Run 026	1484.92	0.64	0.32	0.49	0.27	0.43	0.59	0.65
Run 027	1524.00	0.23	0.33	0.58	0.32	0.44	0.58	0.64
Run 028	1563.08	0.67	0.51	0.20	0.18	0.32	0.40	0.43
Run 029	1602.15	0.34	0.69	0.62	0.24	0.47	0.55	0.64
Run 030	1641.23	0.62	0.53	0.47	0.17	0.32	0.42	0.43
Run 031	1680.31	0.58	0.35	0.70	0.27	0.45	0.62	0.64
Run 032	1719.38	0.21	0.55	0.51	0.39	0.46	0.58	0.65
Run 033	1758.46	0.26	0.56	0.28	0.33	0.45	0.58	0.63
Run 034	1797.54	0.39	0.46	0.65	0.29	0.45	0.63	0.64
Run 035	1836.62	0.37	0.28	0.21	0.31	0.44	0.58	0.64
Run 036	1875.69	0.55	0.38	0.35	0.26	0.45	0.62	0.64
Run 037	1914.77	0.44	0.21	0.57	0.34	0.45	0.59	0.65
Run 038	1953.85	0.32	0.37	0.42	0.36	0.45	0.59	0.65
Run 039	1992.92	0.57	0.60	0.66	0.19	0.32	0.40	0.46
Run 040	2032.00	0.51	0.58	0.26	0.19	0.39	0.54	0.51

3.2 Gaussian Process Model Results and Discussion

Simulations were conducted using the unit load segment finite element model for each of the 160 data points determined by the Latin Hypercube design. Results are presented in Table 17. This was the data input needed to compute the Gaussian Process regression. Root Means Square Error (RMSE) and Mean Absolute Percent Error (MAPE) results are presented in Table 18. For each of the unit load representations, the model with the lowest MAPE and RMSE was selected. The data subset of k=4 was selected as the one with the best goodness of fit for all four models. The overall error level of the GP model was considered low, with an average RMSE of 0.05 and a MAPE of 0.08. The highest error level was for the model with three columns, and it had a RMSE of 0.05 and a MAPE of 0.13. The highest prediction accuracy was presented in the six column model, with a RMSE of 0.03 and a MAPE of 0.03.

Table 18. Root Means Square Error (RMSE) and Mean Absolute Percent Error (MAPE) for the Gaussian Process Prediction for each cross validated data set.

		Model				
Cross validation index (k)	Error Measurement	3 columns	4 columns	5 columns	6 columns	Model Average
1	MAPE	0.26	0.06	0.10	0.05	0.12
2		0.22	0.17	0.07	0.04	0.12
3		0.24	0.06	0.07	0.07	0.11
4		0.13	0.06	0.09	0.03	0.08
5		0.12	0.09	0.08	0.17	0.11
1	RMSE	0.06	0.04	0.05	0.05	0.05
2		0.05	0.07	0.04	0.02	0.05
3		0.08	0.03	0.04	0.06	0.06
4		0.05	0.04	0.06	0.03	0.05
5		0.10	0.05	0.06	0.09	0.08

The complete reports for the selected models are presented in Appendix B. Appendix C provides the Python scripts used to generate the predicted values ($\hat{y}$) for each model. The Gaussian Process model provides a reliable method to efficiently predict the ratio of change in the bending of a unit load segment, with a low error estimate. This is a significant aspect, since finite element modeling places a high initial cost to conduct everyday analysis of unit load design.

4 Study of the significant factors influencing load bridging

4.1 Simplified unit load model scope and limitations

With the goal of better understanding of each of the significant factors influencing load bridging, a detailed analysis was conducted. The GP model was applied to study the behavior of each factor, in an almost One-Factor at a Time (OFAT) style of analysis, but this study also took into consideration major interactions. The results inform and support the decision-making process of unit load design. Given the many interactions acting upon the bending response of the board, the full model should be applied to specific unit load evaluations. The analysis was limited to the dimensions studied in the Latin Hypercube Design in the previous section, since that was the range of the input data of the model. A summary of the factor ranges is shown in Table 19. All other variables not included here were also limited to this project's scope.

Table 19. Factor limiting ranges for each significant variable in the Gaussian Process Model.

Factor	**Factor Range**	
	Minimum	**Maximum**
Unit Load Columns	3	6
Pallet Friction	0.20	0.70
Box Friction	0.20	0.70
Payload Height (mm)	508	2,030

4.2 Analysis of the internal stresses' distribution and trends

The changes in stress distributions when varying different payloads can provide additional insights into how pallet performance can be affected besides the bending response studied.

As previously mentioned, pallets are commonly evaluated applying uniformly distributed loading on the pallet top deck. A similar analysis on the pallet analog developed provides a maximum Von Mises equivalent stress of 6.78 MPa on the center span of the structure, when loaded with a uniform pressure of 4.14 kPa. The aforementioned pressure is equivalent to 109 kg of total load for the unit load segment and the resulting plot is shown in Figure 23. The pallet

analog was modelled after PMMA which has a yield strength of 72 MPa (Altuglas International, 2006). The current internal stresses under uniform loading represent 9.37% of yield.

As it is shown in Figure 24, the Von Mises equivalent stress presents a distribution that closely follows a parabola, with a symmetric distribution along the pallet analog and with the vertex matching the center of the unsupported span.

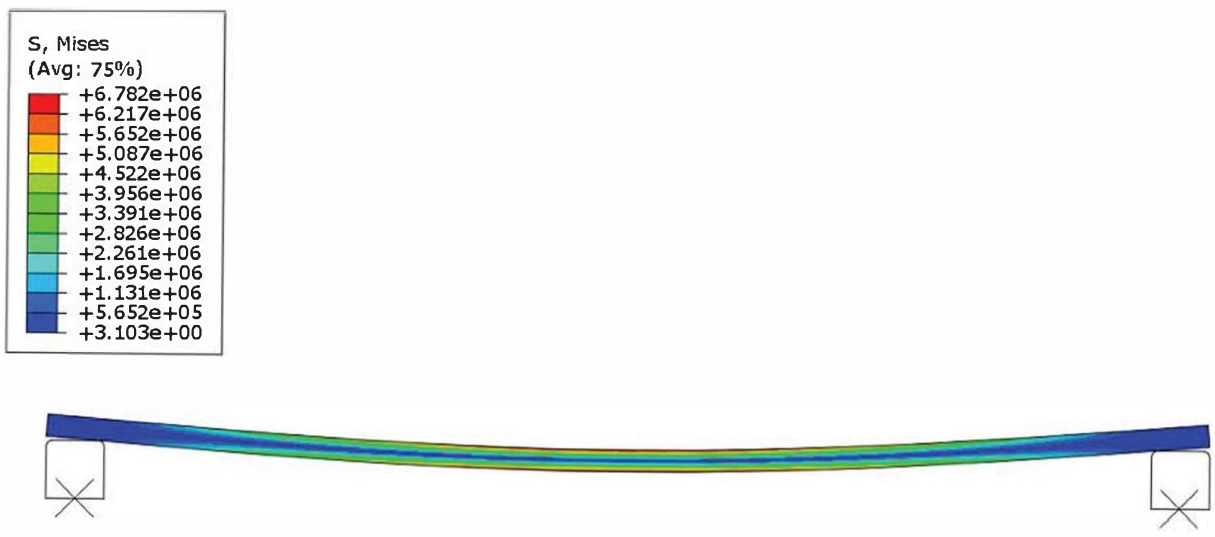

Figure 23. Plot of the equivalent Von Mises stress (Pa) of the pallet analog under uniformly distributed loading of 4.14 kPa.

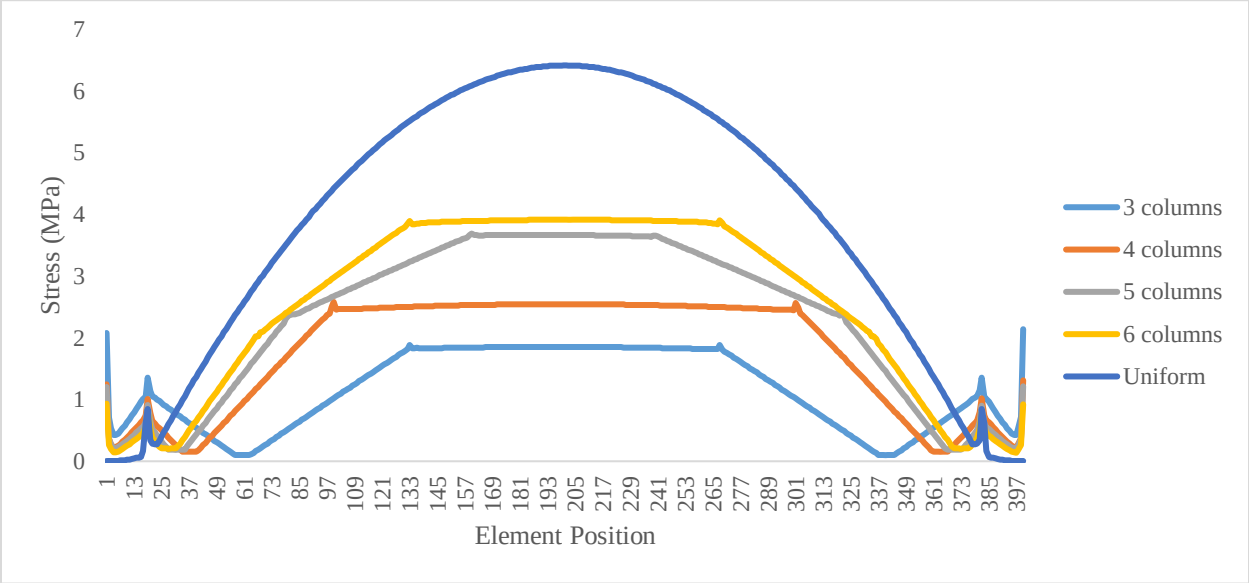

Figure 24. Plot of the maximum equivalent Von Mises stresses (MPa) for the unit load segments under five different payloads.

When discrete loading is applied through the use of stacked corrugated boxes, stress distribution changes. As shown in Figure 24, the distribution of stresses along the pallet analog changes as the payload characteristics are changed. In this example, each one of the payloads has the same characteristics except for the dimensions of the box. Unit load height and all coefficients of friction remained constant. Table 20 shows the percent change for the deflection response and for the equivalent Von Mises stresses. Although the change is not completely equivalent, both variables presented a similar trend of change when decreasing the size of the boxes. Figure 25, Figure 26, Figure 27, and Figure 28 show the equivalent Von Mises stress plots for each of the unit load segments studied. Using the Von Mises stresses for the high strain, ductile material modelled (PMMA), allows for a reasonable estimation of the yield strength of the pallet analog. The reduction in the experienced peak stresses when comparing the specific payloads versus uniform loading indicate that the pallet analog yield strength can increase from 63.7% (6 columns) to 245% (3 columns). This increase is generated exclusively through the load bridging effect.

In analyzing the stress concentrations along the pallet analog, every payload presented high stresses along the ends of the board, where boxes were contacting the corners of the pallet analog and at the location of the rigid supports. Since these pressure concentrations were considered a

result of the modeling simplification, they can be ignored for the purposes of the load bridging analysis. Excluding these sections, most of the stress distributions followed a clear trend, where the stresses present a change in each of the locations where the boxes edges contacted the pallet deck.

The knowledge provided by the trends of the change in the internal stresses, and how the closely relate to the bending response can inform the unit load designers about potential changes in pallet strength performance that must be further validated.

Table 20. Changes in deflection and maximum equivalent stresses from uniformly distributed loading to discrete number of boxes.

	Deflection (mm)	Change	V. Mises Stress (MPa)	Change
Uniform	22.70	-	6.42	-
3 columns	7.72	-66%	1.85	-67%
4 columns	10.44	-54%	2.55	-57%
5 columns	13.39	-41%	3.67	-41%
6 columns	14.53	-36%	3.92	-37%

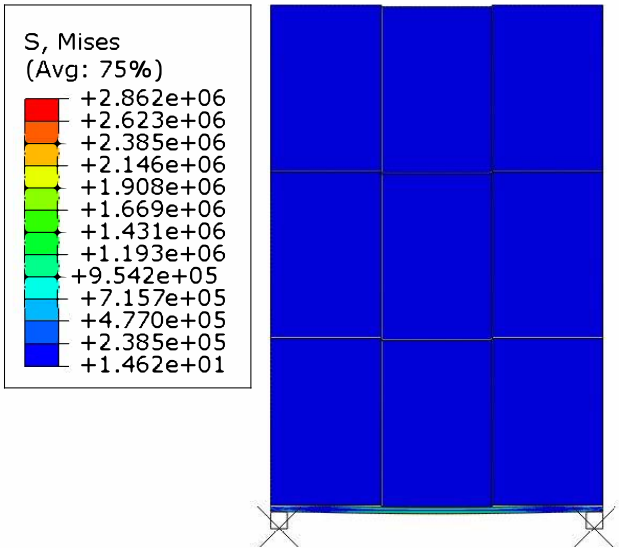

Figure 25. Plot of the equivalent Von Mises (MPa) stress of the unit load segment under a 3 column payload.

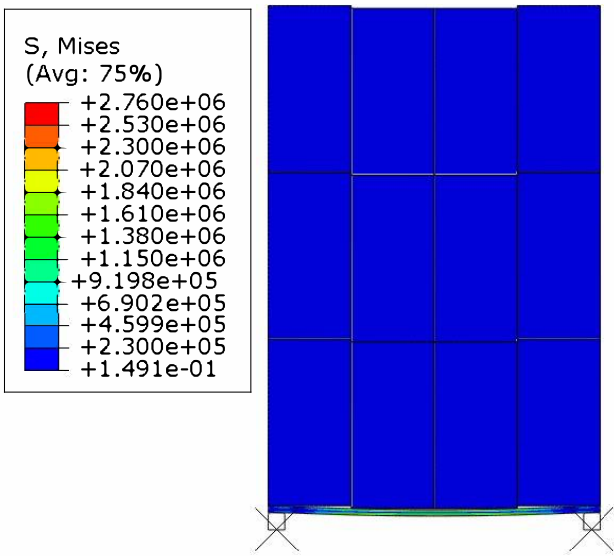

Figure 26. Plot of the equivalent Von Mises (MPa) stress of the unit load segment under a 4 column payload.

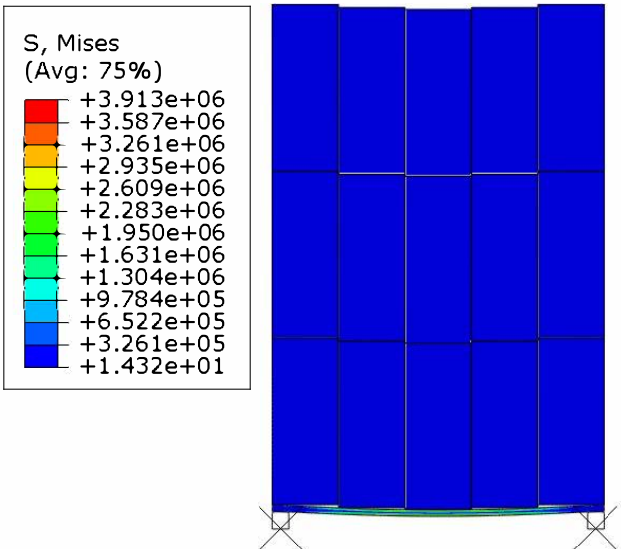

Figure 27. Plot of the equivalent Von Mises (MPa) stress of the unit load segment under a 5 column payload.

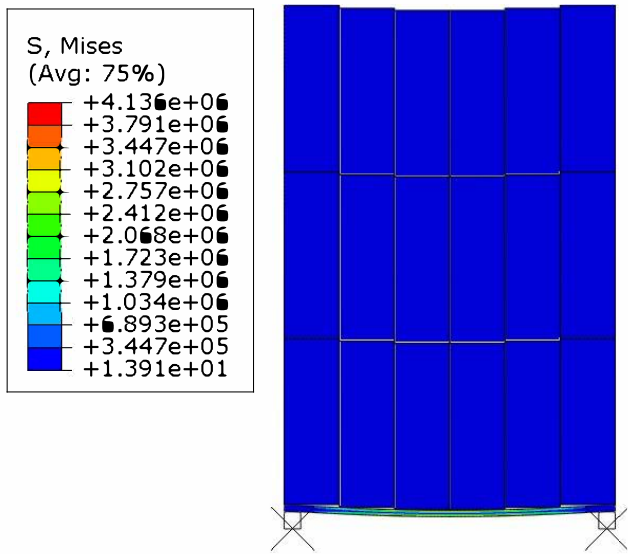

Figure 28. Plot of the equivalent Von Mises (MPa) stress of the unit load segment under a 6 column payload.

4.3 Analysis of the load bridging effects and trends by each significant factor

4.3.1 Effect of number of columns on the bending of a board

Although the Gaussian Process models were formulated independently for unit loads with different numbers of columns, the results can be grouped together to identify relevant trends in the data. Previous researchers have identified that the size of the box has a very significant influence on the load bridging levels that are generated (Clayton et al., 2019; Park et al., 2017). In general, it is commonly assumed that smaller boxes generate higher bending. This hypothesis is based on the application of the discrete load on the pallet deck. Infinitely small boxes will resemble a uniformly distributed load, and therefore, generate the same bending as uniform load applicators. Figure 29 shows that same overall trend for most scenarios studied. It is of high relevance to note that when boxes are longer along the length (three columns), but the payload is relatively short (700 mm) and the box-to-pallet CoF is low (0.30), this observed trend is no longer valid. In this scenario, the unit load with three columns of boxes presented a deflection ratio of 0.65, while that for four columns was 0.43; five columns was 0.59; and six columns was 0.64. Unit loads with these characteristics present a higher deflection than those with smaller boxes, almost matching the same deflection level as a unit load with six columns. The interaction of the box length dimension with low friction properties generated higher deflection than one driven mostly by box

size. As observable in Figure 30, the rotational movement of the boxes when the board was under load was different for the unit load of three columns (Figure 30 (a)) than for the ones with a higher number of columns. The same change in the movement of the boxes was generated by maintaining the number of columns but either increasing the friction coefficient of the pallet (Figure 30 (b)) or the overall height of the payload (Figure 30 (c)). This confirmed that no generalization can be made regarding the effect of box size on load bridging without considering the remaining interacting factors as well. A key aspect in reducing the board deflection was to prevent the rotating movement of the packages. This was possible through many different combinations of factors. Because of this, no specific attempts to quantify a threshold point were made, avoiding the misinterpretation of the model results.

The effect of the pallet friction levels can be observed for a commonly used unit load scenario. The unit load is supported on a 1,219 mm x 1,016 mm wooden pallet (0.45 pallet top deck friction) and contains corrugated boxes made of kraft paper (average box friction of 0.45) that are stacked to a total height of 1,200 mm. Everything else remaining equal, increasing the box length of such a unit load from 169 mm to 338 mm reduces the experienced initial deflection by 60%, from a ratio of 0.64 to 0.25. Taking into account the relationship between box size and pallet performance can influence the design process of tertiary packaging.

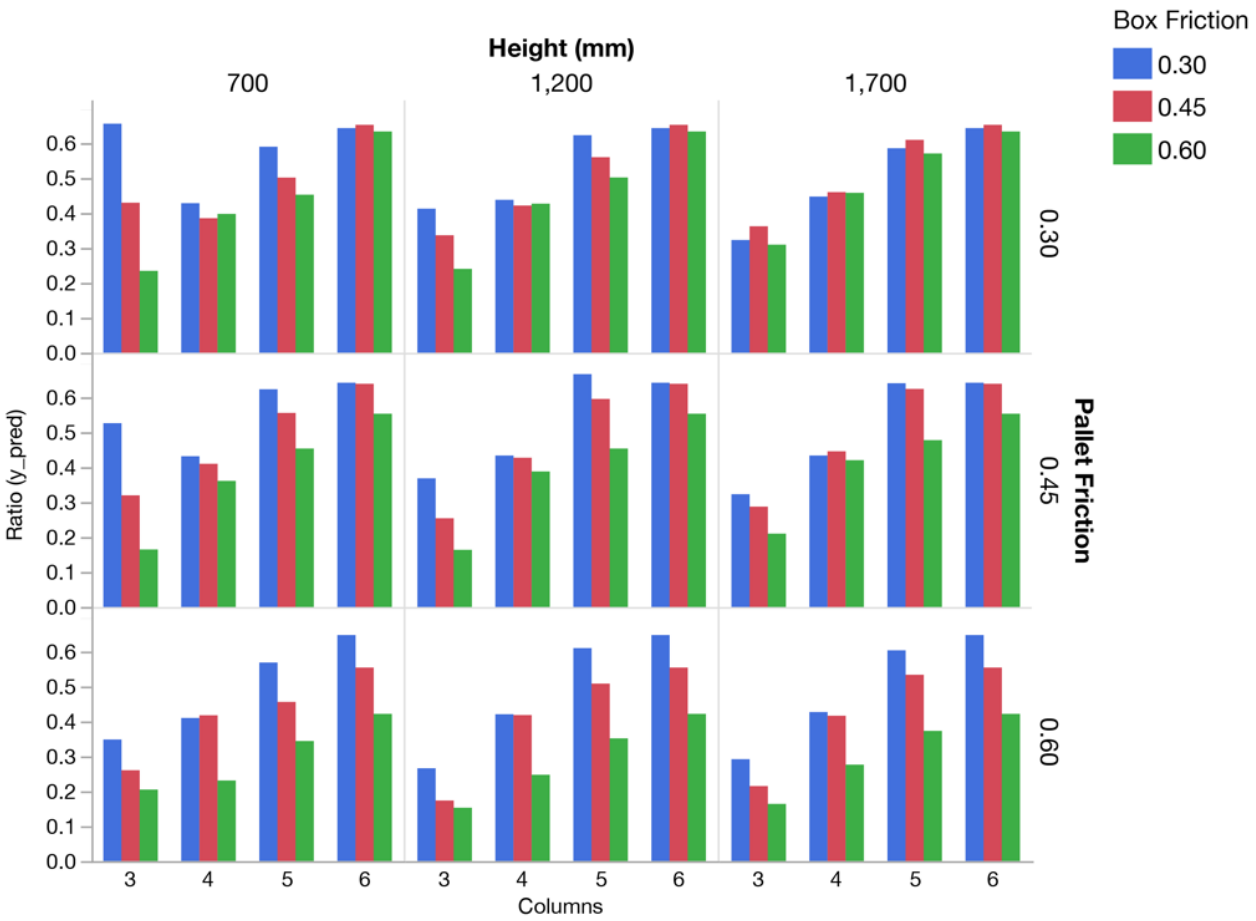

Figure 29. Effect of number of columns on board bending ratio by height (mm), box friction and pallet friction coefficients.

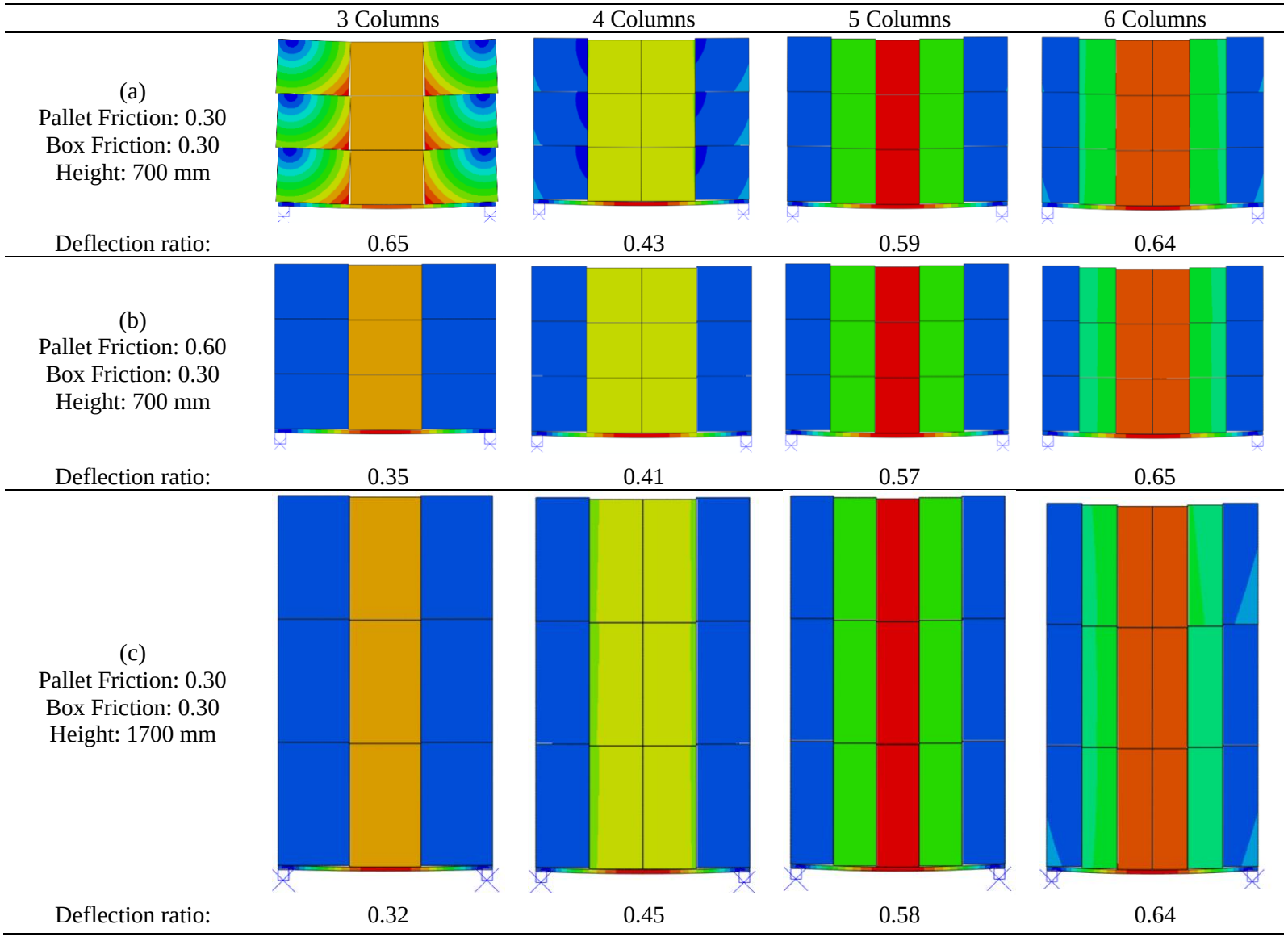

Figure 30. Finite element model simulations for 3, 4, 5, and 6 columns and three combinations of payload height and pallet and box friction coefficients. Colors shown represent displacement (U). Blue equals no movement, red equals large displacements.

4.3.2 Effect of the payload height on the bending ratio of a board

The height of the payload was identified as a significant factor influencing the bending of the pallet deck. When analyzing the height, on a range between 500 mm and 2 m and for a range of friction coefficients and number of columns, it can be observed that the effect of height is highly dependent on the other variables, as shown in Figure 31. Park (2015) conducted preliminary experimentations on the effect of payload height. Using large, corrugated boxes (arranged in two columns), Park identified the fact that by increasing the height of the unit load, there was a significant decrease in the overall board bending response. A similar trend can be observed in the model's response for unit loads consisting of three columns. But, as the boxes become smaller, the effect of height was no longer relevant. The movement of the boxes, such as in Figure 30 for six columns, was mostly downwards. There was no rotational movement on unit loads with low payload heights having the same total weight per column, so the load perceived by the board was not changed, therefore it generated the same board deflection ratios. For the majority of boxes used in the field, changing the height of the boxes or adding additional layers of the same package will not significantly change the resulting deflection.

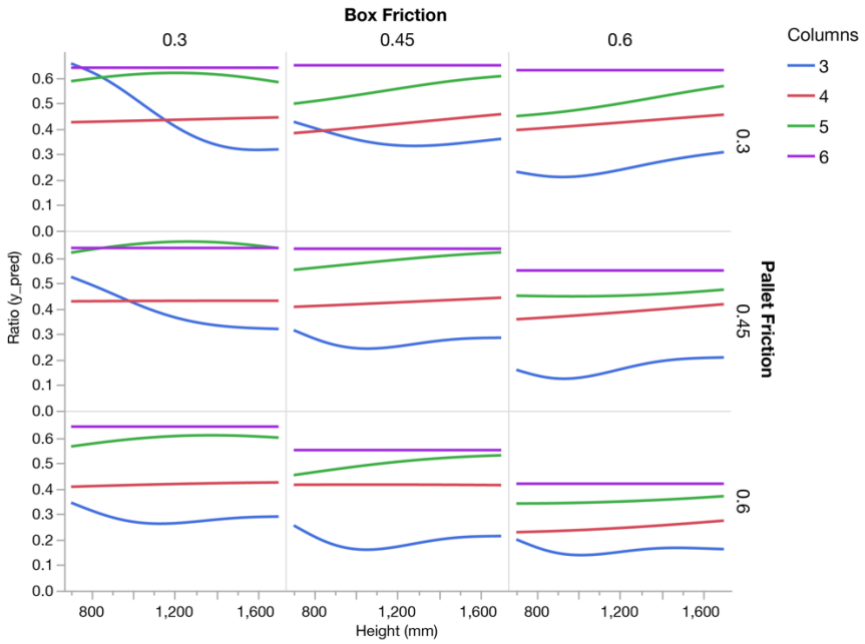

Figure 31. Effect of payload height (mm) on board bending ratio by pallet friction, box friction and number of columns.

4.3.3 Effect of the pallet friction coefficient on the bending ratio of a board

As can be observed in the results (Figure 32), there was an inverse relationship between the deflection ratio of the board and the pallet CoF for most scenarios studied. When the friction of the pallet deck increased, the bending of the board decreased. This trend has the potential to influence the design of plastic pallets. Pallet safe load carrying capacity can be determined by finding the maximum deflection for safe handling or determining the load at which certain pallet components begin to fail (ASTM International, 2009; ISO, 2011a). Plastic pallets, given the commonly low stiffness of their structures, tend to have a maximum carrying capacity determined by the bending level under load. Affecting the resultant bending of the boards by simply increasing the friction can potentially increase the carrying capacity of a pallet. As with other factors, the interactions between number of columns, payload height, and box friction determine the resulting effects, and therefore, it all must be studied as a system. However, unit loads carrying packages with low friction levels, such as the equivalent to returnable plastic containers (RPC), did not present such changes in board deflection, except in the case of larger boxes.

The effect of the pallet friction can be observed for commonly used unit load scenarios. Take a unit load, supported on a 1,219 mm x 1,016 mm pallet, and containing 340 mm x 250 mm x 400 mm corrugated boxes made of kraft paper (with an average box friction of 0.45), and stacked three high (having 1,200 mm in total height). In this scenario, increasing the frictional forces by going from a pallet friction coefficient of 0.30 to 0.60 can decrease the bending response by 48%. Keeping the same characteristics but using smaller boxes, 170 mm x 254 mm x 400 mm (in six columns), and increasing the pallet friction coefficient at the same rate, only decreases the bending response by 15%.

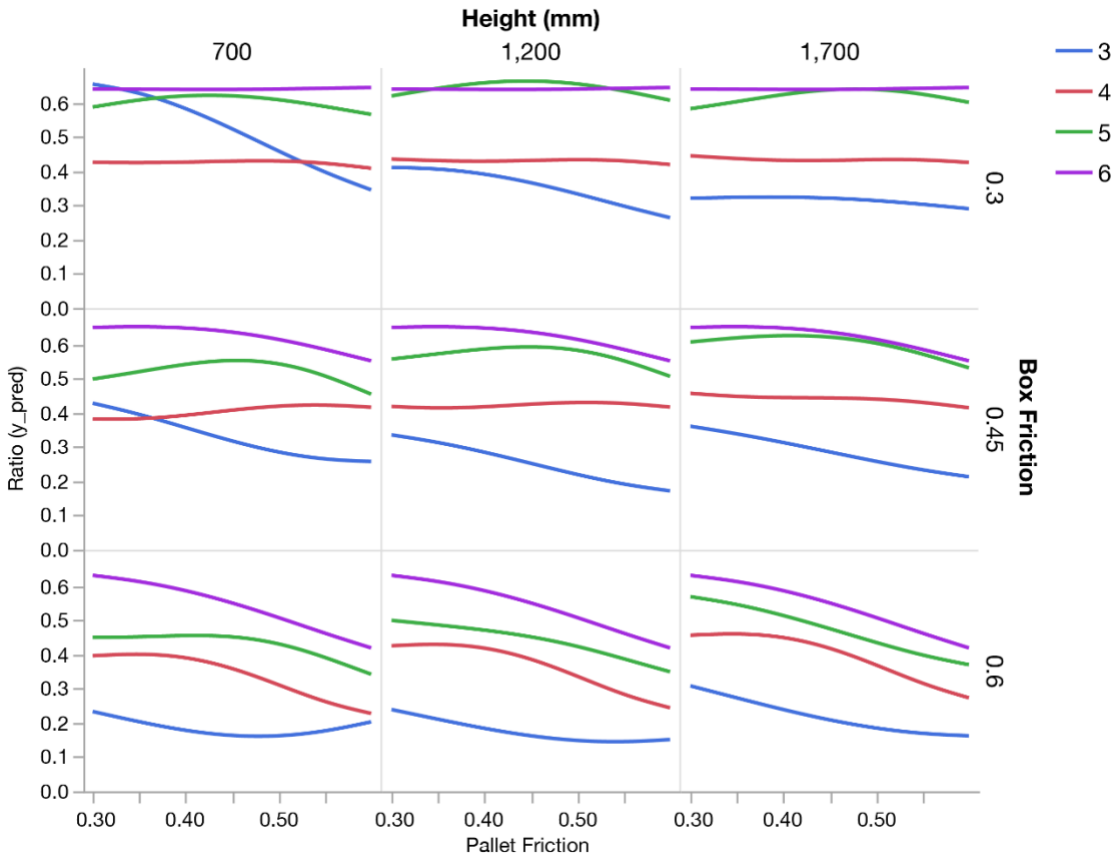

Figure 32. Effect of pallet friction coefficient on board bending ratio by payload height (mm), box friction and number of columns.

4.3.4 Effect of the package friction coefficients on the bending ratio of a board

The friction coefficient of the packages was observed to be a factor that when increased, tended to reduce the bending response of the boards. The rate of change was more pronounced for larger boxes, when there was larger contact area between the boxes. This can be clearly observed in Figure 33. Furthermore, the friction coefficient for the packages were modeled differently for the horizontal and the vertical box surfaces. These components do not affect the bending response equally. Increasing the friction properties of the vertical package surfaces generated a reduction in the bending of the boards for most of the studied scenarios (Figure 34). Alternatively, changes on the frictional properties of the horizontal box surfaces only generated a change in board deflection for unit loads with large boxes (Figure 35). As seen in Figure 30 (a), the unit load with three columns presented a rotational motion of the boxes. Increasing the horizontal friction between boxes reduced this motion and affected the resulting deflection by decreasing it. Unit loads where the aspect ratio or other factors already prevented rotational motion, were not affected by changes in the horizontal CoFs.

The effect of changes in package friction coefficients can be observed for a commonly used unit load scenario. The unit load is supported on a 1200 mm x 1000 mm wooden pallet (0.45 pallet friction) and contains 340 mm x 250 mm x 400 mm corrugated boxes made of kraft paper (average box friction of 0.45) that are stacked three high (1,200 mm total height). By changing the friction of the packages on the vertical surfaces from a coefficient of 0.30 to 0.60, while keeping the horizontal friction fixed at 0.45, it decreases the experienced deflection by 50.4%. The same scenario but with smaller 170 mm x 125 mm x 400 mm corrugated boxes (in six columns) generates a deflection reduction of only 15%. Alternatively, fixing the vertical friction at 0.45, but increasing the horizontal friction coefficient from 0.30 to 0.60 can reduce the deflection by 22.1% for large boxes, but does not generate any significant change in a unit loads carrying small boxes.

A feature that could impact the overall effect of package friction on the bending of a unit loads is the application of containment mechanisms. Methods such as stretch wrapping can restrain the boxes and prevent any rotation or displacement. The increased unitizing forces would increase the overall load bridging effect and potentially reduce the deflection experienced by the unit load. By not considering stretch wrapping or other containment methods commonly utilized, this model provides a conservative estimation of the load bridging effect. Further refinements can be

developed in order to take into account all of the many possible modifications available for unit loads.

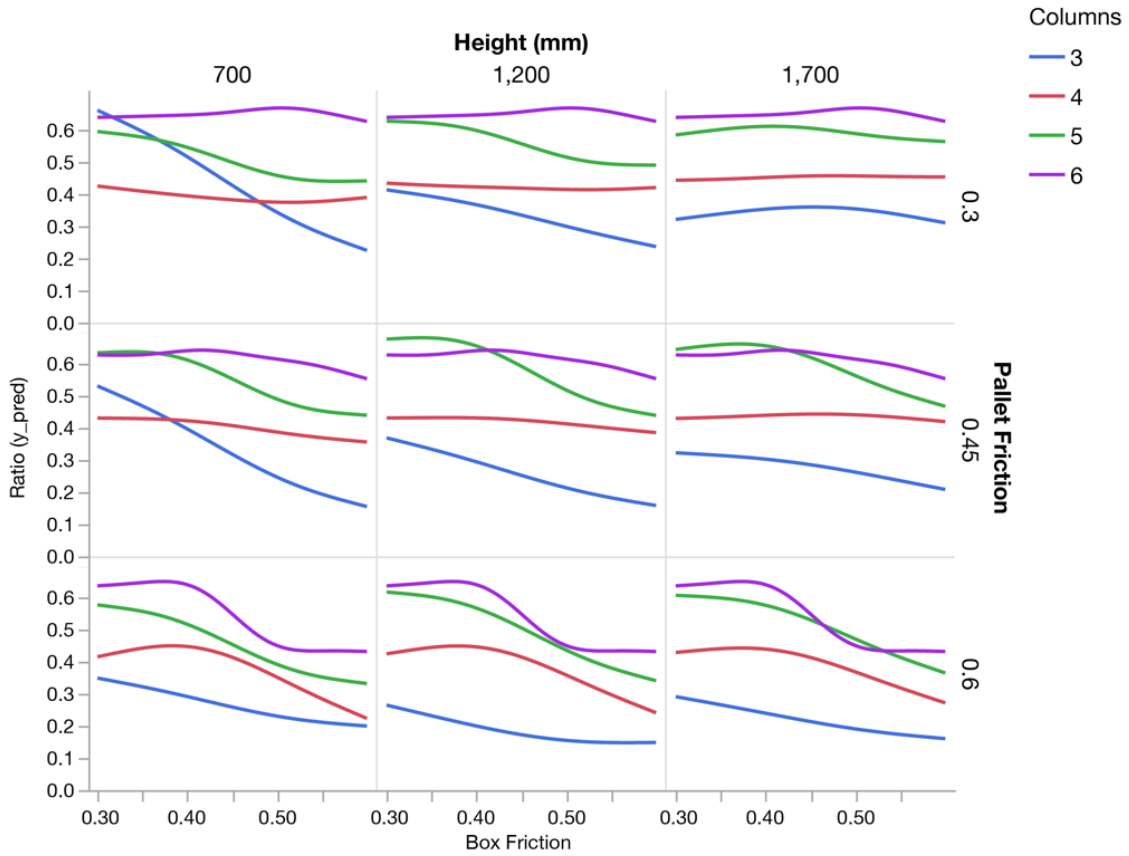

Figure 33. Effect of the friction coefficient of packages on board bending ratio by pallet friction, payload height (mm) and number of columns.

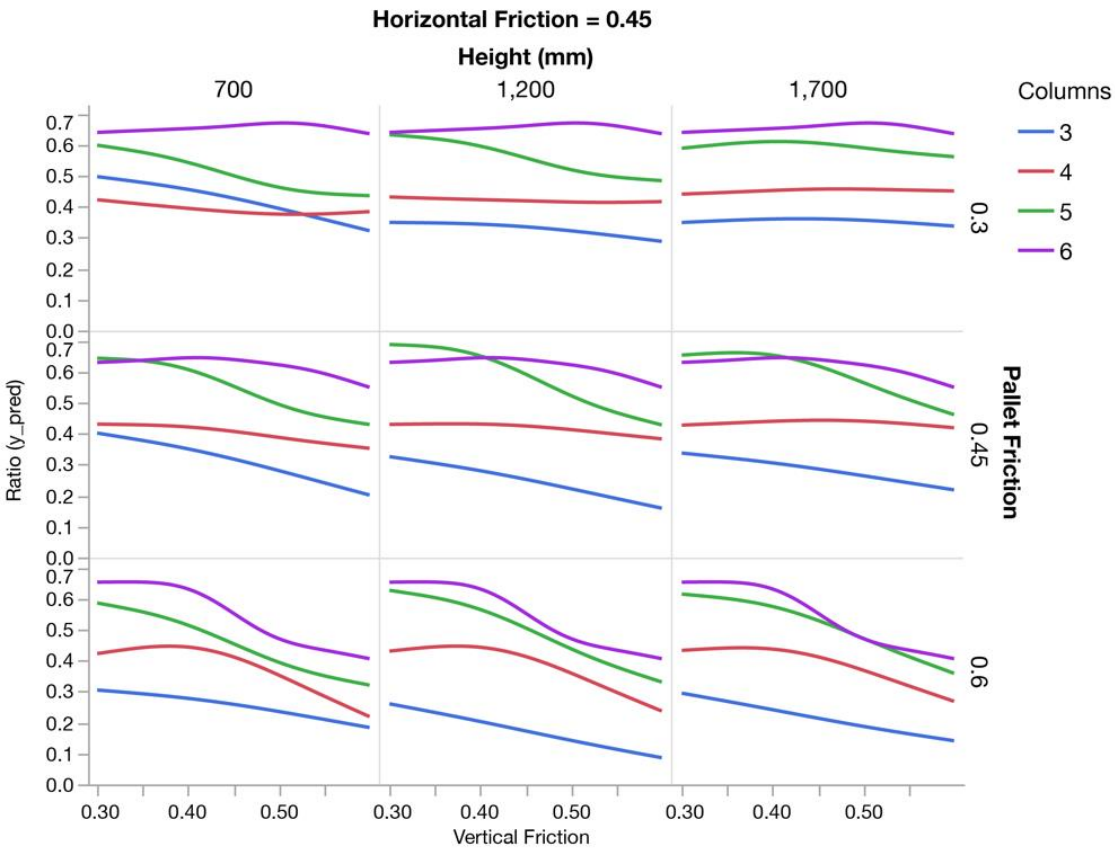

Figure 34. Effect of the friction coefficient of the vertical surface of the packages on board bending ratio by pallet friction, payload height (mm) and number of columns, with a fixed coefficient of friction of the horizontal surface of 0.45.

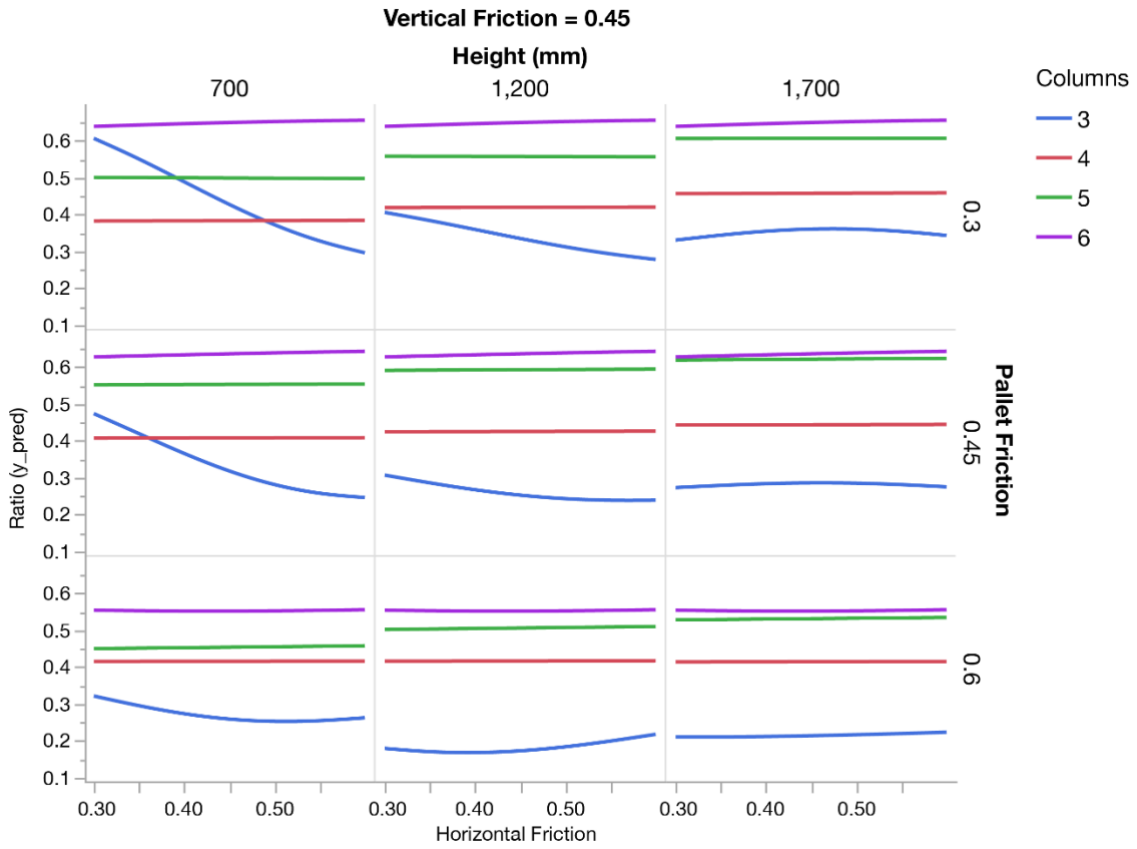

Figure 35. Effect of the friction coefficient of the horizontal surface of the packages on board bending ratio by pallet friction, payload height (mm) and number of columns, with a fixed coefficient of friction of the vertical surface of 0.45.

4.4 Discussion on the factor interactions

After conducting the analysis for the individual factors that influence the load bridging effect, it was evident that the existent interactions between the factors increased the complexity of the trends of the response. Traditional approaches to packaging design have focused on simple adjustment factors for specific characteristics, such as reducing box strength by a certain percent due to environmental conditions. This simplified approach, although useful for dissemination purposes, cannot be applied to the unit load development process. Some factors presented certain trends for common conditions, but when the values of other factors were modified, the trend changed. Due to the complexity of these interactions, it is not reliable to propose individual adjustment factors for each variable, that can estimate the effects of load bridging. To predict the load bridging effect, a simplified model is required to calculate a resulting adjustment. The

Gaussian Process model developed fulfils the expectations of an approachable model that can be utilized in everyday scenarios as part of the unit load design process.

5 Conclusions

After the detailed study and screening of those factors significantly affecting load bridging and the subsequent development of a Gaussian Process Model, the following can be concluded:

- The number of columns in a unit load, the height of the payload, the friction coefficients of the payload's contact with the pallet deck, and the contact friction between packages were all found to be significant factors influencing the bending response of pallet analogs loaded with stacked boxes.
- The Gaussian Process model can act as a surrogate model for the finite element simulation with a prediction error of five percentage points of the estimated deflection ratio.
- Aside from the significance of each studied factor, the interactions between them were found to be of high relevance to the study of load bridging. Load bridging on unit loads must be studied as a system, where variations in any characteristic will potentially influence its effect on the bending response of the remaining factors.
- The number of columns in a unit load affects the bending response. Increased package size reduces unit load bending in most scenarios, but columns' interactions with friction forces and payload height can cause an opposite change in deflection.
- Change in payload height translates to a change in the bending of the boards when supporting large boxes with low payload friction. The deflection of unit loads with smaller boxes tend not to be affected by payload height.
- Pallet top deck friction can influence the bending response of certain unit loads, providing a potentially simple method to improve pallet performance.
- The frictional forces of the packages significantly influence the bending responses of the pallet segments, but the addition of containment methods could potentially restrict this slipping behavior. This shows that containment could limit the effect of package friction on unit load deflection.

The research project also identified that due to the complexity of the factor interactions a simple individual adjustment factor for the load bridging effect of the various unit load factors is not feasible. Therefore, to predict the load bridging effect for unit loads a simplified model, that could be applied to everyday scenarios, is required, increasing the potential applications of the Gaussian Process Model.

6 Acknowledgements

This work was financially supported by the Industrial Affiliate Membership of the Center for Packaging and Unit Load Design at Virginia Tech.

7 References

Altuglas International. (2006). Plexiglass General Information and Physical Properties. Retrieved May 28, 2019, from http://www.plexiglas.com/export/sites/plexiglas/.content/medias/downloads/sheet-docs/plexiglas-general-information-and-physical-properties.pdf

ASTM International. (2009). ASTM D1185-98a(2009) Standard test methods for pallets and related structures employed in materials handling and shipping. https://doi.org/10.1520/D1185-98AR09

Baker, M. (2016). Effect of Pallet Deckboard Stiffness and unit load factors on Corrugated Box Compression Strength. Virginia Tech.

Clayton, A. P., Horvath, L., Bouldin, J., & Gething, B. (2019). Investigation of the effect of column stacked corrugated boxes on load bridging using partial four-way stringer class wooden pallets. Packaging Technology and Science, 32(9), 423–439. https://doi.org/10.1002/pts.2438

Collie, S. T. (1984). Laboratory verification of pallet design procedures (Master's Thesis). Virginia Polytechnic Institute and State University, Blacksburg, VA.

Fagan, B. (1982). Load-support conditions and computerized test apparatus for wood pallets (Master's Thesis). Virginia Polytechnic Institute and State University, Blacksburg, VA.

Hamner, P., & White, M. (2005, November). How to Design Around a Unit Load. Pallet Enterprise, 40–42.

Han, J., White, M., & Hamner, P. (2007). Development of a Finite Element Model of Pallet Deformation and Compressive Stresses on Packaging within Pallet Loads. Journal of Applied Packaging Research, 1(3), 149–162.

ISO. (2011). ISO 8611-1:2011(E) Pallets for materials handling — Flat pallets. Geneva, Switzerland.

Jones, B., & Johnson, R. T. (2009). Design and analysis for the Gaussian process model. Quality and Reliability Engineering International, 25(5), 515–524. https://doi.org/10.1002/qre.1044

Kellicut, K. Q. (1963). Effect of contents and load bearing surface on compressive strength and stacking life of corrugated containers. Tappi, 46(1), 151A-154 A.

Keprate, A., Ratnayake, R. M. C., & Sankararaman, S. (2019). Experimental validation of the adaptive gaussian process regression model used for prediction of stress intensity factor as an

alternative to finite element method. Journal of Offshore Mechanics and Arctic Engineering, 141(2), 1–11. https://doi.org/10.1115/1.4041457

Loferski, J. R. (1985). A Reliability Based Design Procedure for Wood Pallets (PhD Dissertation). Virginia Tech.

Maatouk, H., & Bay, X. (2017). Gaussian Process Emulators for Computer Experiments with Inequality Constraints. Mathematical Geosciences, 49(5), 557–582. https://doi.org/10.1007/s11004-017-9673-2

Molina, E., Horvath, L., & White, M. S. (2018). Investigation of pallet stacking pattern on unit load bridging. Packaging Technology and Science, 31(10), 653–663. https://doi.org/10.1002/pts.2406

Monaghan, J., & Marcondes, J. (1992). Technical notes: Overhang and pallet gap effects on the performance of corrugated fiberboard boxes. Transactions of the ASAE, 35(6), 1945–1947. https://doi.org/10.13031/2013.28820

Morrissette, S. M. (2020). Investigation into the Load Bridging Effect for Block Class Pallets as a Function of Package Size and Pallet Stiffness (Masters Thesis). Virginia Tech.

Morrissette, S. M., Horvath, L., & DeLack, K. (2020). Investigation into the load bridging effect for block class pallets as a function of package size and pallet stiffness. Packaging Technology and Science, 1–19. https://doi.org/10.1002/pts.2539

O'Dell, R., Clarke, J. W., & White, M. S. (1998). Relationship of friction characteristics and pallet performance. Virginia Tech Center for Unit Load Design, 1(1). Retrieved from https://secure.hosting.vt.edu/www.unitload.vt.edu/private/library/VT1000.pdf

Park, J. (2015). Investigation of fundamental relationships to improve the sustainability of unit loads (Ph.D. Dissertation). Virginia Polytechnic Institute and State University.

Park, J., Horvath, L., White, M. S., Phanthanousy, S., Araman, P., & Bush, R. J. (2017). The influence of package size and flute type of corrugated boxes on load bridging in unit loads. Packaging Technology and Science, 30(1–2), 33–43. https://doi.org/10.1002/pts.2279

Phanthanousy, S. (2017). The Effect of the Stiffness of Unit Load Components on Pallet Deflection and Box Compression Strength. Retrieved from https://vtechworks.lib.vt.edu/handle/10919/86203

Quesenberry, C., Horvath, L., Bouldin, J., & White, M. S. (2020). The effect of pallet top deck stiffness on the compression strength of asymmetrically supported corrugated boxes. Packaging Technology and Science, (July), 1–12. https://doi.org/10.1002/pts.2533

Research and Markets. (2019, June). Pallet Market: Global Industry Trends, Share, Size, Growth, Opportunity and Forecast 2019-2024. Research and Markets.

Twede, D., Selke, S. E. M., Kamdem, D.-P., & Shires, D. (2014). Cartons, crates and corrugated board: handbook of paper and wood packaging technology (2nd.). DEStech Publications, Inc.

Vasudevan, S., Ramos, F., Nettleton, E., & Durrant-Whyte, H. (2009). Gaussian process modeling of large-scale terrain. Journal of Field Robotics, 26(10), 812–840. https://doi.org/10.1002/rob.20309

Wallin, W. B. (1979). Analysis for Safe Load and Deflection for Wooden Pallets and Related Structures. Princeton, West Virginia.

Yoo, J. (2011). Modeling compressive stress distributions at the interface between a pallet deck and distribution packaging (Doctoral dissertation). Virginia Tech.

Summary, conclusions, and recommendations for future research

1 Summary

In this research project, the load bridging effect on unit loads was studied in-depth. The main payload characteristic factors affecting the pallet bending response were identified and characterized. Additionally, the interactions between the different factors were studied. A finite element model of a simplified unit load was developed and validated, with the goal to replicate the effect studied. Additionally, a Gaussian Process model was created as an alternative to a more efficient approach to the study of the phenomenon investigated.

The models developed, as well as the main findings will allow unit load designers to consider the changes in pallet bending response when evaluating specific payloads. Improving the unit load design process can allow for the optimization of material consumption in pallet manufacturing operations as well as reducing the overall costs related to distribution.

2 Conclusions

Following the main objective of the research project, this study focused on the understanding of the load bridging effect in unit loads. Taking into consideration the scope of the model, the following can be concluded.

- A two-dimensional finite element model of a simplified unit load was successfully developed and validated for the most common loads. The developed model is capable of accurately predicting the bending response change of a pallet segment when the payload characteristics are modified.
- A deep characterization of the identified significant factors influencing the load bridging effect was conducted.
- Given the acting complex interactions in the studied phenomena, load bridging on unit loads must be studied as a system. Analyzing individual variables, while

ignoring the effects of others, can prevent unit load designers from predicting the actual changes in pallet deflection.

- In order to simplify the implicit dynamic finite element model, a Gaussian Process Model was developed. The resulting formulation for the changes in the ratio of pallet deflection can be more easily adopted.
- Dimensions of the boxes, height of the unit load and the coefficient of frictions among the different components were identified as the factors influencing load bridging and the resulting pallet deflection.
- Pallet analog yield strength could increase by more than 60% when taking into consideration the load bridging effect.
- The model developed presents an opportunity to improve the pallet and unit load design methodology. Accounting for the factors identified can allow designers to select potentially problematic unit loads and further investigate.
- The results presented provide a guideline towards the change in trends of pallet deflection as payload configuration is modified. It is not the intent of the author to directly modify the safe carrying capacity of pallets. Pallet designs must be properly verified by the currently accepted methodologies. This model allows for the identification of payloads that can potentially generate larger deformation. Pallet designs must be tested with such payloads.

3 Recommendations for future research

The methods developed in this study represent a first approach to a comprehensive load bridging model for unit loads. To further expand the knowledge in the underlying mechanical behavior and to extend the adoption of the proposed methods in pallet design, the following is recommended for future research projects.

- Expand the model to explore the effects of load bridging on different types of packages besides corrugated boxes. Not all of the assumptions and simplifications of this study will hold when varying the payload characteristics and as such, modifications should be included.
- Include in the model the effect on bending response for interlocked layers of packages stacked in the unit load.

- Study the effects of multiple pallet support conditions besides warehouse beam racking. Supply chains where no warehouse racking is present will benefit of the knowledge of the load bridging effect for additional support conditions.
- Study the effects of applying stretch wrap and other load containment methods.
- Expanding the model limits to include different payload and support conditions might require adjusting the model to include three dimensional effects. This will allow an increase in the supply chain scenarios where the model can be utilized.
- This model focused exclusively on pallet bending response. Further studies should be conducted to evaluate the effects of load bridging on pallet strength.
- Further experimental validation of the model results should be conducted for multiple pallet designs and sets of packages. This can help identify possible sources of variability not currently accounted.
- Development of a standalone software application for the design of unit loads based on the Gaussian Process Model formulas can facilitate the adoption of the model in day-to-day unit load design operations.

3.1 Project Limitations

The project was conducted considering the following limitations:

- In the development of the finite element model of the unit load segment, a board was used as a pallet analog. The study does not consider the effect of different pallet designs.
- Time-dependent material properties, such as creep of the pallet analog for extended periods under load were not considered.
- The simplified load bridging model developed using the Gaussian Process regression is limited to the ranges of values where each variable was validated. Although unit loads outside of these ranges exist, they are not considered for the prediction properties of the model.

Appendix A: Finite element simulation results for the fractional factorial screening design

Table B.1. Factor level combinations for each run of the fractional factorial 2_{IV}^{7-1} design and deflection results (mm) and as a ratio of the uniformly loaded pallet deflection.

	Factor							Responses	
	Weight	**Columns**	**Layers**	**Pallet Friction**	**Box Friction**	**MOE**	**Height**	**Pallet Deflection**	**Ratio[a]**
Units	kg	Ordinal	Ordinal			GPa	m	mm	
Low (-)	109	3	3	0.2	0.2	2.76	0.762		
High (+)	218	5	5	0.6	0.6	8.27	1.778		
Run 001	–	–	–	–	–	–	–	19.94	0.88
Run 002	–	–	–	–	–	+	+	2.36	0.31
Run 003	–	–	–	–	+	–	+	8.36	0.37
Run 004	–	–	–	–	+	+	–	4.55	0.60
Run 005	–	–	–	+	–	–	+	8.18	0.36
Run 006	–	–	–	+	–	+	–	2.29	0.30
Run 007	–	–	–	+	+	–	–	3.30	0.14
Run 008	–	–	–	+	+	+	+	2.11	0.28
Run 009	–	–	+	–	–	–	+	7.24	0.32
Run 010	–	–	+	–	–	+	–	6.63	0.88
Run 011	–	–	+	–	+	–	–	11.51	0.51
Run 012	–	–	+	–	+	+	+	2.62	0.35
Run 013	–	–	+	+	–	–	–	13.39	0.59
Run 014	–	–	+	+	–	+	+	2.49	0.33
Run 015	–	–	+	+	+	–	+	3.99	0.17
Run 016	–	–	+	+	+	+	–	1.32	0.18
Run 017	–	+	–	–	–	–	+	13.56	0.60
Run 018	–	+	–	–	–	+	–	5.79	0.77
Run 019	–	+	–	–	+	–	–	12.60	0.55
Run 020	–	+	–	–	+	+	+	4.45	0.59
Run 021	–	+	–	+	–	–	–	11.63	0.51
Run 022	–	+	–	+	–	+	+	4.37	0.58
Run 023	–	+	–	+	+	–	+	8.94	0.39
Run 024	–	+	–	+	+	+	–	3.18	0.42
Run 025	–	+	+	–	–	–	–	18.11	0.80
Run 026	–	+	+	–	–	+	+	4.39	0.58
Run 027	–	+	+	–	+	–	+	13.46	0.59
Run 028	–	+	+	–	+	+	–	3.99	0.53
Run 029	–	+	+	+	–	–	+	13.16	0.58
Run 030	–	+	+	+	–	+	–	3.99	0.53

	Factor							Responses	
	Weight	**Columns**	**Layers**	**Pallet Friction**	**Box Friction**	**MOE**	**Height**	**Pallet Deflection**	**Ratio[a]**
Run 031	−	+	+	+	+	−	−	8.05	0.35
Run 032	−	+	+	+	+	+	+	3.33	0.44
Run 033	+	−	−	−	−	−	−	34.74	0.77
Run 034	+	−	−	−	−	+	+	4.83	0.33
Run 035	+	−	−	−	+	−	+	14.43	0.32
Run 036	+	−	−	−	+	+	−	7.07	0.48
Run 037	+	−	−	+	−	−	+	12.83	0.29
Run 038	+	−	−	+	−	+	−	4.51	0.31
Run 039	+	−	−	+	+	−	−	5.29	0.12
Run 040	+	−	−	+	+	+	+	3.04	0.21
Run 041	+	−	+	−	−	−	+	14.64	0.33
Run 042	+	−	+	−	−	+	−	12.89	0.88
Run 043	+	−	+	−	+	−	−	20.46	0.46
Run 044	+	−	+	−	+	+	+	5.50	0.37
Run 045	+	−	+	+	−	−	−	20.61	0.46
Run 046	+	−	+	+	−	+	+	5.24	0.36
Run 047	+	−	+	+	+	−	+	5.96	0.13
Run 048	+	−	+	+	+	+	−	2.61	0.18
Run 049	+	+	−	−	−	−	+	25.94	0.58
Run 050	+	+	−	−	−	+	−	9.45	0.64
Run 051	+	+	−	−	+	−	−	28.00	0.62
Run 052	+	+	−	−	+	+	+	8.39	0.57
Run 053	+	+	−	+	−	−	−	24.06	0.54
Run 054	+	+	−	+	−	+	+	8.47	0.58
Run 055	+	+	−	+	+	−	+	14.35	0.32
Run 056	+	+	−	+	+	+	−	5.27	0.36
Run 057	+	+	+	−	−	−	−	26.49	0.59
Run 058	+	+	+	−	−	+	+	8.39	0.57
Run 059	+	+	+	−	+	−	+	25.44	0.57
Run 060	+	+	+	−	+	+	−	7.86	0.53
Run 061	+	+	+	+	−	−	+	26.30	0.59
Run 062	+	+	+	+	−	+	−	7.19	0.49
Run 063	+	+	+	+	+	−	−	12.90	0.29
Run 064	+	+	+	+	+	+	+	5.95	0.40

[a] 'Ratio' refers to the ratio of deflection of the experimental unit from the deflection under uniformly distributed loading.

Appendix B: Gaussian Process Model reports

Table C.1. Model report for the 3 column-unit load Gaussian Process Model.

Column	Theta	Total Sensitivity	Main Effect	Height (mm) Interaction	Pallet Friction Interaction	Vertical Friction Interaction	Horizontal Friction Interaction
Height (mm)	2.69E-06	0.2715855	0.1455754	.	0.0158222	0.0123887	0.0977991
Pallet Friction	10.605077	0.3928196	0.3074511	0.0158222	.	0.0267726	0.0427738
Vertical Friction	5.143414	0.2682	0.2270755	0.0123887	0.0267726	.	0.0019632
Horizontal Friction	7.9340513	0.2099791	0.067443	0.0977991	0.0427738	0.0019632	.

μ	**σ^2**
0.3150199	0.0151404

-2*LogLikelihood

-69.0752

Table C.2. Model report for the 4 column-unit load Gaussian Process Model.

Column	Theta	Total Sensitivity	Main Effect	Height (mm) Interaction	Pallet Friction Interaction	Vertical Friction Interaction	Horizontal Friction Interaction
Height (mm)	1.48E-07	0.0737937	0.0541573	.	0.0051113	0.014525	9.06E-08
Pallet Friction	21.962287	0.6274388	0.3068785	0.0051113	.	0.3154295	1.95E-05
Vertical Friction	33.95775	0.6194135	0.2883838	0.014525	0.3154295	.	0.0010753
Horizontal Friction	0.0738977	0.0011266	3.17E-05	9.06E-08	1.95E-05	0.0010753	.

μ	**σ^2**
0.4019256	0.0055786

-2*LogLikelihood

-130.7308

Table C.3. Model report for the 5 column-unit load Gaussian Process Model.

Column	Theta	Total Sensitivity	Main Effect	Height (mm) Interaction	Pallet Friction Interaction	Vertical Friction Interaction	Horizontal Friction Interaction
Height (mm)	6.87E-07	0.0879232	0.0520318	.	0.0047046	0.0311776	9.23E-06
Pallet Friction	21.215255	0.3384798	0.2167599	0.0047046	.	0.1168647	0.0001506
Vertical Friction	33.373971	0.7135215	0.5653476	0.0311776	0.1168647	.	0.0001316
Horizontal Friction	0.0835701	0.0005557	0.0002642	9.23E-06	0.0001506	0.0001316	.

μ	**σ^2**
0.49101	0.0071159

-2*LogLikelihood

-107.9988

Table C.4. Model report for the 6 column-unit load Gaussian Process Model.

Column	Theta	Total Sensitivity	Main Effect	Height (mm) Interaction	Pallet Friction Interaction	Vertical Friction Interaction	Horizontal Friction Interaction
Height (mm)	0	0	0	.	0	0	0
Pallet Friction	13.248404	0.6710739	0.3252035	0	.	0.345048	0.0008224
Vertical Friction	192.92906	0.6687176	0.3038749	0	0.345048	.	0.0197947
Horizontal Friction	1.686846	0.0214602	0.0008431	0	0.0008224	0.0197947	.

μ	**σ^2**
0.5931393	0.0080952

-2*LogLikelihood

-98.22023

Appendix D: Python Scripts for the predicted value calculation of the Gaussian Process Model

D.1. Formula for the Gaussian Process Model for 3 columns

```
from __future__ import division
import jmp_score as jmp
from math import *
import numpy as np


""" ==================================================================
 Copyright(C) 2018 SAS Institute Inc.All rights reserved.

 Notice:
 The following permissions are granted provided that the
 above copyright and this notice appear in the score code and
 any related documentation. Permission to copy, modify
 and distribute the score code generated using
 JMP(R) software is limited to customers of SAS Institute Inc. ("SAS")
 and successive third parties, all without any warranty, express or
 implied, or any other obligation by SAS. SAS and all other SAS
 Institute Inc. product and service names are registered
 trademarks or trademarks of SAS Institute Inc. in the USA
 and other countries. Except as contained in this notice,
 the name of the SAS Institute Inc. and JMP shall not be used in
 the advertising or promotion of products or services without
 prior written authorization from SAS Institute Inc.
 ================================================================== """

""" Python code generated by JMP v15.0.0 """

def getModelMetadata():
        return {"creator": u"Gaussian Process", "modelName": u"", "predicted": u"Ratio", "table": u"Columns=3", "version": u"15.0.0", "timestamp": u"2020-08-31T19:49:08Z"}


def getInputMetadata():
   return {
      u"Height (mm)": "float",
      u"Horizontal_Friction": "float",
      u"Pallet_Friction": "float",
      u"Vertical_Friction": "float"
         }


def getOutputMetadata():
   return {
      u"Ratio Prediction Formula": "float"
         }


def score(indata, outdata):
   outdata[u"Ratio Prediction Formula"] = 0.315019924054793 + -0.149667248995762 * jmp.exp(-((0.0000026891432172166 * jmp.pow((-2032 + indata[u"Height (mm)"]), 2) + 5.14341401748062 * jmp.pow((-0.58 + indata[u"Vertical_Friction"]), 2) +
```

10.6050768355277 * jmp.pow((-0.51 + indata[u"Pallet_Friction"]), 2) + 7.9340513075143 * jmp.pow((-0.26 + indata[u"Horizontal_Friction"]), 2)))) + -0.0377542145678315 * jmp.exp(-((0.0000026891432172166 * jmp.pow((-1992.92 + indata[u"Height (mm)"]), 2) + 7.9340513075143 * jmp.pow((-0.66 + indata[u"Horizontal_Friction"]), 2) + 5.14341401748062 * jmp.pow((-0.6 + indata[u"Vertical_Friction"]), 2) + 10.6050768355277 * jmp.pow((-0.57 + indata[u"Pallet_Friction"]), 2)))) + 0.0575822939756754 * jmp.exp(-((0.0000026891432172166 * jmp.pow((-1953.85 + indata[u"Height (mm)"]), 2) + 7.9340513075143 * jmp.pow((-0.42 + indata[u"Horizontal_Friction"]), 2) + 5.14341401748062 * jmp.pow((-0.37 + indata[u"Vertical_Friction"]), 2) + 10.6050768355277 * jmp.pow((-0.32 + indata[u"Pallet_Friction"]), 2)))) + 0.00996204670573888 * jmp.exp(-((0.0000026891432172166 * jmp.pow((-1914.77 + indata[u"Height (mm)"]), 2) + 7.9340513075143 * jmp.pow((-0.57 + indata[u"Horizontal_Friction"]), 2) + 10.6050768355277 * jmp.pow((-0.44 + indata[u"Pallet_Friction"]), 2) + 5.14341401748062 * jmp.pow((-0.21 + indata[u"Vertical_Friction"]), 2)))) + 0.0916249136166858 * jmp.exp(-((0.0000026891432172166 * jmp.pow((-1875.69 + indata[u"Height (mm)"]), 2) + 10.6050768355277 * jmp.pow((-0.55 + indata[u"Pallet_Friction"]), 2) + 5.14341401748062 * jmp.pow((-0.38 + indata[u"Vertical_Friction"]), 2) + 7.9340513075143 * jmp.pow((-0.35 + indata[u"Horizontal_Friction"]), 2)))) + 0.0306887017655656 * jmp.exp(-((0.0000026891432172166 * jmp.pow((-1836.62 + indata[u"Height (mm)"]), 2) + 10.6050768355277 * jmp.pow((-0.37 + indata[u"Pallet_Friction"]), 2) + 5.14341401748062 * jmp.pow((-0.28 + indata[u"Vertical_Friction"]), 2) + 7.9340513075143 * jmp.pow((-0.21 + indata[u"Horizontal_Friction"]), 2)))) + -0.0031342382936451 * jmp.exp(-((0.0000026891432172166 * jmp.pow((-1797.54 + indata[u"Height (mm)"]), 2) + 7.9340513075143 * jmp.pow((-0.65 + indata[u"Horizontal_Friction"]), 2) + 5.14341401748062 * jmp.pow((-0.46 + indata[u"Vertical_Friction"]), 2) + 10.6050768355277 * jmp.pow((-0.39 + indata[u"Pallet_Friction"]), 2)))) + -0.0863634839333545 * jmp.exp(-((0.0000026891432172166 * jmp.pow((-1758.46 + indata[u"Height (mm)"]), 2) + 5.14341401748062 * jmp.pow((-0.56 + indata[u"Vertical_Friction"]), 2) + 7.9340513075143 * jmp.pow((-0.28 + indata[u"Horizontal_Friction"]), 2) + 10.6050768355277 * jmp.pow((-0.26 + indata[u"Pallet_Friction"]), 2)))) + 0.341919686027407 * jmp.exp(-((0.0000026891432172166 * jmp.pow((-1719.38 + indata[u"Height (mm)"]), 2) + 5.14341401748062 * jmp.pow((-0.55 + indata[u"Vertical_Friction"]), 2) + 7.9340513075143 * jmp.pow((-0.51 + indata[u"Horizontal_Friction"]), 2) + 10.6050768355277 * jmp.pow((-0.21 + indata[u"Pallet_Friction"]), 2)))) + -0.162787147854361 * jmp.exp(-((0.0000026891432172166 * jmp.pow((-1641.23 + indata[u"Height (mm)"]), 2) + 10.6050768355277 * jmp.pow((-0.62 + indata[u"Pallet_Friction"]), 2) + 5.14341401748062 * jmp.pow((-0.53 + indata[u"Vertical_Friction"]), 2) + 7.9340513075143 * jmp.pow((-0.47 + indata[u"Horizontal_Friction"]), 2)))) + -0.281758115207761 * jmp.exp(-((0.0000026891432172166 * jmp.pow((-1602.15 + indata[u"Height (mm)"]), 2) + 5.14341401748062 * jmp.pow((-0.69 + indata[u"Vertical_Friction"]), 2) + 7.9340513075143 * jmp.pow((-0.62 + indata[u"Horizontal_Friction"]), 2) + 10.6050768355277 * jmp.pow((-0.34 + indata[u"Pallet_Friction"]), 2)))) + -0.0392642088660763 * jmp.exp(-((0.0000026891432172166 * jmp.pow((-1563.08 + indata[u"Height (mm)"]), 2) + 10.6050768355277 * jmp.pow((-0.67 + indata[u"Pallet_Friction"]), 2) + 5.14341401748062 * jmp.pow((-0.51 + indata[u"Vertical_Friction"]), 2) + 7.9340513075143 * jmp.pow((-0.2 + indata[u"Horizontal_Friction"]), 2)))) + -0.101838423068741 * jmp.exp(-((0.0000026891432172166 * jmp.pow((-1524 + indata[u"Height (mm)"]), 2) + 7.9340513075143 * jmp.pow((-0.58 + indata[u"Horizontal_Friction"]), 2) + 5.14341401748062 * jmp.pow((-0.33 + indata[u"Vertical_Friction"]), 2) + 10.6050768355277 * jmp.pow((-0.23 + indata[u"Pallet_Friction"]), 2)))) + -0.00648900253696268 * jmp.exp(-((0.0000026891432172166 * jmp.pow((-1484.92 + indata[u"Height (mm)"]), 2) + 10.6050768355277 * jmp.pow((-0.64 + indata[u"Pallet_Friction"]), 2) + 7.9340513075143 * jmp.pow((-0.49 + indata[u"Horizontal_Friction"]), 2) + 5.14341401748062 * jmp.pow((-0.32 + indata[u"Vertical_Friction"]), 2)))) + 0.0142741159676444 * jmp.exp(-((0.0000026891432172166 * jmp.pow((-1445.85 + indata[u"Height (mm)"]), 2) + 5.14341401748062 * jmp.pow((-0.7 + indata[u"Vertical_Friction"]), 2) + 10.6050768355277 * jmp.pow((-0.49 + indata[u"Pallet_Friction"]), 2) + 7.9340513075143 * jmp.pow((-0.38 + indata[u"Horizontal_Friction"]), 2)))) + 0.141507043535488 * jmp.exp(-((0.0000026891432172166 * jmp.pow((-1406.77 + indata[u"Height (mm)"]), 2) + 10.6050768355277 * jmp.pow((-0.53 + indata[u"Pallet_Friction"]), 2) + 7.9340513075143 * jmp.pow((-0.32 + indata[u"Horizontal_Friction"]), 2) + 5.14341401748062 * jmp.pow((-0.2 + indata[u"Vertical_Friction"]), 2)))) + -0.34535406102884 * jmp.exp(-((0.0000026891432172166 * jmp.pow((-1367.69 + indata[u"Height (mm)"]), 2) + 7.9340513075143 * jmp.pow((-0.37 + indata[u"Horizontal_Friction"]), 2) + 10.6050768355277 * jmp.pow((-0.3 + indata[u"Pallet_Friction"]), 2) + 5.14341401748062 * jmp.pow((-0.23 + indata[u"Vertical_Friction"]), 2)))) + 0.326126957975666 * jmp.exp(-((0.0000026891432172166 * jmp.pow((-1328.62 + indata[u"Height (mm)"]), 2) + 7.9340513075143 * jmp.pow((-0.48 + indata[u"Horizontal_Friction"]), 2) + 5.14341401748062 * jmp.pow((-0.47 + indata[u"Vertical_Friction"]), 2) + 10.6050768355277 * jmp.pow((-0.41 + indata[u"Pallet_Friction"]), 2)))) + 0.0829135061033895 * jmp.exp(-((0.0000026891432172166 * jmp.pow((-1211.38 + indata[u"Height (mm)"]), 2) + 7.9340513075143 * jmp.pow((-0.56 + indata[u"Horizontal_Friction"]), 2) + 10.6050768355277 * jmp.pow((-0.42 + indata[u"Pallet_Friction"]), 2) + 5.14341401748062 * jmp.pow((-0.25 + indata[u"Vertical_Friction"]), 2)))) + 0.0352831370645952 * jmp.exp(-((0.0000026891432172166 * jmp.pow((-1172.31 + indata[u"Height (mm)"]), 2) + 5.14341401748062 * jmp.pow((-0.65 + indata[u"Vertical_Friction"]), 2) + 7.9340513075143 * jmp.pow((-0.46 + indata[u"Horizontal_Friction"]), 2) + 10.6050768355277 * jmp.pow((-0.29 + indata[u"Pallet_Friction"]), 2)))) + -0.0639270016272973 * jmp.exp(-((0.0000026891432172166 * jmp.pow((-1094.15 + indata[u"Height (mm)"]), 2) + 10.6050768355277 * jmp.pow((-0.6 + indata[u"Pallet_Friction"]), 2) + 5.14341401748062 * jmp.pow((-0.41 + indata[u"Vertical_Friction"]), 2) + 7.9340513075143 * jmp.pow((-0.33 + indata[u"Horizontal_Friction"]), 2)))) + 0.155941940885416 * jmp.exp(-((0.0000026891432172166 * jmp.pow((-1016 + indata[u"Height (mm)"]), 2) + 10.6050768355277 * jmp.pow((-0.69 + indata[u"Pallet_Friction"]), 2) + 5.14341401748062 * jmp.pow((-0.62 + indata[u"Vertical_Friction"]), 2) + 7.9340513075143 * jmp.pow((-0.52 + indata[u"Horizontal_Friction"]), 2)))) + -0.298720893154552 * jmp.exp(-((0.0000026891432172166 * jmp.pow((-937.85 + indata[u"Height (mm)"]), 2) + 10.6050768355277 * jmp.pow((-0.65 + indata[u"Pallet_Friction"]), 2) + 5.14341401748062 * jmp.pow((-0.64 + indata[u"Vertical_Friction"]), 2) + 7.9340513075143 *

```
jmp.pow((-0.29 + indata[u"Horizontal_Friction"]), 2)))) + -0.0531175409282043 * jmp.exp(-((0.0000026891432172166 * jmp.pow((-
859.69 + indata[u"Height (mm)"]), 2) + 10.6050768355277 * jmp.pow((-0.7 + indata[u"Pallet_Friction"]), 2) + 7.9340513075143 *
jmp.pow((-0.53 + indata[u"Horizontal_Friction"]), 2) + 5.14341401748062 * jmp.pow((-0.29 + indata[u"Vertical_Friction"]), 2)))) + -
0.16296792923761 * jmp.exp(-((0.0000026891432172166 * jmp.pow((-820.62 + indata[u"Height (mm)"]), 2) + 7.9340513075143 *
jmp.pow((-0.55 + indata[u"Horizontal_Friction"]), 2) + 5.14341401748062 * jmp.pow((-0.34 + indata[u"Vertical_Friction"]), 2) +
10.6050768355277 * jmp.pow((-0.25 + indata[u"Pallet_Friction"]), 2)))) + -0.743356069805181 * jmp.exp(-
((0.0000026891432172166 * jmp.pow((-781.54 + indata[u"Height (mm)"]), 2) + 5.14341401748062 * jmp.pow((-0.61 +
indata[u"Vertical_Friction"]), 2) + 10.6050768355277 * jmp.pow((-0.48 + indata[u"Pallet_Friction"]), 2) + 7.9340513075143 *
jmp.pow((-0.44 + indata[u"Horizontal_Friction"]), 2)))) + 0.459956187057059 * jmp.exp(-((0.0000026891432172166 * jmp.pow((-
742.46 + indata[u"Height (mm)"]), 2) + 7.9340513075143 * jmp.pow((-0.3 + indata[u"Horizontal_Friction"]), 2) + 5.14341401748062
* jmp.pow((-0.3 + indata[u"Vertical_Friction"]), 2) + 10.6050768355277 * jmp.pow((-0.28 + indata[u"Pallet_Friction"]), 2)))) +
0.46796576758358 * jmp.exp(-((0.0000026891432172166 * jmp.pow((-703.38 + indata[u"Height (mm)"]), 2) + 5.14341401748062 *
jmp.pow((-0.52 + indata[u"Vertical_Friction"]), 2) + 10.6050768355277 * jmp.pow((-0.46 + indata[u"Pallet_Friction"]), 2) +
7.9340513075143 * jmp.pow((-0.23 + indata[u"Horizontal_Friction"]), 2)))) + 0.0809169262401329 * jmp.exp(-
((0.0000026891432172166 * jmp.pow((-664.31 + indata[u"Height (mm)"]), 2) + 5.14341401748062 * jmp.pow((-0.67 +
indata[u"Vertical_Friction"]), 2) + 7.9340513075143 * jmp.pow((-0.61 + indata[u"Horizontal_Friction"]), 2) + 10.6050768355277 *
jmp.pow((-0.33 + indata[u"Pallet_Friction"]), 2)))) + -0.306613406030312 * jmp.exp(-((0.0000026891432172166 * jmp.pow((-586.15
+ indata[u"Height (mm)"]), 2) + 10.6050768355277 * jmp.pow((-0.61 + indata[u"Pallet_Friction"]), 2) + 7.9340513075143 *
jmp.pow((-0.34 + indata[u"Horizontal_Friction"]), 2) + 5.14341401748062 * jmp.pow((-0.24 + indata[u"Vertical_Friction"]), 2)))) +
0.0907343239646985 * jmp.exp(-((0.0000026891432172166 * jmp.pow((-547.08 + indata[u"Height (mm)"]), 2) + 7.9340513075143
* jmp.pow((-0.64 + indata[u"Horizontal_Friction"]), 2) + 10.6050768355277 * jmp.pow((-0.47 + indata[u"Pallet_Friction"]), 2) +
5.14341401748062 * jmp.pow((-0.26 + indata[u"Vertical_Friction"]), 2)))) + 0.455715436667746 * jmp.exp(-
((0.0000026891432172166 * jmp.pow((-508 + indata[u"Height (mm)"]), 2) + 10.6050768355277 * jmp.pow((-0.66 +
indata[u"Pallet_Friction"]), 2) + 5.14341401748062 * jmp.pow((-0.48 + indata[u"Vertical_Friction"]), 2) + 7.9340513075143 *
jmp.pow((-0.41 + indata[u"Horizontal_Friction"]), 2))))

    return outdata[u"Ratio Prediction Formula"]
```

D.2. Formula for the Gaussian Process Model for 4 columns

```
from __future__ import division
import jmp_score as jmp
from math import *
import numpy as np


""" ==================================================================
 Copyright(C) 2018 SAS Institute Inc.All rights reserved.

 Notice:
 The following permissions are granted provided that the
 above copyright and this notice appear in the score code and
 any related documentation. Permission to copy, modify
 and distribute the score code generated using
 JMP(R) software is limited to customers of SAS Institute Inc. ("SAS")
 and successive third parties, all without any warranty, express or
 implied, or any other obligation by SAS. SAS and all other SAS
 Institute Inc. product and service names are registered
 trademarks or trademarks of SAS Institute Inc. in the USA
 and other countries. Except as contained in this notice,
 the name of the SAS Institute Inc. and JMP shall not be used in
 the advertising or promotion of products or services without
 prior written authorization from SAS Institute Inc.
 ================================================================== """

""" Python code generated by JMP v15.0.0 """

def getModelMetadata():
        return {"creator": u"Gaussian Process", "modelName": u"", "predicted": u"Ratio", "table": u"Columns=4", "version": u"15.0.0", "timestamp": u"2020-08-31T19:58:15Z"}


def getInputMetadata():
    return {
        u"Height (mm)": "float",
        u"Horizontal_Friction": "float",
        u"Pallet_Friction": "float",
        u"Vertical_Friction": "float"
            }


def getOutputMetadata():
    return {
        u"Ratio Prediction Formula": "float"
            }


def score(indata, outdata):
    outdata[u"Ratio Prediction Formula"] = 0.401925596054757 + 0.198513736651184 * jmp.exp(-((0.0000001484831488128 * jmp.pow((-2032 + indata[u"Height (mm)"]), 2) + 33.9577496496067 * jmp.pow((-0.58 + indata[u"Vertical_Friction"]), 2) + 21.9622867242468 * jmp.pow((-0.51 + indata[u"Pallet_Friction"]), 2) + 0.0738977186050841 * jmp.pow((-0.26 + indata[u"Horizontal_Friction"]), 2)))) + 0.0528549747884317 * jmp.exp(-((0.0000001484831488128 * jmp.pow((-1992.92 + indata[u"Height (mm)"]), 2) + 0.0738977186050841 * jmp.pow((-0.66 + indata[u"Horizontal_Friction"]), 2) + 33.9577496496067 * jmp.pow((-0.6 + indata[u"Vertical_Friction"]), 2) + 21.9622867242468 * jmp.pow((-0.57 + indata[u"Pallet_Friction"]), 2)))) + -0.0147587158733636 * jmp.exp(-((0.0000001484831488128 * jmp.pow((-1953.85 + indata[u"Height (mm)"]), 2) + 0.0738977186050841 * jmp.pow((-0.42 + indata[u"Horizontal_Friction"]), 2) + 33.9577496496067 * jmp.pow((-0.37 + indata[u"Vertical_Friction"]), 2) + 21.9622867242468 * jmp.pow((-0.32 + indata[u"Pallet_Friction"]), 2)))) + -0.179814823461886 *
```

jmp.exp(-((0.0000001484831488128 * jmp.pow((-1914.77 + indata[u"Height (mm)"]), 2) + 0.0738977186050841 * jmp.pow((-0.57 + indata[u"Horizontal_Friction"]), 2) + 21.9622867242468 * jmp.pow((-0.44 + indata[u"Pallet_Friction"]), 2) + 33.9577496496067 * jmp.pow((-0.21 + indata[u"Vertical_Friction"]), 2)))) + -0.284297862006475 * jmp.exp(-((0.0000001484831488128 * jmp.pow((-1875.69 + indata[u"Height (mm)"]), 2) + 21.9622867242468 * jmp.pow((-0.55 + indata[u"Pallet_Friction"]), 2) + 33.9577496496067 * jmp.pow((-0.38 + indata[u"Vertical_Friction"]), 2) + 0.0738977186050841 * jmp.pow((-0.35 + indata[u"Horizontal_Friction"]), 2)))) + 0.255250015263726 * jmp.exp(-((0.0000001484831488128 * jmp.pow((-1836.62 + indata[u"Height (mm)"]), 2) + 21.9622867242468 * jmp.pow((-0.37 + indata[u"Pallet_Friction"]), 2) + 33.9577496496067 * jmp.pow((-0.28 + indata[u"Vertical_Friction"]), 2) + 0.0738977186050841 * jmp.pow((-0.21 + indata[u"Horizontal_Friction"]), 2)))) + 0.34753361803903 * jmp.exp(-((0.0000001484831488128 * jmp.pow((-1797.54 + indata[u"Height (mm)"]), 2) + 0.0738977186050841 * jmp.pow((-0.65 + indata[u"Horizontal_Friction"]), 2) + 33.9577496496067 * jmp.pow((-0.46 + indata[u"Vertical_Friction"]), 2) + 21.9622867242468 * jmp.pow((-0.39 + indata[u"Pallet_Friction"]), 2)))) + -0.0911056788800588 * jmp.exp(-((0.0000001484831488128 * jmp.pow((-1758.46 + indata[u"Height (mm)"]), 2) + 33.9577496496067 * jmp.pow((-0.56 + indata[u"Vertical_Friction"]), 2) + 0.0738977186050841 * jmp.pow((-0.28 + indata[u"Horizontal_Friction"]), 2) + 21.9622867242468 * jmp.pow((-0.26 + indata[u"Pallet_Friction"]), 2)))) + 0.276511975728018 * jmp.exp(-((0.0000001484831488128 * jmp.pow((-1719.38 + indata[u"Height (mm)"]), 2) + 33.9577496496067 * jmp.pow((-0.55 + indata[u"Vertical_Friction"]), 2) + 0.0738977186050841 * jmp.pow((-0.51 + indata[u"Horizontal_Friction"]), 2) + 21.9622867242468 * jmp.pow((-0.21 + indata[u"Pallet_Friction"]), 2)))) + 0.0919632186892546 * jmp.exp(-((0.0000001484831488128 * jmp.pow((-1602.15 + indata[u"Height (mm)"]), 2) + 33.9577496496067 * jmp.pow((-0.69 + indata[u"Vertical_Friction"]), 2) + 0.0738977186050841 * jmp.pow((-0.62 + indata[u"Horizontal_Friction"]), 2) + 21.9622867242468 * jmp.pow((-0.34 + indata[u"Pallet_Friction"]), 2)))) + -0.298536872141072 * jmp.exp(-((0.0000001484831488128 * jmp.pow((-1563.08 + indata[u"Height (mm)"]), 2) + 21.9622867242468 * jmp.pow((-0.67 + indata[u"Pallet_Friction"]), 2) + 33.9577496496067 * jmp.pow((-0.51 + indata[u"Vertical_Friction"]), 2) + 0.0738977186050841 * jmp.pow((-0.2 + indata[u"Horizontal_Friction"]), 2)))) + -0.154601708293927 * jmp.exp(-((0.0000001484831488128 * jmp.pow((-1445.85 + indata[u"Height (mm)"]), 2) + 33.9577496496067 * jmp.pow((-0.7 + indata[u"Vertical_Friction"]), 2) + 21.9622867242468 * jmp.pow((-0.49 + indata[u"Pallet_Friction"]), 2) + 0.0738977186050841 * jmp.pow((-0.38 + indata[u"Horizontal_Friction"]), 2)))) + 0.538766840761848 * jmp.exp(-((0.0000001484831488128 * jmp.pow((-1406.77 + indata[u"Height (mm)"]), 2) + 21.9622867242468 * jmp.pow((-0.53 + indata[u"Pallet_Friction"]), 2) + 0.0738977186050841 * jmp.pow((-0.32 + indata[u"Horizontal_Friction"]), 2) + 33.9577496496067 * jmp.pow((-0.2 + indata[u"Vertical_Friction"]), 2)))) + 0.0399787888782095 * jmp.exp(-((0.0000001484831488128 * jmp.pow((-1367.69 + indata[u"Height (mm)"]), 2) + 0.0738977186050841 * jmp.pow((-0.37 + indata[u"Horizontal_Friction"]), 2) + 21.9622867242468 * jmp.pow((-0.3 + indata[u"Pallet_Friction"]), 2) + 33.9577496496067 * jmp.pow((-0.23 + indata[u"Vertical_Friction"]), 2)))) + -0.1903782604921 * jmp.exp(-((0.0000001484831488128 * jmp.pow((-1328.62 + indata[u"Height (mm)"]), 2) + 0.0738977186050841 * jmp.pow((-0.48 + indata[u"Horizontal_Friction"]), 2) + 33.9577496496067 * jmp.pow((-0.47 + indata[u"Vertical_Friction"]), 2) + 21.9622867242468 * jmp.pow((-0.41 + indata[u"Pallet_Friction"]), 2)))) + -0.224208473100283 * jmp.exp(-((0.0000001484831488128 * jmp.pow((-1289.54 + indata[u"Height (mm)"]), 2) + 33.9577496496067 * jmp.pow((-0.42 + indata[u"Vertical_Friction"]), 2) + 21.9622867242468 * jmp.pow((-0.38 + indata[u"Pallet_Friction"]), 2) + 0.0738977186050841 * jmp.pow((-0.24 + indata[u"Horizontal_Friction"]), 2)))) + 0.272537666372577 * jmp.exp(-((0.0000001484831488128 * jmp.pow((-1250.46 + indata[u"Height (mm)"]), 2) + 33.9577496496067 * jmp.pow((-0.43 + indata[u"Vertical_Friction"]), 2) + 0.0738977186050841 * jmp.pow((-0.39 + indata[u"Horizontal_Friction"]), 2) + 21.9622867242468 * jmp.pow((-0.2 + indata[u"Pallet_Friction"]), 2)))) + -0.475166291767345 * jmp.exp(-((0.0000001484831488128 * jmp.pow((-1211.38 + indata[u"Height (mm)"]), 2) + 0.0738977186050841 * jmp.pow((-0.56 + indata[u"Horizontal_Friction"]), 2) + 21.9622867242468 * jmp.pow((-0.42 + indata[u"Pallet_Friction"]), 2) + 33.9577496496067 * jmp.pow((-0.25 + indata[u"Vertical_Friction"]), 2)))) + -0.0884125152632931 * jmp.exp(-((0.0000001484831488128 * jmp.pow((-1172.31 + indata[u"Height (mm)"]), 2) + 33.9577496496067 * jmp.pow((-0.65 + indata[u"Vertical_Friction"]), 2) + 0.0738977186050841 * jmp.pow((-0.46 + indata[u"Horizontal_Friction"]), 2) + 21.9622867242468 * jmp.pow((-0.29 + indata[u"Pallet_Friction"]), 2)))) + 0.788353941100435 * jmp.exp(-((0.0000001484831488128 * jmp.pow((-1094.15 + indata[u"Height (mm)"]), 2) + 21.9622867242468 * jmp.pow((-0.6 + indata[u"Pallet_Friction"]), 2) + 33.9577496496067 * jmp.pow((-0.41 + indata[u"Vertical_Friction"]), 2) + 0.0738977186050841 * jmp.pow((-0.33 + indata[u"Horizontal_Friction"]), 2)))) + 0.550871258957875 * jmp.exp(-((0.0000001484831488128 * jmp.pow((-1016 + indata[u"Height (mm)"]), 2) + 21.9622867242468 * jmp.pow((-0.69 + indata[u"Pallet_Friction"]), 2) + 33.9577496496067 * jmp.pow((-0.62 + indata[u"Vertical_Friction"]), 2) + 0.0738977186050841 * jmp.pow((-0.52 + indata[u"Horizontal_Friction"]), 2)))) + -0.259705180657399 * jmp.exp(-((0.0000001484831488128 * jmp.pow((-976.92 + indata[u"Height (mm)"]), 2) + 0.0738977186050841 * jmp.pow((-0.6 + indata[u"Horizontal_Friction"]), 2) + 21.9622867242468 * jmp.pow((-0.56 + indata[u"Pallet_Friction"]), 2) + 33.9577496496067 * jmp.pow((-0.44 + indata[u"Vertical_Friction"]), 2)))) + -0.645950283389929 * jmp.exp(-((0.0000001484831488128 * jmp.pow((-937.85 + indata[u"Height (mm)"]), 2) + 21.9622867242468 * jmp.pow((-0.65 + indata[u"Pallet_Friction"]), 2) + 33.9577496496067 * jmp.pow((-0.64 + indata[u"Vertical_Friction"]), 2) + 0.0738977186050841 * jmp.pow((-0.29 + indata[u"Horizontal_Friction"]), 2)))) + -0.381232180673959 * jmp.exp(-((0.0000001484831488128 * jmp.pow((-898.77 + indata[u"Height (mm)"]), 2) + 33.9577496496067 * jmp.pow((-0.57 + indata[u"Vertical_Friction"]), 2) + 0.0738977186050841 * jmp.pow((-0.25 + indata[u"Horizontal_Friction"]), 2) + 21.9622867242468 * jmp.pow((-0.24 + indata[u"Pallet_Friction"]), 2)))) + -0.528345325153237 * jmp.exp(-((0.0000001484831488128 * jmp.pow((-820.62 + indata[u"Height (mm)"]), 2) + 0.0738977186050841 * jmp.pow((-0.55 + indata[u"Horizontal_Friction"]), 2) + 33.9577496496067 * jmp.pow((-0.34 + indata[u"Vertical_Friction"]), 2) + 21.9622867242468 * jmp.pow((-0.25 + indata[u"Pallet_Friction"]), 2)))) + 0.00339884955120239 * jmp.exp(-((0.0000001484831488128 * jmp.pow((-

781.54 + indata[u"Height (mm)"]), 2) + 33.9577496496067 * jmp.pow((-0.61 + indata[u"Vertical_Friction"]), 2) + 21.9622867242468 * jmp.pow((-0.48 + indata[u"Pallet_Friction"]), 2) + 0.0738977186050841 * jmp.pow((-0.44 + indata[u"Horizontal_Friction"]), 2)))) + 0.415384812873294 * jmp.exp(-((0.0000001484831488128 * jmp.pow((-742.46 + indata[u"Height (mm)"]), 2) + 0.0738977186050841 * jmp.pow((-0.3 + indata[u"Horizontal_Friction"]), 2) + 33.9577496496067 * jmp.pow((-0.3 + indata[u"Vertical_Friction"]), 2) + 21.9622867242468 * jmp.pow((-0.28 + indata[u"Pallet_Friction"]), 2)))) + 0.246990952391946 * jmp.exp(-((0.0000001484831488128 * jmp.pow((-664.31 + indata[u"Height (mm)"]), 2) + 33.9577496496067 * jmp.pow((-0.67 + indata[u"Vertical_Friction"]), 2) + 0.0738977186050841 * jmp.pow((-0.61 + indata[u"Horizontal_Friction"]), 2) + 21.9622867242468 * jmp.pow((-0.33 + indata[u"Pallet_Friction"]), 2)))) + 0.114234082242217 * jmp.exp(-((0.0000001484831488128 * jmp.pow((-625.23 + indata[u"Height (mm)"]), 2) + 0.0738977186050841 * jmp.pow((-0.43 + indata[u"Horizontal_Friction"]), 2) + 21.9622867242468 * jmp.pow((-0.43 + indata[u"Pallet_Friction"]), 2) + 33.9577496496067 * jmp.pow((-0.39 + indata[u"Vertical_Friction"]), 2)))) + -0.448790782455563 * jmp.exp(-((0.0000001484831488128 * jmp.pow((-586.15 + indata[u"Height (mm)"]), 2) + 21.9622867242468 * jmp.pow((-0.61 + indata[u"Pallet_Friction"]), 2) + 0.0738977186050841 * jmp.pow((-0.34 + indata[u"Horizontal_Friction"]), 2) + 33.9577496496067 * jmp.pow((-0.24 + indata[u"Vertical_Friction"]), 2)))) + 0.187046491049111 * jmp.exp(-((0.0000001484831488128 * jmp.pow((-547.08 + indata[u"Height (mm)"]), 2) + 0.0738977186050841 * jmp.pow((-0.64 + indata[u"Horizontal_Friction"]), 2) + 21.9622867242468 * jmp.pow((-0.47 + indata[u"Pallet_Friction"]), 2) + 33.9577496496067 * jmp.pow((-0.26 + indata[u"Vertical_Friction"]), 2)))) + -0.114886269728468 * jmp.exp(-((0.0000001484831488128 * jmp.pow((-508 + indata[u"Height (mm)"]), 2) + 21.9622867242468 * jmp.pow((-0.66 + indata[u"Pallet_Friction"]), 2) + 33.9577496496067 * jmp.pow((-0.48 + indata[u"Vertical_Friction"]), 2) + 0.0738977186050841 * jmp.pow((-0.41 + indata[u"Horizontal_Friction"]), 2))))

```
return outdata[u"Ratio Prediction Formula"]
```

D.3. Formula for the Gaussian Process Model for 5 columns

```
from __future__ import division
import jmp_score as jmp
from math import *
import numpy as np


""" ==================================================================
 Copyright(C) 2018 SAS Institute Inc.All rights reserved.

 Notice:
 The following permissions are granted provided that the
 above copyright and this notice appear in the score code and
 any related documentation. Permission to copy, modify
 and distribute the score code generated using
 JMP(R) software is limited to customers of SAS Institute Inc. ("SAS")
 and successive third parties, all without any warranty, express or
 implied, or any other obligation by SAS. SAS and all other SAS
 Institute Inc. product and service names are registered
 trademarks or trademarks of SAS Institute Inc. in the USA
 and other countries. Except as contained in this notice,
 the name of the SAS Institute Inc. and JMP shall not be used in
 the advertising or promotion of products or services without
 prior written authorization from SAS Institute Inc.
 ================================================================== """

""" Python code generated by JMP v15.0.0 """

def getModelMetadata():
        return {"creator": u"Gaussian Process", "modelName": u"", "predicted": u"Ratio", "table": u"Columns=5", "version": u"15.0.0", "timestamp": u"2020-08-31T19:59:16Z"}


def getInputMetadata():
    return {
        u"Height (mm)": "float",
        u"Horizontal_Friction": "float",
        u"Pallet_Friction": "float",
        u"Vertical_Friction": "float"
            }


def getOutputMetadata():
    return {
        u"Ratio Prediction Formula": "float"
            }


def score(indata, outdata):
    outdata[u"Ratio Prediction Formula"] = 0.491009963402697 + -0.0748344176712304 * jmp.exp(-((0.0000006871399355687 * jmp.pow((-1992.92 + indata[u"Height (mm)"]), 2) + 0.0835700586855658 * jmp.pow((-0.66 + indata[u"Horizontal_Friction"]), 2) + 33.3739713268205 * jmp.pow((-0.6 + indata[u"Vertical_Friction"]), 2) + 21.2152551067792 * jmp.pow((-0.57 + indata[u"Pallet_Friction"]), 2)))) + -0.442846996058811 * jmp.exp(-((0.0000006871399355687 * jmp.pow((-1953.85 + indata[u"Height (mm)"]), 2) + 0.0835700586855658 * jmp.pow((-0.42 + indata[u"Horizontal_Friction"]), 2) + 33.3739713268205 * jmp.pow((-0.37 + indata[u"Vertical_Friction"]), 2) + 21.2152551067792 * jmp.pow((-0.32 + indata[u"Pallet_Friction"]), 2)))) + 0.152348960712861 * jmp.exp(-((0.0000006871399355687 * jmp.pow((-1914.77 + indata[u"Height (mm)"]), 2) + 0.0835700586855658 * jmp.pow((-0.57 + indata[u"Horizontal_Friction"]), 2) + 21.2152551067792 * jmp.pow((-0.44 + indata[u"Pallet_Friction"]), 2) + 33.3739713268205 * jmp.pow((-0.21 + indata[u"Vertical_Friction"]), 2)))) + 0.0143944994589447 *
```

jmp.exp(-((0.0000006871399355687 * jmp.pow((-1875.69 + indata[u"Height (mm)"]), 2) + 21.2152551067792 * jmp.pow((-0.55 + indata[u"Pallet_Friction"]), 2) + 33.3739713268205 * jmp.pow((-0.38 + indata[u"Vertical_Friction"]), 2) + 0.0835700586855658 * jmp.pow((-0.35 + indata[u"Horizontal_Friction"]), 2)))) + -0.153605109467535 * jmp.exp(-((0.0000006871399355687 * jmp.pow((-1836.62 + indata[u"Height (mm)"]), 2) + 21.2152551067792 * jmp.pow((-0.37 + indata[u"Pallet_Friction"]), 2) + 33.3739713268205 * jmp.pow((-0.28 + indata[u"Vertical_Friction"]), 2) + 0.0835700586855658 * jmp.pow((-0.21 + indata[u"Horizontal_Friction"]), 2)))) + 0.780191495778637 * jmp.exp(-((0.0000006871399355687 * jmp.pow((-1797.54 + indata[u"Height (mm)"]), 2) + 0.0835700586855658 * jmp.pow((-0.65 + indata[u"Horizontal_Friction"]), 2) + 33.3739713268205 * jmp.pow((-0.46 + indata[u"Vertical_Friction"]), 2) + 21.2152551067792 * jmp.pow((-0.39 + indata[u"Pallet_Friction"]), 2)))) + -0.0455593884631675 * jmp.exp(-((0.0000006871399355687 * jmp.pow((-1758.46 + indata[u"Height (mm)"]), 2) + 33.3739713268205 * jmp.pow((-0.56 + indata[u"Vertical_Friction"]), 2) + 0.0835700586855658 * jmp.pow((-0.28 + indata[u"Horizontal_Friction"]), 2) + 21.2152551067792 * jmp.pow((-0.26 + indata[u"Pallet_Friction"]), 2)))) + 0.073359686792354 * jmp.exp(-((0.0000006871399355687 * jmp.pow((-1719.38 + indata[u"Height (mm)"]), 2) + 33.3739713268205 * jmp.pow((-0.55 + indata[u"Vertical_Friction"]), 2) + 0.0835700586855658 * jmp.pow((-0.51 + indata[u"Horizontal_Friction"]), 2) + 21.2152551067792 * jmp.pow((-0.21 + indata[u"Pallet_Friction"]), 2)))) + -0.0278231933606738 * jmp.exp(-((0.0000006871399355687 * jmp.pow((-1641.23 + indata[u"Height (mm)"]), 2) + 21.2152551067792 * jmp.pow((-0.62 + indata[u"Pallet_Friction"]), 2) + 33.3739713268205 * jmp.pow((-0.53 + indata[u"Vertical_Friction"]), 2) + 0.0835700586855658 * jmp.pow((-0.47 + indata[u"Horizontal_Friction"]), 2)))) + 0.195516498185493 * jmp.exp(-((0.0000006871399355687 * jmp.pow((-1602.15 + indata[u"Height (mm)"]), 2) + 33.3739713268205 * jmp.pow((-0.69 + indata[u"Vertical_Friction"]), 2) + 0.0835700586855658 * jmp.pow((-0.62 + indata[u"Horizontal_Friction"]), 2) + 21.2152551067792 * jmp.pow((-0.34 + indata[u"Pallet_Friction"]), 2)))) + 0.264114242864018 * jmp.exp(-((0.0000006871399355687 * jmp.pow((-1524 + indata[u"Height (mm)"]), 2) + 0.0835700586855658 * jmp.pow((-0.58 + indata[u"Horizontal_Friction"]), 2) + 33.3739713268205 * jmp.pow((-0.33 + indata[u"Vertical_Friction"]), 2) + 21.2152551067792 * jmp.pow((-0.23 + indata[u"Pallet_Friction"]), 2)))) + -0.0421680374031931 * jmp.exp(-((0.0000006871399355687 * jmp.pow((-1484.92 + indata[u"Height (mm)"]), 2) + 21.2152551067792 * jmp.pow((-0.64 + indata[u"Pallet_Friction"]), 2) + 0.0835700586855658 * jmp.pow((-0.49 + indata[u"Horizontal_Friction"]), 2) + 33.3739713268205 * jmp.pow((-0.32 + indata[u"Vertical_Friction"]), 2)))) + -0.342528970575507 * jmp.exp(-((0.0000006871399355687 * jmp.pow((-1445.85 + indata[u"Height (mm)"]), 2) + 33.3739713268205 * jmp.pow((-0.7 + indata[u"Vertical_Friction"]), 2) + 21.2152551067792 * jmp.pow((-0.49 + indata[u"Pallet_Friction"]), 2) + 0.0835700586855658 * jmp.pow((-0.38 + indata[u"Horizontal_Friction"]), 2)))) + 0.036181654857164 * jmp.exp(-((0.0000006871399355687 * jmp.pow((-1406.77 + indata[u"Height (mm)"]), 2) + 21.2152551067792 * jmp.pow((-0.53 + indata[u"Pallet_Friction"]), 2) + 0.0835700586855658 * jmp.pow((-0.32 + indata[u"Horizontal_Friction"]), 2) + 33.3739713268205 * jmp.pow((-0.2 + indata[u"Vertical_Friction"]), 2)))) + 0.0273001364577141 * jmp.exp(-((0.0000006871399355687 * jmp.pow((-1367.69 + indata[u"Height (mm)"]), 2) + 0.0835700586855658 * jmp.pow((-0.37 + indata[u"Horizontal_Friction"]), 2) + 21.2152551067792 * jmp.pow((-0.3 + indata[u"Pallet_Friction"]), 2) + 33.3739713268205 * jmp.pow((-0.23 + indata[u"Vertical_Friction"]), 2)))) + -1.41903131049454 * jmp.exp(-((0.0000006871399355687 * jmp.pow((-1328.62 + indata[u"Height (mm)"]), 2) + 0.0835700586855658 * jmp.pow((-0.48 + indata[u"Horizontal_Friction"]), 2) + 33.3739713268205 * jmp.pow((-0.47 + indata[u"Vertical_Friction"]), 2) + 21.2152551067792 * jmp.pow((-0.41 + indata[u"Pallet_Friction"]), 2)))) + 0.838638599869705 * jmp.exp(-((0.0000006871399355687 * jmp.pow((-1289.54 + indata[u"Height (mm)"]), 2) + 33.3739713268205 * jmp.pow((-0.42 + indata[u"Vertical_Friction"]), 2) + 21.2152551067792 * jmp.pow((-0.38 + indata[u"Pallet_Friction"]), 2) + 0.0835700586855658 * jmp.pow((-0.24 + indata[u"Horizontal_Friction"]), 2)))) + 0.400191407554078 * jmp.exp(-((0.0000006871399355687 * jmp.pow((-1133.23 + indata[u"Height (mm)"]), 2) + 0.0835700586855658 * jmp.pow((-0.67 + indata[u"Horizontal_Friction"]), 2) + 33.3739713268205 * jmp.pow((-0.66 + indata[u"Vertical_Friction"]), 2) + 21.2152551067792 * jmp.pow((-0.52 + indata[u"Pallet_Friction"]), 2)))) + -0.294442321909093 * jmp.exp(-((0.0000006871399355687 * jmp.pow((-1094.15 + indata[u"Height (mm)"]), 2) + 21.2152551067792 * jmp.pow((-0.6 + indata[u"Pallet_Friction"]), 2) + 33.3739713268205 * jmp.pow((-0.41 + indata[u"Vertical_Friction"]), 2) + 0.0835700586855658 * jmp.pow((-0.33 + indata[u"Horizontal_Friction"]), 2)))) + 0.30307831311714 * jmp.exp(-((0.0000006871399355687 * jmp.pow((-1016 + indata[u"Height (mm)"]), 2) + 21.2152551067792 * jmp.pow((-0.69 + indata[u"Pallet_Friction"]), 2) + 33.3739713268205 * jmp.pow((-0.62 + indata[u"Vertical_Friction"]), 2) + 0.0835700586855658 * jmp.pow((-0.52 + indata[u"Horizontal_Friction"]), 2)))) + 0.723964536985593 * jmp.exp(-((0.0000006871399355687 * jmp.pow((-976.92 + indata[u"Height (mm)"]), 2) + 0.0835700586855658 * jmp.pow((-0.6 + indata[u"Horizontal_Friction"]), 2) + 21.2152551067792 * jmp.pow((-0.56 + indata[u"Pallet_Friction"]), 2) + 33.3739713268205 * jmp.pow((-0.44 + indata[u"Vertical_Friction"]), 2)))) + -0.534235772596599 * jmp.exp(-((0.0000006871399355687 * jmp.pow((-937.85 + indata[u"Height (mm)"]), 2) + 21.2152551067792 * jmp.pow((-0.65 + indata[u"Pallet_Friction"]), 2) + 33.3739713268205 * jmp.pow((-0.64 + indata[u"Vertical_Friction"]), 2) + 0.0835700586855658 * jmp.pow((-0.29 + indata[u"Horizontal_Friction"]), 2)))) + 0.151363230279477 * jmp.exp(-((0.0000006871399355687 * jmp.pow((-859.69 + indata[u"Height (mm)"]), 2) + 21.2152551067792 * jmp.pow((-0.7 + indata[u"Pallet_Friction"]), 2) + 0.0835700586855658 * jmp.pow((-0.53 + indata[u"Horizontal_Friction"]), 2) + 33.3739713268205 * jmp.pow((-0.29 + indata[u"Vertical_Friction"]), 2)))) + -0.377003314336225 * jmp.exp(-((0.0000006871399355687 * jmp.pow((-820.62 + indata[u"Height (mm)"]), 2) + 0.0835700586855658 * jmp.pow((-0.55 + indata[u"Horizontal_Friction"]), 2) + 33.3739713268205 * jmp.pow((-0.34 + indata[u"Vertical_Friction"]), 2) + 21.2152551067792 * jmp.pow((-0.25 + indata[u"Pallet_Friction"]), 2)))) + 0.169214360135111 * jmp.exp(-((0.0000006871399355687 * jmp.pow((-781.54 + indata[u"Height (mm)"]), 2) + 33.3739713268205 * jmp.pow((-0.61 + indata[u"Vertical_Friction"]), 2) + 21.2152551067792 * jmp.pow((-0.48 + indata[u"Pallet_Friction"]), 2) + 0.0835700586855658 * jmp.pow((-0.44 + indata[u"Horizontal_Friction"]), 2)))) + 0.229263839312546 * jmp.exp(-((0.0000006871399355687 * jmp.pow((-742.46 + indata[u"Height (mm)"]), 2) + 0.0835700586855658

```
* jmp.pow((-0.3 + indata[u"Horizontal_Friction"]), 2) + 33.3739713268205 * jmp.pow((-0.3 + indata[u"Vertical_Friction"]), 2) +
21.2152551067792 * jmp.pow((-0.28 + indata[u"Pallet_Friction"]), 2)))) + -0.0301804754712044 * jmp.exp(-
((0.0000006871399355687 * jmp.pow((-703.38 + indata[u"Height (mm)"]), 2) + 33.3739713268205 * jmp.pow((-0.52 +
indata[u"Vertical_Friction"]), 2) + 21.2152551067792 * jmp.pow((-0.46 + indata[u"Pallet_Friction"]), 2) + 0.0835700586855658 *
jmp.pow((-0.23 + indata[u"Horizontal_Friction"]), 2)))) + -0.103008626950518 * jmp.exp(-((0.0000006871399355687 * jmp.pow((-
664.31 + indata[u"Height (mm)"]), 2) + 33.3739713268205 * jmp.pow((-0.67 + indata[u"Vertical_Friction"]), 2) +
0.0835700586855658 * jmp.pow((-0.61 + indata[u"Horizontal_Friction"]), 2) + 21.2152551067792 * jmp.pow((-0.33 +
indata[u"Pallet_Friction"]), 2)))) + 0.0743112203444423 * jmp.exp(-((0.0000006871399355687 * jmp.pow((-625.23 + indata[u"Height
(mm)"]), 2) + 0.0835700586855658 * jmp.pow((-0.43 + indata[u"Horizontal_Friction"]), 2) + 21.2152551067792 * jmp.pow((-0.43 +
indata[u"Pallet_Friction"]), 2) + 33.3739713268205 * jmp.pow((-0.39 + indata[u"Vertical_Friction"]), 2)))) + -0.0513912644883757 *
jmp.exp(-((0.0000006871399355687 * jmp.pow((-586.15 + indata[u"Height (mm)"]), 2) + 21.2152551067792 * jmp.pow((-0.61 +
indata[u"Pallet_Friction"]), 2) + 0.0835700586855658 * jmp.pow((-0.34 + indata[u"Horizontal_Friction"]), 2) + 33.3739713268205 *
jmp.pow((-0.24 + indata[u"Vertical_Friction"]), 2)))) + -0.112899762524901 * jmp.exp(-((0.0000006871399355687 * jmp.pow((-
547.08 + indata[u"Height (mm)"]), 2) + 0.0835700586855658 * jmp.pow((-0.64 + indata[u"Horizontal_Friction"]), 2) +
21.2152551067792 * jmp.pow((-0.47 + indata[u"Pallet_Friction"]), 2) + 33.3739713268205 * jmp.pow((-0.26 +
indata[u"Vertical_Friction"]), 2)))) + -0.381873720933703 * jmp.exp(-((0.0000006871399355687 * jmp.pow((-508 + indata[u"Height
(mm)"]), 2) + 21.2152551067792 * jmp.pow((-0.66 + indata[u"Pallet_Friction"]), 2) + 33.3739713268205 * jmp.pow((-0.48 +
indata[u"Vertical_Friction"]), 2) + 0.0835700586855658 * jmp.pow((-0.41 + indata[u"Horizontal_Friction"]), 2))))

    return outdata[u"Ratio Prediction Formula"]
```

D.4. Formula for the Gaussian Process Model for 6 columns

```
from __future__ import division
import jmp_score as jmp
from math import *
import numpy as np


""" ================================================================
 Copyright(C) 2018 SAS Institute Inc.All rights reserved.

 Notice:
 The following permissions are granted provided that the
 above copyright and this notice appear in the score code and
 any related documentation. Permission to copy, modify
 and distribute the score code generated using
 JMP(R) software is limited to customers of SAS Institute Inc. ("SAS")
 and successive third parties, all without any warranty, express or
 implied, or any other obligation by SAS. SAS and all other SAS
 Institute Inc. product and service names are registered
 trademarks or trademarks of SAS Institute Inc. in the USA
 and other countries. Except as contained in this notice,
 the name of the SAS Institute Inc. and JMP shall not be used in
 the advertising or promotion of products or services without
 prior written authorization from SAS Institute Inc.
 ================================================================ """

""" Python code generated by JMP v15.0.0 """

def getModelMetadata():
        return {"creator": u"Gaussian Process", "modelName": u"", "predicted": u"Ratio", "table": u"Columns=6", "version": u"15.0.0", "timestamp": u"2020-08-31T19:59:48Z"}


def getInputMetadata():
    return {
        u"Horizontal_Friction": "float",
        u"Pallet_Friction": "float",
        u"Vertical_Friction": "float"
            }


def getOutputMetadata():
    return {
        u"Ratio Prediction Formula": "float"
            }


def score(indata, outdata):
    outdata[u"Ratio Prediction Formula"] = 0.593139334951414 + 0.00943096438698837 * jmp.exp(-((1.68684597555766 * jmp.pow((-0.7 + indata[u"Horizontal_Friction"]), 2) + 13.2484044550356 * jmp.pow((-0.58 + indata[u"Pallet_Friction"]), 2) + 192.929055892264 * jmp.pow((-0.35 + indata[u"Vertical_Friction"]), 2)))) + 0.226530602498753 * jmp.exp(-((1.68684597555766 * jmp.pow((-0.67 + indata[u"Horizontal_Friction"]), 2) + 192.929055892264 * jmp.pow((-0.66 + indata[u"Vertical_Friction"]), 2) + 13.2484044550356 * jmp.pow((-0.52 + indata[u"Pallet_Friction"]), 2)))) + 0.222846325965564 * jmp.exp(-((1.68684597555766 * jmp.pow((-0.66 + indata[u"Horizontal_Friction"]), 2) + 192.929055892264 * jmp.pow((-0.6 + indata[u"Vertical_Friction"]), 2) + 13.2484044550356 * jmp.pow((-0.57 + indata[u"Pallet_Friction"]), 2)))) + -0.0772641883839807 * jmp.exp(-((1.68684597555766 * jmp.pow((-0.64 + indata[u"Horizontal_Friction"]), 2) + 13.2484044550356 * jmp.pow((-0.47 + indata[u"Pallet_Friction"]), 2) + 192.929055892264 * jmp.pow((-0.26 + indata[u"Vertical_Friction"]), 2)))) + 0.203233452312261 * jmp.exp(-((1.68684597555766 * jmp.pow((-0.6 + indata[u"Horizontal_Friction"]), 2) + 13.2484044550356 * jmp.pow((-0.56 + indata[u"Pallet_Friction"]), 2) + 192.929055892264 *
```

```
jmp.pow((-0.44 + indata[u"Vertical_Friction"]), 2)))) + 0.334619842772528 * jmp.exp(-((1.68684597555766 * jmp.pow((-0.58 +
indata[u"Horizontal_Friction"]), 2) + 192.929055892264 * jmp.pow((-0.33 + indata[u"Vertical_Friction"]), 2) + 13.2484044550356 *
jmp.pow((-0.23 + indata[u"Pallet_Friction"]), 2)))) + 0.0357608316172623 * jmp.exp(-((1.68684597555766 * jmp.pow((-0.57 +
indata[u"Horizontal_Friction"]), 2) + 13.2484044550356 * jmp.pow((-0.44 + indata[u"Pallet_Friction"]), 2) + 192.929055892264 *
jmp.pow((-0.21 + indata[u"Vertical_Friction"]), 2)))) + 0.0359067465074916 * jmp.exp(-((1.68684597555766 * jmp.pow((-0.56 +
indata[u"Horizontal_Friction"]), 2) + 13.2484044550356 * jmp.pow((-0.42 + indata[u"Pallet_Friction"]), 2) + 192.929055892264 *
jmp.pow((-0.25 + indata[u"Vertical_Friction"]), 2)))) + -0.47571616974978 * jmp.exp(-((1.68684597555766 * jmp.pow((-0.55 +
indata[u"Horizontal_Friction"]), 2) + 192.929055892264 * jmp.pow((-0.34 + indata[u"Vertical_Friction"]), 2) + 13.2484044550356 *
jmp.pow((-0.25 + indata[u"Pallet_Friction"]), 2)))) + 0.0279779366384816 * jmp.exp(-((1.68684597555766 * jmp.pow((-0.48 +
indata[u"Horizontal_Friction"]), 2) + 192.929055892264 * jmp.pow((-0.47 + indata[u"Vertical_Friction"]), 2) + 13.2484044550356 *
jmp.pow((-0.41 + indata[u"Pallet_Friction"]), 2)))) + 0.35131645943198 * jmp.exp(-((1.68684597555766 * jmp.pow((-0.42 +
indata[u"Horizontal_Friction"]), 2) + 192.929055892264 * jmp.pow((-0.37 + indata[u"Vertical_Friction"]), 2) + 13.2484044550356 *
jmp.pow((-0.32 + indata[u"Pallet_Friction"]), 2)))) + 0.00881003602613707 * jmp.exp(-((1.68684597555766 * jmp.pow((-0.37 +
indata[u"Horizontal_Friction"]), 2) + 13.2484044550356 * jmp.pow((-0.3 + indata[u"Pallet_Friction"]), 2) + 192.929055892264 *
jmp.pow((-0.23 + indata[u"Vertical_Friction"]), 2)))) + -0.0841392979961282 * jmp.exp(-((13.2484044550356 * jmp.pow((-0.7 +
indata[u"Pallet_Friction"]), 2) + 1.68684597555766 * jmp.pow((-0.53 + indata[u"Horizontal_Friction"]), 2) + 192.929055892264 *
jmp.pow((-0.29 + indata[u"Vertical_Friction"]), 2)))) + -0.24451841183761 * jmp.exp(-((13.2484044550356 * jmp.pow((-0.69 +
indata[u"Pallet_Friction"]), 2) + 192.929055892264 * jmp.pow((-0.62 + indata[u"Vertical_Friction"]), 2) + 1.68684597555766 *
jmp.pow((-0.52 + indata[u"Horizontal_Friction"]), 2)))) + 0.228695610802868 * jmp.exp(-((13.2484044550356 * jmp.pow((-0.67 +
indata[u"Pallet_Friction"]), 2) + 192.929055892264 * jmp.pow((-0.51 + indata[u"Vertical_Friction"]), 2) + 1.68684597555766 *
jmp.pow((-0.2 + indata[u"Horizontal_Friction"]), 2)))) + -0.587849879725133 * jmp.exp(-((13.2484044550356 * jmp.pow((-0.66 +
indata[u"Pallet_Friction"]), 2) + 192.929055892264 * jmp.pow((-0.48 + indata[u"Vertical_Friction"]), 2) + 1.68684597555766 *
jmp.pow((-0.41 + indata[u"Horizontal_Friction"]), 2)))) + -0.181987711289532 * jmp.exp(-((13.2484044550356 * jmp.pow((-0.65 +
indata[u"Pallet_Friction"]), 2) + 192.929055892264 * jmp.pow((-0.64 + indata[u"Vertical_Friction"]), 2) + 1.68684597555766 *
jmp.pow((-0.29 + indata[u"Horizontal_Friction"]), 2)))) + 0.191184662785231 * jmp.exp(-((13.2484044550356 * jmp.pow((-0.64 +
indata[u"Pallet_Friction"]), 2) + 1.68684597555766 * jmp.pow((-0.49 + indata[u"Horizontal_Friction"]), 2) + 192.929055892264 *
jmp.pow((-0.32 + indata[u"Vertical_Friction"]), 2)))) + -0.191733316453697 * jmp.exp(-((13.2484044550356 * jmp.pow((-0.62 +
indata[u"Pallet_Friction"]), 2) + 192.929055892264 * jmp.pow((-0.53 + indata[u"Vertical_Friction"]), 2) + 1.68684597555766 *
jmp.pow((-0.47 + indata[u"Horizontal_Friction"]), 2)))) + 0.0476301032376704 * jmp.exp(-((13.2484044550356 * jmp.pow((-0.61 +
indata[u"Pallet_Friction"]), 2) + 1.68684597555766 * jmp.pow((-0.34 + indata[u"Horizontal_Friction"]), 2) + 192.929055892264 *
jmp.pow((-0.24 + indata[u"Vertical_Friction"]), 2)))) + 0.448620128729714 * jmp.exp(-((13.2484044550356 * jmp.pow((-0.6 +
indata[u"Pallet_Friction"]), 2) + 192.929055892264 * jmp.pow((-0.41 + indata[u"Vertical_Friction"]), 2) + 1.68684597555766 *
jmp.pow((-0.33 + indata[u"Horizontal_Friction"]), 2)))) + -0.450917350311948 * jmp.exp(-((13.2484044550356 * jmp.pow((-0.55 +
indata[u"Pallet_Friction"]), 2) + 192.929055892264 * jmp.pow((-0.38 + indata[u"Vertical_Friction"]), 2) + 1.68684597555766 *
jmp.pow((-0.35 + indata[u"Horizontal_Friction"]), 2)))) + 0.0158599433865497 * jmp.exp(-((13.2484044550356 * jmp.pow((-0.37 +
indata[u"Pallet_Friction"]), 2) + 192.929055892264 * jmp.pow((-0.28 + indata[u"Vertical_Friction"]), 2) + 1.68684597555766 *
jmp.pow((-0.21 + indata[u"Horizontal_Friction"]), 2)))) + 0.0353260957007769 * jmp.exp(-((192.929055892264 * jmp.pow((-0.69 +
indata[u"Vertical_Friction"]), 2) + 1.68684597555766 * jmp.pow((-0.62 + indata[u"Horizontal_Friction"]), 2) + 13.2484044550356 *
jmp.pow((-0.34 + indata[u"Pallet_Friction"]), 2)))) + -0.214402145297626 * jmp.exp(-((192.929055892264 * jmp.pow((-0.67 +
indata[u"Vertical_Friction"]), 2) + 1.68684597555766 * jmp.pow((-0.61 + indata[u"Horizontal_Friction"]), 2) + 13.2484044550356 *
jmp.pow((-0.33 + indata[u"Pallet_Friction"]), 2)))) + 0.231170297924968 * jmp.exp(-((192.929055892264 * jmp.pow((-0.65 +
indata[u"Vertical_Friction"]), 2) + 1.68684597555766 * jmp.pow((-0.46 + indata[u"Horizontal_Friction"]), 2) + 13.2484044550356 *
jmp.pow((-0.29 + indata[u"Pallet_Friction"]), 2)))) + -0.220328343588647 * jmp.exp(-((192.929055892264 * jmp.pow((-0.61 +
indata[u"Vertical_Friction"]), 2) + 13.2484044550356 * jmp.pow((-0.48 + indata[u"Pallet_Friction"]), 2) + 1.68684597555766 *
jmp.pow((-0.44 + indata[u"Horizontal_Friction"]), 2)))) + 0.00762776493348111 * jmp.exp(-((192.929055892264 * jmp.pow((-0.57 +
indata[u"Vertical_Friction"]), 2) + 1.68684597555766 * jmp.pow((-0.25 + indata[u"Horizontal_Friction"]), 2) + 13.2484044550356 *
jmp.pow((-0.24 + indata[u"Pallet_Friction"]), 2)))) + -0.0205956119217474 * jmp.exp(-((192.929055892264 * jmp.pow((-0.55 +
indata[u"Vertical_Friction"]), 2) + 1.68684597555766 * jmp.pow((-0.51 + indata[u"Horizontal_Friction"]), 2) + 13.2484044550356 *
jmp.pow((-0.21 + indata[u"Pallet_Friction"]), 2)))) + 0.260984201468229 * jmp.exp(-((192.929055892264 * jmp.pow((-0.52 +
indata[u"Vertical_Friction"]), 2) + 13.2484044550356 * jmp.pow((-0.46 + indata[u"Pallet_Friction"]), 2) + 1.68684597555766 *
jmp.pow((-0.23 + indata[u"Horizontal_Friction"]), 2)))) + 0.0305325225149831 * jmp.exp(-((192.929055892264 * jmp.pow((-0.43 +
indata[u"Vertical_Friction"]), 2) + 1.68684597555766 * jmp.pow((-0.39 + indata[u"Horizontal_Friction"]), 2) + 13.2484044550356 *
jmp.pow((-0.2 + indata[u"Pallet_Friction"]), 2)))) + -0.204612103086104 * jmp.exp(-((192.929055892264 * jmp.pow((-0.42 +
indata[u"Vertical_Friction"]), 2) + 13.2484044550356 * jmp.pow((-0.38 + indata[u"Pallet_Friction"]), 2) + 1.68684597555766 *
jmp.pow((-0.24 + indata[u"Horizontal_Friction"]), 2))))

    return outdata[u"Ratio Prediction Formula"]
```

D.5. JMP Score Function, required as helper module.

```
mport math
import numpy as np

# ----------------------------------------------------------------
# jmp_score.py
# Helper module with functions supporting the Python language
# scoring code generated by JMP
#
# Required by customer code: Yes
# ----------------------------------------------------------------


# return the index of the max value found in an array
# or -1 if all are missing
def max_array(len, lst):
    maxval = -float('inf')
    maxidx = 0
    count_miss = 0

    for i in range(0, len):
        if is_missing(lst[i]):
            count_miss = count_miss + 1
        elif maxval < lst[i]:
            maxval = lst[i]
            maxidx = i
    return -1 if (count_miss == len) else maxidx


# return the index of the min value found in an array
# or -1 if all are missing
def min_array(len, lst):
    minval = float('inf')
    minidx = 0
    count_miss = 0

    for i in range(0, len):
        if is_missing(lst[i]):
            count_miss = count_miss + 1
        elif minval > lst[i]:
            minval = lst[i]
            minidx = i
    return -1 if (count_miss == len) else minidx


def is_missing(x):
    return math.isnan(x) or math.isinf(x) or x is None


def exp(x):
    try:
        return math.exp(x)
    except OverflowError:
        return float('inf')


def pow(a, b=2):
```

```
    try:
        return math.pow(a, b)
    except OverflowError:
        return float('inf')


# Also known as logist or logistic
def squish(x):
    return 1.0 / (1.0 + exp(-x))


def squash(x):
    return 1.0 / (1.0 + exp(x))


# Returns true if the numbers are identical using straight comparison.
# If necessary, replace with a suitable comparison using a value of EPSILON
# appropriate for your domain.
def numeq(x, y):
    return x == y
    # return Math.abs(a - b) < EPSILON;


def vec_diag(M):
    """
    Returns the diagonal elements of the square matrix as a vector.
    """
    return np.diag(M).reshape(M.shape[0], 1)


def vec_quadratic(S, X):
    """
    Evaluates as Vec Diag( X * S * X` ).
    """
    if S.shape[1] == X.shape[0]:
        return vec_diag(np.dot(X.T, np.dot(S, X)))
    return vec_diag(np.dot(X, np.dot(S, X.T)))


def sum(S):
    """
    Return the sum of array elements treating missing (NaN) as zero.

    To match JMP's behavior, check if all elements are missing in
    which case missing is returned.
    """
    if np.all(np.isnan(S)):
        return np.nan
    return np.nansum(S)
```

Appendix D. Python Scripts for parametric modification of Abaqus CAE models

The following scripts can be used to modify the base finite element model used in Chapter 1 and to retrieve data efficiently. Script 1 allows the user to copy the model and change the values of the input variables. It can be used to generate multiple copies based on array inputs of the variables.

Scripts 2 and 3 allow for the retrieval of images and data of the solved model. Although results can be generated for large runs, it is recommended to review the results for each individual run.

1 Script 1: Parametric creation of unit loads for the finite element method.

```
# ============================================================
# ============================================================
# ============================================================
# ============================================================
# Paste all the input variables from the Script_Generator.xlsx

from part import *
from material import *
from section import *
from assembly import *
from step import *
from interaction import *
from load import *
from mesh import *
from optimization import *
from job import *
from sketch import *
from visualization import *
from connectorBehavior import *

Runs          = [ ] #Insert here names (string) of new models to copy
COF_pall      = [] #Pallet friction for each model copy
COF_ver       = [] #Vertical box friction for each model copy
COF_hor       = [] #Horizontal box friction for each model copy
new_height    = [] #Unit load height for each model copy
```

```
columns         = [] #Number of columns for each model copy
density         = [] #Box density for each model copy
master_models = [0,1,'2C3L_master_30in','3C3L_master_30in','4C3L_master_30in',
                        '5C3L_master_30in','6C3L_master_30in','7C3L_Master_30in','8C3L_Mas
                ter_30in',
                        '9C3L_Master_30in'] #name of the original models that will be copied and
                modified

original_height = 30 #original unit load height
layers = 3       #number of layers of the original unit loads
pallet_MOE  = 400000 #modify for the new copies
new_box_height  = [x/3 for x in new_height]
i = 0
for iRun in Runs:
    mdb.Model(name=iRun, objectToCopy=mdb.models[master_models[columns[i]]])
    #change horizontal friction
    mdb.models[iRun].interactionProperties['Box-Box-Horizontal'].tangentialBehavior.setValues(
        table=((COF_hor[i], ), ))
    #change vertical friction
    mdb.models[iRun].interactionProperties['Box-Box-Vertical'].tangentialBehavior.setValues(
        table=((COF_ver[i], ), ))
    #change pallet friction
    mdb.models[iRun].interactionProperties['PlexiPallet-Box'].tangentialBehavior.setValues(
        table=((COF_pall[i], ), ))
     #change pallet stiffness
    mdb.models[iRun].materials['Plexi'].elastic.setValues(table=((
        pallet_MOE, 0.35), ))
     #change box density
    mdb.models[iRun].materials['Box_Material'].density.setValues(
        table=((density[i], ), ))
    box_height_int = (new_height[i] / 3)
    #check that layers is not parametric
    box_height = str(new_box_height[i])
    translate_Y = (new_height[i] - original_height) / 3
    ## adjust the size of the box sketch
    mdb.models[iRun].ConstrainedSketch(name='__edit__'
        , objectToCopy=
        mdb.models[iRun].parts['Box'].features['Shell planar-1'].sketch)
    mdb.models[iRun].sketches['__edit__'].parameters['BoxHeight'].setValues(
        expression=box_height)
    mdb.models[iRun].parts['Box'].features['Shell planar-1'].setValues(
        sketch=mdb.models[iRun].sketches['__edit__'])
    del mdb.models[iRun].sketches['__edit__']
    mdb.models[iRun].parts['Box'].regenerate()
    mdb.models[iRun].rootAssembly.regenerate()
    if columns[i] == 2:
```

```
        #if to select the right boxes to move
        mdb.models[iRun].rootAssembly.translate(instanceList=('Box_L3_C1','Box_L3_C2'),
vector=(0.0, translate_Y,0.0))

mdb.models[iRun].rootAssembly.translate(instanceList=('Box_L2_C1','Box_L3_C1','Box_L2_C
2','Box_L3_C2'), vector=(0.0, translate_Y, 0.0))
    elif columns[i] == 3:

mdb.models[iRun].rootAssembly.translate(instanceList=('Box_L3_C1','Box_L3_C2','Box_L3_C
3'), vector=(0.0, translate_Y,0.0))

mdb.models[iRun].rootAssembly.translate(instanceList=('Box_L2_C1','Box_L3_C1','Box_L2_C
2','Box_L3_C2','Box_L2_C3','Box_L3_C3'), vector=(0.0, translate_Y, 0.0))
    elif columns[i] == 4:

mdb.models[iRun].rootAssembly.translate(instanceList=('Box_L3_C1','Box_L3_C2','Box_L3_C
3','Box_L3_C4'), vector=(0.0, translate_Y, 0.0))

mdb.models[iRun].rootAssembly.translate(instanceList=('Box_L2_C1','Box_L3_C1','Box_L2_C
2','Box_L3_C2','Box_L2_C3','Box_L3_C3','Box_L2_C4','Box_L3_C4'), vector=(0.0,
translate_Y, 0.0))
    elif columns[i] == 5:

mdb.models[iRun].rootAssembly.translate(instanceList=('Box_L3_C1','Box_L3_C2','Box_L3_C
3','Box_L3_C4','Box_L3_C5'), vector=(0.0, translate_Y,0.0))

mdb.models[iRun].rootAssembly.translate(instanceList=('Box_L2_C1','Box_L3_C1','Box_L2_C
2','Box_L3_C2','Box_L2_C3','Box_L3_C3','Box_L2_C4','Box_L3_C4','Box_L2_C5','Box_L3_C
5'), vector=(0.0, translate_Y, 0.0))
    elif columns[i] == 6:

mdb.models[iRun].rootAssembly.translate(instanceList=('Box_L3_C1','Box_L3_C2','Box_L3_C
3','Box_L3_C4','Box_L3_C5','Box_L3_C6'), vector=(0.0, translate_Y,0.0))

mdb.models[iRun].rootAssembly.translate(instanceList=('Box_L2_C1','Box_L3_C1','Box_L2_C
2','Box_L3_C2','Box_L2_C3','Box_L3_C3','Box_L2_C4','Box_L3_C4','Box_L2_C5','Box_L3_C
5','Box_L2_C6','Box_L3_C6'), vector=(0.0, translate_Y, 0.0))
    elif columns[i] == 7:

mdb.models[iRun].rootAssembly.translate(instanceList=('Box_L3_C1','Box_L3_C2','Box_L3_C
3','Box_L3_C4','Box_L3_C5','Box_L3_C6','Box_L3_C7'), vector=(0.0, translate_Y,0.0))

mdb.models[iRun].rootAssembly.translate(instanceList=('Box_L2_C1','Box_L3_C1','Box_L2_C
2','Box_L3_C2','Box_L2_C3','Box_L3_C3','Box_L2_C4','Box_L3_C4','Box_L2_C5','Box_L3_C
5','Box_L2_C6','Box_L3_C6','Box_L2_C7','Box_L3_C7'), vector=(0.0, translate_Y, 0.0))
    elif columns[i] == 8:
```

```
mdb.models[iRun].rootAssembly.translate(instanceList=('Box_L3_C1','Box_L3_C2','Box_L3_C
3','Box_L3_C4','Box_L3_C5','Box_L3_C6','Box_L3_C7','Box_L3_C8'), vector=(0.0,
translate_Y,0.0))

mdb.models[iRun].rootAssembly.translate(instanceList=('Box_L2_C1','Box_L3_C1','Box_L2_C
2','Box_L3_C2','Box_L2_C3','Box_L3_C3','Box_L2_C4','Box_L3_C4','Box_L2_C5','Box_L3_C
5','Box_L2_C6','Box_L3_C6','Box_L2_C7','Box_L3_C7','Box_L2_C8','Box_L3_C8'),
vector=(0.0, translate_Y, 0.0))
    elif columns[i] == 9:

mdb.models[iRun].rootAssembly.translate(instanceList=('Box_L3_C1','Box_L3_C2','Box_L3_C
3','Box_L3_C4','Box_L3_C5','Box_L3_C6','Box_L3_C7','Box_L3_C8','Box_L3_C9'),
vector=(0.0, translate_Y,0.0))

mdb.models[iRun].rootAssembly.translate(instanceList=('Box_L2_C1','Box_L3_C1','Box_L2_C
2','Box_L3_C2','Box_L2_C3','Box_L3_C3','Box_L2_C4','Box_L3_C4','Box_L2_C5','Box_L3_C
5','Box_L2_C6','Box_L3_C6','Box_L2_C7','Box_L3_C7','Box_L2_C8','Box_L3_C8','Box_L2_C
9','Box_L3_C9'), vector=(0.0, translate_Y,0.0))

    else:
        pass
    mdb.models[iRun].parts['Box'].generateMesh()
    mdb.models[iRun].rootAssembly.regenerate()
    mdb.models[iRun].rootAssembly.regenerate()
    i = i + 1
    mdb.Job(name=iRun, model=iRun, description='', type=ANALYSIS,
        atTime=None, waitMinutes=0, waitHours=0, queue=None, memory=90,
        memoryUnits=PERCENTAGE, getMemoryFromAnalysis=True,
        explicitPrecision=SINGLE, nodalOutputPrecision=SINGLE, echoPrint=OFF,
        modelPrint=OFF, contactPrint=OFF, historyPrint=OFF, userSubroutine='',
        scratch='', resultsFormat=ODB, multiprocessingMode=DEFAULT, numCpus=8,
        numDomains=8, numGPUs=0)
    mdb.jobs[iRun].writeInput(consistencyChecking=OFF)
```

2 Script 2: Automated Abaqus script for the retrieval of the results for the deflection of the board.

```
#THIS WORKS TO OBTAIN THE DISPLACEMENT AT THE PALLETCENTER

from abaqus import *
from abaqusConstants import *
import visualization
```

```
paths_model = ['C:\Users\edu88.HOKIES\Documents\ACTIVE_FEA_RUNS\_480lbs\Results
Retrieval\_5C3L_30in_6p_2box_400_480lb.odb'] #modify to show file location
model_id = ['_5C3L_30in_6p_2box_400_480lb'] #modify to show file name
count = 0
for i in paths_model:
    odb = session.openOdb(name=i)
    lastFrame = odb.steps['GravityLoad'].frames[-1]
    displacement=lastFrame.fieldOutputs['U']
    center = odb.rootAssembly.instances['PALLET'].nodeSets["NEUTRALAXISCENTER"]
    centerDisplacement = displacement.getSubset(region=center)
    centerValues = centerDisplacement.values
    #print ('odb', centerValues[0].nodeLabel, centerValues[0].data, lastFrame.frameValue,
file=results)
    results = open('results2.txt', 'a')
    astr = str(model_id[count]) +' Frame: '+str(lastFrame.frameValue)+':
'+str(centerValues[0].data)+ '\n'
    count += 1
    results.write(astr)
    results.close()
    odb.close()
```

3 Script 3: Automated Abaqus script for the retrieval of an image of the deformed model for each run.

```
from abaqus import *
from abaqusConstants import *
from caeModules import *
import visualization
#This statement provides access to the commands that replicate the functionality of the
Visualization module in Abaqus/CAE (Abaqus/Viewer).
pathFolder = 'C:/Users/edu88.HOKIES/Documents/ACTIVE_FEA_RUNS/_480lbs/Results
Retrieval/'
paths_name= ['_5C3L_30in_6p_2box_400_480lb.odb']
names = ['_5C3L_30in_6p_2box_400_480lb']
j = 0
for i in paths_name:
    paths_model = pathFolder + i
    myViewport = session.Viewport(name=i, width=400, height=168)
    #This statement creates a new viewport in the session. The new viewport is assigned to the
variable myViewport. The origin and the size of the viewport assume the default values.
```

```
    odbPath = paths_model
    #This statement creates a path to the tutorial output database.
    myOdb = session.openOdb(name=odbPath)
    #This statement uses the path variable odbPath to open the output database and to assign it to
the variable myOdb.
    myViewport.setValues(displayedObject=myOdb)
    #This statement displays the default plot of the output database in the viewport.
    myViewport.odbDisplay.setPrimaryVariable(variableLabel='U', outputPosition=NODAL,
refinement=(INVARIANT,'Magnitude'), )
    myViewport.odbDisplay.display.setValues(plotState=(CONTOURS_ON_DEF, ))
    myViewport.odbDisplay.commonOptions.setValues(visibleEdges=FEATURE)
    session.printOptions.setValues(vpDecorations=OFF, reduceColors=False)
    #myViewport.viewportAnnotationOptions.setValues(compass=OFF, state=OFF, title=OFF,
legend=OFF, triad=OFF)
    myViewport.viewportAnnotationOptions.setValues(compass=OFF, titlePosition=(22, 10),
        triadSize=3,  triadPosition=(2, 2), statePosition=(5, 8))
    session.printToFile(fileName=names[j],format=TIFF, canvasObjects=(myViewport, ))
    #myViewport.close()
    del myViewport
    myOdb.close()
    j += 1


triadFont='-*-verdana-medium-r-normal-*-*-80-*-*-p-*-*-*',
titleFont='-*-verdana-medium-r-normal-*-*-80-*-*-p-*-*-*',
stateFont='-*-verdana-medium-r-normal-*-*-80-*-*-p-*-*-*'
```